Fall 2009

Wind turbine vibration study: a data driven methodology

Zijun Zhang
University of Iowa

WIND TURBINE VIBRATION STUDY: A DATA-DRIVEN METHODOLOGY

by

Zijun Zhang

A thesis submitted in partial fulfillment
of the requirements for the Master of Science
degree in Industrial Engineering
in the Graduate College of
The University of Iowa

December 2009

Thesis Supervisor: Professor Andrew Kusiak

Graduate College
The University of Iowa
Iowa City, Iowa

CERTIFICATE OF APPROVAL

_____

MASTER'S THESIS

_____

This is to certify that the Master's Thesis of

Zijun Zhang

has been approved by the Examining Committee
for the thesis requirement for the Master of Science degree
in Industrial Engineering at the December 2009 graduation.

Thesis Committee: _____
Andrew Kusiak, Thesis Supervisor

_____
Yong Chen

_____
Kate Cowles

To My Parents and Family

Hope is a waking dream.

Aristotle

ACKNOWLEDGMENTS

I would like to express my sincere gratitude to my advisor Professor Andrew Kusiak, for his devotion to this research. He has been the most instrumental person for my academic and research achievements. He provided the motivation, encouragement, guidance and advice which have prepared me for the challenges of future life. I was fortunately exposed to industrial applications while working in the Intelligent Systems Laboratory. This invaluable experience has allowed me to maintain a balance between theory and practice leading to realistic solutions.

I would like to thank Professor Yong Chen and Professor Kate Cowles for serving on my Thesis Committee and providing valuable suggestions and feedback on my research.

I am also grateful for the financial support from Iowa Energy Center and MidAmerican Energy Company. The energy experts from company and Iowa Energy Center have extended invaluable information for this research.

I thank all the members of the Intelligent Systems Laboratory who have worked with me and provided advice, reviews and suggestions. Special thanks to my colleagues: Dr. Zhe Song, who worked with me to solve challenging problems in wind energy domain; Wenyan Li, who shared her research experience with me; Mingyang Li, who enhanced my research capability through frequent communication and collaboration; and Robert A. Hamel, who discussed with me in wind energy topics and provided access to industrial data.

And finally, and most importantly, I would like to express my sincere gratitude to my parents, who solidly supported me in my academic pursuit.

ABSTRACT

Vibrations of a wind turbine have a negative impact on its performance and therefore approaches to effectively control turbines are sought by wind industry. The body of previous research on wind turbine vibrations has focused on physics-based models. Such models come with limitations as some ideal assumptions do not reflect reality. In this Thesis a data-driven approach to analyze the wind turbine vibrations is introduced.

Improvements in the data collection of information system allow collection of large volumes of industrial process data. Although the sufficient information is contained in collected data, they cannot be fully utilized to solve the challenging industrial modeling issues. Data-mining is a novel science offers platform to identify models or recognize patterns from large data set. Various successful applications of data mining proved its capability in extracting models accurately describing the processes of interest.

The vibrations of a wind turbine originate at various sources. This Thesis focuses on mitigating vibrations with wind turbine control. Data mining algorithms are utilized to construct vibration models of a wind turbine that are represented by two parameters, drive train acceleration and tower acceleration. An evolutionary strategy algorithm is employed to optimize the wind turbine performance expressed with three objectives, power generation, vibration of wind turbine drive train, and vibration of wind turbine tower.

The methodology presented in the Thesis is applicable to industrial processes other than wind industry.

TABLE OF CONTENTS

LIST OF TABLES

LIST OF FIGURES

CHAPTER 1.

INTRODUCTION

Recent years have seen growing interest in renewable energy. This increase is driven, in part, by growing awareness of the energy cost, climate changes, supply uncertainty, and environment concerns.

Wind energy is recognized as one of the most important sources of renewable energy and this awareness has translated in expansion of investments in this area. In 2008, the U.S. Department of Energy has produced a report aiming at increasing contribution of wind energy to the electricity supply to 20% by 2030. However, challenging issues, such as higher operation, maintenance and market costs than other conventional energy sources in many areas across the country, create a great barrier on this road. To accomplish this ambitious goal, numerous questions of wind energy need to be addressed, including providing control strategies to mitigate wind turbine vibrations.

Research in conventional power systems has introduced numerous simulation models for analysis of different operational scenarios of those systems. Yet, a commercial wind farm includes a large number (dozens to hundreds) of megawatt-class turbines with static and dynamic characteristics that differ from the conventional power plants. Therefore, the modeling template developed for conventional power generating facilities is not compatible with modeling wind turbines. Novel methodologies to model wind turbine systems are needed by wind energy industry.

The research in wind energy has intensified in recent years. Areas with the most research progress include the design of wind turbines [1, 2], the design and reliability of wind farms [3, 4, 5], the control of wind turbines [6, 7, 8, 9], wind energy conversion [10, 11], the prediction of wind power [12, 13], and condition monitoring of wind turbines [14, 15]. Although numerous novel modeling methods were addressed in the literature, the major focus was on developing accurate power prediction models compare to other topics. Wind turbine vibrations impact performance and life-cycle of wind turbines and

therefore it deserves further studies. Mitigating the vibrations of a wind turbine can potentially prevent material fatigue, reduce number of component failures, improve power quality and extend life-cycle of some components, such as gearbox. This in turn translates into increased turbine availability and reduced maintenance costs.

The goal of the Thesis is to analyze wind turbine vibrations and developing nonlinear and nonparametric models to optimize wind turbine performance in considering three objectives, maximization of the power produced by a wind turbine, and reduction of vibrations of the turbine's drive train and tower.

Researchers introduced models to predict wind power and describe vibrations of components of a wind turbine. Nevertheless, the majority of the published research falls into parametric and physics-based models. It is widely recognized such models usually involve assumptions, and therefore they may not adequately represent reality.

1.1 Review of wind turbine vibration research

The sources of wind turbine vibrations [16] are diverse and due to the large size of wind turbines, conducting laboratory experiments with such systems is difficult. Thus, the past wind turbine vibration research has primarily focused on the building models based on first principles and simulation. Leithead *et al.* [17] studied dynamics of variable speed wind turbines and design of models to control wind turbines. Fadaeinedjad *et al.* [18] investigated the impact of voltage sag on vibration of the wind turbine tower. They used three simulation programs, TrubSim, FAST and Simulink, to model wind turbines. Murtagh *et al.* [19] investigated control wind turbine vibration by incorporating a passive control device. A passive control method using a tuned mass damper to mitigate vibrations of the blades and tower of a wind turbine was introduced. The research reported in [20] discussed the estimation of aeroelastic damping of operational wind turbine modes based on experiments.

The physics-based or simulation based wind turbine vibration models introduced in the past research provided a solid foundation of understanding the nature of wind turbine vibrations. Unfortunately, these models involve assumptions that the industry finds restrictive. Therefore, new and more effective approaches are needed.

1.2 Review of approaches for building predictive models

Accurate prediction of wind power is essential for integration of commercial wind farms with the electric grid. Prediction of wind speed is one of the elements of power prediction. Numerous approaches to predicting wind speed have been developed. Louka *et al.* [21] applied Kalman filters to enhance wind speed prediction using hourly data. Flores *et al.* [22] employed neural networks for hourly prediction of wind speed and designed a control system for active power generation. El-Fouly *et al.* [23] developed a linear time-series strategy to predict hourly wind speed and direction. Power prediction researches also have been addressed in various published literature. Damousis *et al.* [24] used a fuzzy logic model trained by a genetic algorithm to predict wind speed and power over 0.5 to 2 hour horizons. Contaxis *et al.* [25] introduced an ARMA model to predict power produced by wind turbine in a study of short term scheduling issue. Anahua *et al.* [26] presented a stochastic differential equation to estimate power by describe power generation as a Markov process. Landberg *et al.* [27] predict the power produced by a wind farm through establishing a model by using the data from the weather prediction model (HIRLAM) and the local weather model (WASP).

In the published literature on wind and power prediction, statistical model, physics-based model and climate model have been widely discussed. However, the published research has mainly concentrated on long-time predictions, e.g., hourly predictions. To control of a wind turbine, accurate short-term power prediction models, such as 1-min or 10-s power prediction models are needed. Due to the higher sampling frequency of data, the stochastic nature of the wind speed was more significant and it

makes modeling its behavior a challenge. The past states of wind speed, temperature, humidity, latitude, terrain topography, air pressure and other factors all impact wind speed. Thus, the quality of power predicted for a wind turbine is dependent on the accuracy of wind speed prediction. The previous research [13] has demonstrated suitability of the data-driven approach

1.3 Computational intelligence and optimization

New theories and advances in computational intelligence, fuzzy logic, and image processing offer alternatives to model and solve problems in energy systems.

Chu *et al.* [28] applied a neural network to predict the performance index and non-analytical constraints, thus speeding up the trial-and-error approach of finding the optimal operating points optimizing a boiler's combustion process. Rusinowski *et al.* [29] focused on finding an optimal travelling rate of the grid and an optimal height of the fuel layer. Büche *et al.* [30] applied an evolutionary computation algorithm to find an optimal design of a burner to reduce NOx emissions as well as pressure fluctuation. Wang *et al.* [31] applied a naïve intelligent control algorithm to determine the best air supply for a boiler. Cass *et al.* [32] combined the neural network and evolutionary computation techniques to determine an optimal fuel/air ratio.

Kusiak *et al.* [33] addressed anticipatory control of wind turbine by integrating data mining and evolutionary strategy algorithms. Li *et al.* [34] introduced a hybrid genetic and immune algorithm to solve the optimization problem of internal electric connection system of large offshore wind farms. Prats *et al.* [35] applied fuzzy control techniques to improve wind energy capture for variable speed and variable pitch wind turbines. Sareni *et al.* [36] developed multi-objective genetic algorithm to study the optimal design of a small passive wind turbine generator by considering the size, power generation and other issues.

1.4 Thesis structure

Figure 1.1 illustrates the structure of the Thesis. Five data mining algorithms, Neural Network, Support Vector Machine, Standard C&R Tree, Boosting Tree and Random Forests are used to construct models for wind turbine vibrations. Chapter 2 presents analysis of wind turbine vibration data collected from SCADA systems in time and frequency domain. In Chapter 3, modeling wind turbine vibrations in drive train and tower by data-mining algorithms are discussed. Chapter 4 presents optimization model of wind turbine performance.

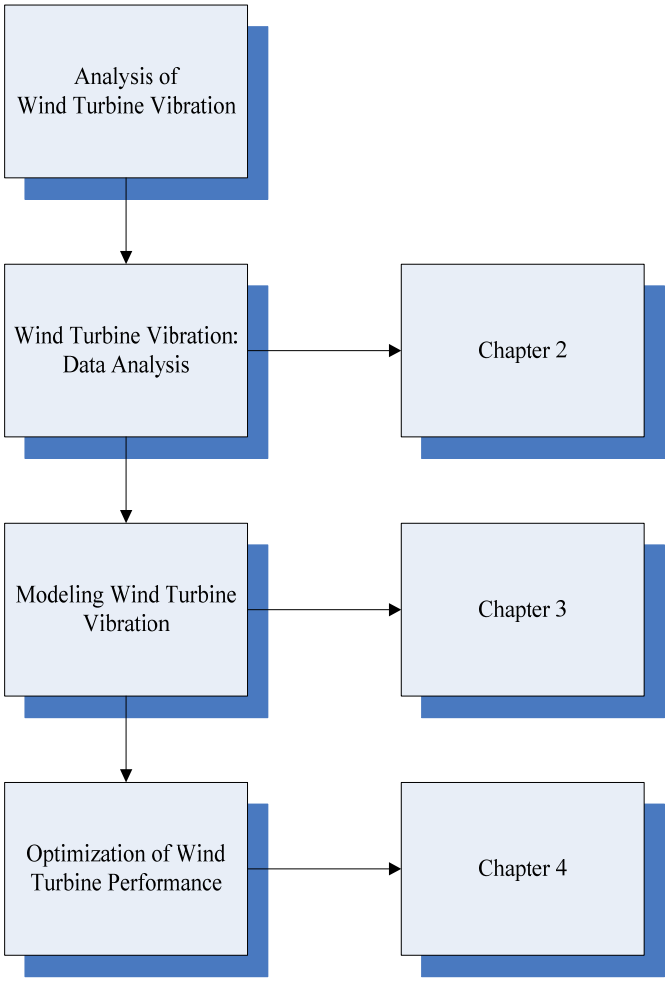

Figure 1.1 The Thesis structure

In Chapter 2, three approaches, namely the predictor importance analysis, the global sensitivity analysis, and the correlation coefficient analysis, are applied to determine turbine parameters that could potentially mitigate turbine vibrations. In the frequency domain analysis, Fourier analysis transforms time domain data into frequency domain to demonstrate another approach to vibration studies.

In Chapter 3, application of wavelet analysis in smoothing data is discussed as sensors to measure drive train acceleration and tower acceleration are noise sensitive.

In Chapter 4 a framework for wind turbine performance optimization is presented. Data mining and evolutionary algorithms are integrated to model and solve multi-objective optimization model of maximizing power generation, and reducing vibrations of the drive train and the tower. Tuning parameters of evolutionary strategy algorithm is discussed to improve computational efficiency. Three weight assignment cases are discussed and computational gains in power maximization and vibration reduction are presented.

CAPTER 2.

ANALYSIS OF WIND TURBINE VIBRATION

2.1 Introduction

In this chapter, analysis of wind turbine vibration in the time domain and the frequency domain is introduced. Two parameters the drive train acceleration and the tower acceleration are utilized to represent the wind turbine vibration.

The sources of wind turbine vibrations [16] are diverse. The focus of this research is on vibrations attributed to the control of wind turbines, e.g., control of the generator torque and blade pitch angle. Data partitioning strategy is applied to divide data set according to fixed range of wind speed so that impact of wind speed in wind turbine vibration can be mitigated and vibrations associated to control parameters of wind turbine can be emphasized.

The basis of the time domain analysis is statistical and data-driven methodologies. Three approaches, namely the predictor importance analysis, the global sensitivity analysis, and the correlation coefficient analysis, are applied to determine turbine parameters that could potentially mitigate turbine vibrations. In the frequency domain analysis, data is transformed from time domain to frequency domain by Fourier analysis and this approach offers an alternative angle to understand wind turbine vibration.

2.2. Data description

In this research, data sets collected by the SCADA system at two variable speed 1.5MW turbines of a large wind farm are used. Each data set contains average values of more than 120 parameters, including vibration parameters, all stored at 10-second (10-s) intervals and thus the sampling frequency is 0.1Hz. Although the SCADA system contains values of many parameters, only some of them are of interest to vibration analysis. The literature and domain expertise was used to select a list of parameters that

could be potentially relevant to the research discussed in this paper. Table 2.1 illustrates the format of the data used in this research.

Table 2.1 Sample data set

Observation No.	Time	Torque Value [%]	Wind Speed [m/s]	…	Drive Train Acceleration [mm/s2]	Tower Acceleration [mm/s2]
1	10/1/08 12:00 AM	22.10	5.77	…	25.67	29.31
2	10/1/08 12:00 AM	22.60	6.45	…	24.78	30.26
3	10/1/08 12:00 AM	23.10	6.07	…	23.89	31.21
…	…	…	…	…	…	…
60482	10/8/08 12:00 AM	0.00	2.74	…	18.01	29.34

As illustrated in Table 2.1, the values of all parameters contained in the data set, such as torque, wind speed, wind deviation, drive train acceleration, and tower acceleration, are time stamped. The wind turbine vibration is indicated by two important parameters, the drive train acceleration reflecting vibrations of the drive train, and the tower acceleration reflecting vibrations of the tower. The accelerometer measuring the drive train acceleration is attached at the rear bottom of nacelle and the tower acceleration accelerometer is located near the nacelle and tower connection.

2.3 Data pre-processing

Since the data set is stored at 10-s intervals, the month-long data set considered in this research is large, and it contains errors caused by malfunction of sensors, mechanical systems, and the data collection system. Those errors usually appear as missing values,

values that are out of range, and invalid values. For example, the net power produced by a wind turbine should be a positive number, which is usually between 0 and its rated power. Thus, filtering erroneous values is a significant step in data-driven research. However, once the error logic is discovered, the data cleaning process can be automated.

After filtering the errors and invalid values, three derived parameters are created based on the original SCADA data. The first one is the wind deviation (yaw error), which is defined as the difference between the wind direction and the nacelle position. The next two are the rate of change of torque and the rate of change of the pitch angle. The rate of change of torque (referred to as torque rate) is the difference between the current torque value and the torque value at the preceding time 10-s interval (see Eq. (2.1)). The rate of change of pitch angle (referred to as blade pitch angle rate) is the difference between the current pitch angle and the pitch angle preceding the 10-s time interval (see Eq. (2.2)).

$$\text{Torque Rate} = \text{Torque Value}(t) - \text{Torque Value}(t-1) \tag{2.1}$$

$$\text{Pitch Angle Rate} = \text{Pitch Angle}(t) - \text{Pitch Angle}(t-1) \tag{2.2}$$

The two derived parameters (see Eqs (2.1) and (2.2)) provide additional information about wind turbine vibrations from the rate of change perspective.

In the time domain analysis, the entire data set is used for training models, and it is decomposed into three partitions based on the wind speed values: wind speed in the interval [3.5 m/s, 7 m/s), [7 m/s, 12 m/s), and [>=12 m/s]. This rather arbitrary partitioning is based on the sigmoid shape of power curve and provides a way to isolate the turbine vibrations attributed to both the drive train and the tower from the impact of other factors such as the wind itself, malfunctions of mechanical systems (e.g., shaft misalignments), and so on (see Table 2.2).

Table 2.2 Three data subsets

Wind Turbine 1		
Data Partition No.	Wind Speed	Number of Data Points
1	[3.5m/s, 7m/s)	77593 10-s observations
2	[7m/s, 12m/s)	103148 10-s observations
3	[>=12m/s]	21525 10-s observations
Wind Turbine 2		
Data Partition No.	Wind Speed	Number of Data Points
1	[3.5m/s, 7m/s)	63554 10-s observations
2	[7m/s, 12m/s)	103115 10-s observations
3	[>= 12m/s]	11855 10-s observations

Although the volume of data collected at the wind farm is large, some data samples are biased, i.e., some observations included in the population dominate other data points. A typical biased data sample of torque values included in Data Partition 1 of Turbine 1 (see Table 2.2) is illustrated in the histogram of Fig. 2.1.

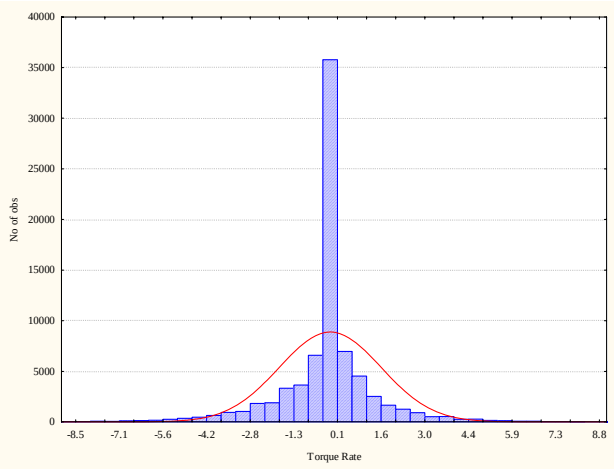

Figure 2.1 Torque histogram for data partition 1 of turbine 1

It is obvious from the histogram in Fig. 1 that the torque rates in the interval [-0.84, 0.84] have a much higher frequency than the values in other intervals. Thus, the number of observations in this interval needs to be reduced from about 36000 to 7000. This has been accomplished with a random sampling without a replacement scheme. The histogram of torque values after sampling is presented in Fig. 2.2.

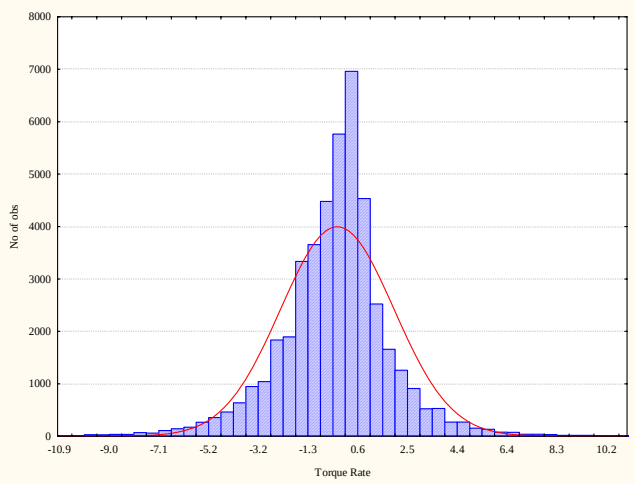

Figure 2.2 Torque histogram for data partition 1 of turbine 1 after sampling

2.4 Data analysis of wind turbine vibration in time domain

In this research, several parameters measured by sensors or derived from data, such as torque, torque rate, wind speed, wind deviation, blade pitch angle (average of the three measured pitch angles, one for each blade), and the blade pitch rate, are considered as the major factors potentially impacting the turbine vibrations. These parameters are selected mainly based on domain knowledge and study of the wind energy literature [37, 38].

The tower and drive train accelerations are recorded by the SCADA system. As there are two similar measured values offered by the sensor installed on the drive train,

the average value of drive train acceleration is considered for simplicity of analysis. Three different data approaches are applied to quantitatively analyze the impact of each of the selected parameters on the turbine vibrations reflected by the drive train acceleration and the tower acceleration. The data analysis approaches include the predictor importance analysis, the global sensitivity analysis, and the correlation coefficient analysis, and they are applied to each of the three data partitions of Table 2.2. Predictor importance is determined by the boosting regression tree algorithm [39, 40]. The predictor importance statistics, e.g., the sum of the squares' errors, are computed for each split during the process of building trees, and the best predictor parameter is then is selected. An average statistic is computed over all trees and all splits. The predictor parameter with the highest value is assigned the value of 100, and other parameters are assigned lower values. The global sensitivity analysis ranks the importance of inputs on the model extracted by a neural network approach [41, 42, 43]. It examines the contribution of uncertainty of all inputs to the output of the model simultaneously, rather than individually, to determine the order of parameter importance. The correlation coefficient [44] is a statistical approach to analyze the relationship between predictors and the target based on their affinity.

2.4.1 Analysis of data set with wind speed between 3.5m/s and 7m/s

For Data Partition 1 of Table 2.2, the wind speed of both turbines is in the interval [3.5 m/s, 7 m/s). Due to the fact that the wind speed is rather low, its impact on the drive train and the tower is likely to be minimal.

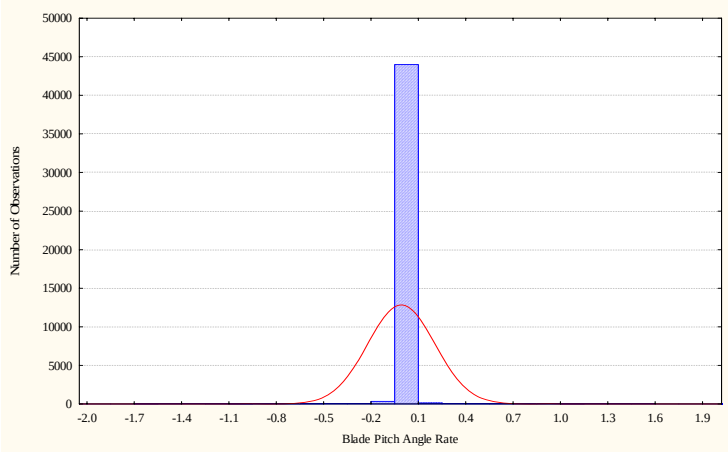

Figure 2.3 Histogram of the blade pitch angle rate of turbine 1 in data partition 1

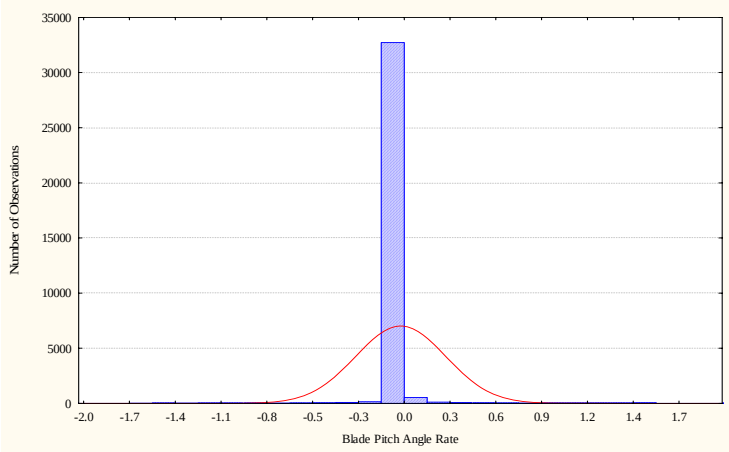

Figure 2.4 Histogram of the blade pitch angle rate of turbine 2 in data partition 1

It is also known that for low wind speeds, the blade pitch angle remains mostly constant for most pitch controlled turbines as shown in Figure 2.3 and Figure 2.4; therefore, this parameter could be excluded in the analysis. Table 2.3 shows the impact of predictors (measured with the predictor importance) on the drive train acceleration and the average tower acceleration of the two turbines.

Table 2.3 Ranking produced by predictor importance analysis for two turbines for data partition 1

Predictor	Drive Train Acceleration		Tower Acceleration	
	Turbine 1 Predictor Rank	Turbine 2 Predictor Rank	Turbine 1 Predictor Rank	Turbine 2 Predictor Rank
Torque Value	100	100	90	95
Torque Rate	79	94	100	98
Wind Deviation	54	57	91	93
Blade Pitch Angle	54	66	67	100
Wind Speed	47	46	51	82

The values of the predictor rank in Table 2.3 are generated by the boosting tree regression algorithm. The predictor importance varies by the predictor (e.g., Torque Value, Torque Rate) and the target (i.e., Drive Train Acceleration, Tower Acceleration).

The global sensitivity rankings produced by a neural network are provided in Table 2.4. Although the scale used to rank the predictors is different than the one used in Table 2.3, a higher ranking value indicates that the contribution of the corresponding parameter for making predictions is higher.

Table 2.4 Rankings produced by the global sensitivity analysis for two turbines for data partition 1

Predictor	Drive Train Acceleration		Tower Acceleration	
	Turbine 1 Predictor Rank	Turbine 2 Predictor Rank	Turbine 1 Predictor Rank	Turbine 2 Predictor Rank
Torque Value	3.27	3.87	3.27	1.25
Torque Rate	1.55	2.02	1.11	1.04
Wind Deviation	1.03	1.00	1.02	1.01
Blade Pitch Angle	1.02	1.01	1.07	1.00
Wind Speed	1.96	1.33	1.64	1.05

Table 2.5 illustrates the correlation coefficient between predictors and two accelerations. A higher value of the correlation coefficient indicates a stronger dependence between a predictor and the vibration.

Table 2.5 Rankings produced by the correlation coefficient analysis for two turbines for data partition 1

Predictor	Drive Train Acceleration		Tower Acceleration	
	Turbine 1 Correlation Coefficient	Turbine 2 Correlation Coefficient	Turbine 1 Correlation Coefficient	Turbine 2 Correlation Coefficient
Torque Value	0.74	0.50	0.30	0.11
Torque Rate	-0.23	-0.22	-0.05	0.01
Wind Deviation	0.14	0.04	0.09	0.05
Blade Pitch Angle	-0.36	-0.19	-0.17	-0.06
Wind Speed	0.55	0.28	0.17	-0.03

In the boosting tree regression analysis, a higher predictor rank points to a stronger impact of the predictor on a target variable (here vibration). The nature of the global sensitivity analysis is similar to the regression boosting tree analysis. However, the correlation coefficient analysis offers a different concept. A positive correlation coefficient implies that the two variables are positively and linearly correlated, while a

negative correlation coefficient indicates the inverse relationship. A higher value of the correlation coefficient indicates a more obvious linear relationship between the corresponding variables. In Table 2.3, the rank of the torque in respect to the drive train acceleration is 100, the highest of all other parameters. In Table 2.4, the rank value of torque is also the highest for both two turbines. In Table 2.5, the correlation coefficient between the torque value and the drive train acceleration is the highest, which means that the vibrations of the drive train are strongly associated with the torque value. These observations indicate that in the speed interval [3.5 m/s, 7 m/s) large values of the torque potentially contribute to higher acceleration of the drive train. The torque rate of change is another variable with a strong impact on vibrations of the drive train of a wind turbine. In the boosting tree regression analysis, the torque rate of change ranked after the torque value for both turbines. In the global sensitivity analysis, it is ranked third for Turbine 1 and second for Turbine 2. The wind speed turns out to be more important for Turbine 1 than for Turbine 2. The correlation coefficient in Table 2.5 provides a different result for the torque rate, as it emphasizes the linear relationship rather than the non-linear relationship between the corresponding variables. In this case, the results of the first two analyses provide more valuable information and indicate that the torque rate of change is another factor (after torque value) strongly associated with the vibrations of the turbine drive train.

For the tower vibration, no single parameter consistently scores the highest rank in all three analyses. However, the rank values in Table 2.3 and Table 2.4 indicate that the torque value is more important than most other variables for both turbines. In Table 2.3, the rank of torque value is 90 for Turbine 1 and 95 for Turbine 2. In Table 2.4, the rank of torque value is 3.27 for Turbine 1 and 1.25 for Turbine 2. In conclusion, although the rankings for a turbine tower provided by the three analyses are somehow different, it is apparent that the torque is associated with the vibrations at the turbine tower.

2.4.2 Analysis of data set with wind speed between 7m/s and 12m/s

In Data Partition 2 of Table 2.1, the wind speed falls in the interval [7 m/s, 12 m/s). Figure 2.5 and 2.6 illustrate the blade pitch angle rate (i.e., the change of pitch angle in the consecutive time points (see Eq. (2)) for the data sets of two turbines.

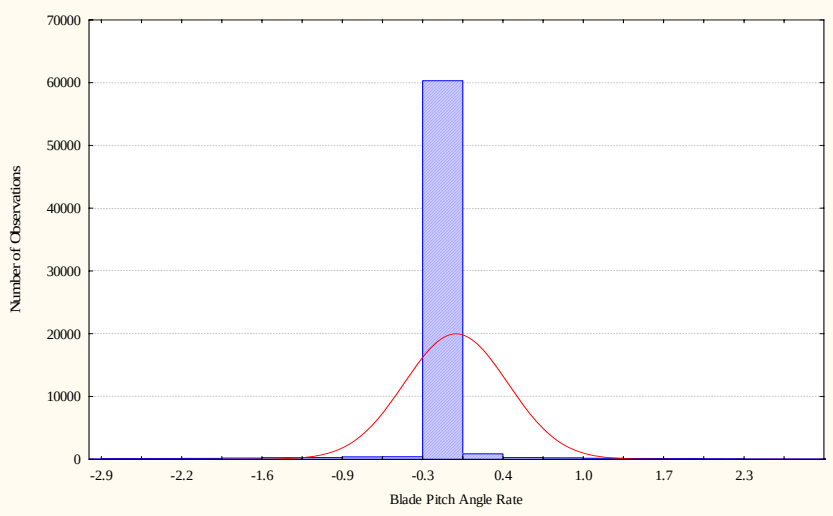

Figure 2.5 Histogram of the blade pitch angle rate of turbine 1 in data partition 2

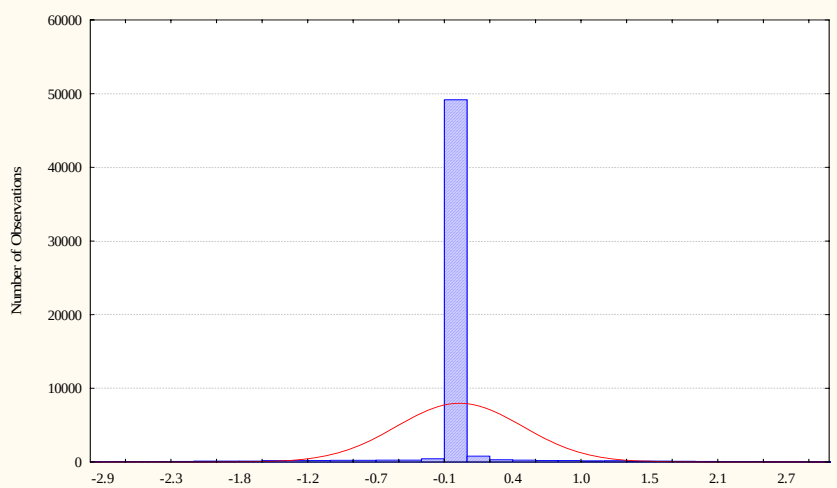

Figure 2.6 Histogram of the blade pitch angle rate of turbine 2 in data partition 2

The blade pitch angle of two wind turbines (see Figsure 5 and 6) does not significantly change. Table 2.6 shows the results of the predictor importance analysis of two turbines in Data Partition 2. Table 2.7 illustrates the results of the global sensitivity analysis for the two turbines. Table 8 presents the results of the correlation coefficient analysis in this scenario.

Table 2.6 Ranking produced by the predictor importance analysis for two turbines in data partition 2

Predictor Importance Analysis	Drive Train Acceleration		Tower Acceleration	
	Turbine 1 Predictor Rank	Turbine 2 Predictor Rank	Turbine 1 Predictor Rank	Turbine 2 Predictor Rank
Torque Value	100	100	100	98
Torque Rate	86	95	84	100
Wind Deviation	42	47	39	48
Blade Pitch Angle	71	76	71	81
Wind Speed	69	55	80	76

Table 2.7 Rankings produced by the global sensitivity analysis for two turbines in data partition 2

Global Sensitivity Analysis	Drive Train Acceleration		Tower Acceleration	
	Turbine 1 Predictor Rank	Turbine 2 Predictor Rank	Turbine 1 Predictor Rank	Turbine 2 Predictor Rank
Torque Value	3.87	3.77	1.25	1.17
Torque Rate	2.02	1.90	1.04	1.11
Wind Deviation	1.00	1.00	1.01	1.01
Blade Pitch Angle	1.01	1.02	1.00	1.01
Wind Speed	1.33	1.42	1.05	1.17

Table 2.8 Rankings produced by the correlation coefficient analysis for two turbines in data partition 2

Correlation Coefficient Analysis	Drive Train Acceleration		Tower Acceleration	
	Turbine 1 Correlation Coefficient	Turbine 2 Correlation Coefficient	Turbine 1 Correlation Coefficient	Turbine 2 Correlation Coefficient
Torque Value	0.69	0.51	0.52	0.38
Torque Rate	0.08	0.12	0.08	0.14
Wind Deviation	0.02	0.03	0.00	0.01
Blade Pitch Angle	0.25	0.23	0.23	0.23
Wind Speed	0.63	0.48	0.48	0.35

Torque value is considered as the most important variable in vibration analysis of the drive train. In Table 2.6, the rank of torque value is 100 for both turbines. Table 2.7 confirms the results of Table 2.6. In Table 2.8, the correlation coefficient between the torque value and the drive train acceleration is the highest. These results confirm that the torque value is the most significant parameter related to vibrations of the drive train. Torque rate could be considered as the second most important parameter associated with the drive train vibration. The blade pitch angle could be another parameter potentially

causing the wind turbine vibrations, as confirmed by the predictor importance analysis and correlation coefficient analysis.

In analyzing tower accelerations, the torque value ranks highest for Turbine 1 (Table 2.6). It also scores the second highest rank (98) for Turbine 2. The global sensitivity analysis (Table 2.7) shows that the torque value is also important, as it gets ranked close to other parameters. In Table 2.8, the correlation coefficient between the torque value and the tower acceleration is the highest. The torque rate and blade pitch angle are also important factors related to the tower acceleration. In the predictor importance analysis, the rank values of the torque rate and the blade pitch angle for both turbines are higher than 70. In Table 2.7, the rank values of the variables besides torque value are similar. In Table 2.8, the blade pitch angle shows a higher correlation with the tower acceleration than the torque rate. In conclusion, although the results from different analyses point to different importance of parameters, the results imply that the torque rate and blade pitch angle are strongly associated with the tower acceleration.

2.4.3 Analysis of data set with wind speed higher than 12m/s

In this scenario, all the wind speeds are higher than 12 m/s. As the torque value does not frequently change (see Figure 2.7 and 2.8) it is not considered in the analysis discussed in this section. The predictor importance is reported in Table 2.9; Table 2.10 shows the results of the global sensitivity analysis, and Table 2.11 presents the results of the correlation coefficient analysis. This scenario (speed above 12 m/s) is considered to be high wind speed, and it is likely that some vibrations of the wind turbine are contributed by the wind.

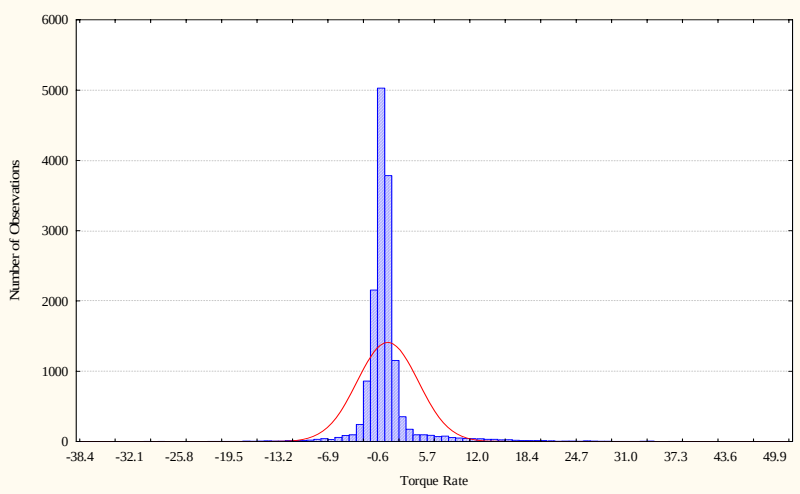

Figure 2.7 Histogram of torque rate of turbine 1 in data partition 3

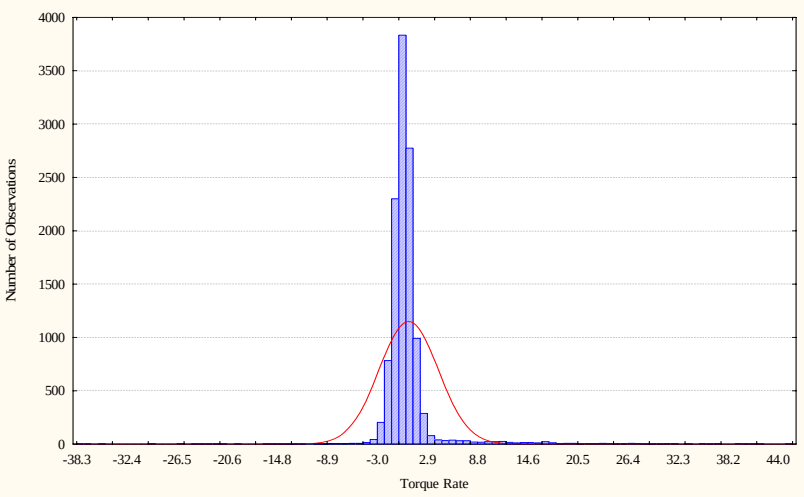

Figure 2.8 Histogram of torque rate of turbine 2 in data partition 3

The analysis of the drive train acceleration data has revealed that the association of the blade pitch angle with turbine vibrations is the strongest of all parameters. In Table 2.9, the predictor importance analysis ranks the blade pitch angle as the most important factor. In Table 2.10, the rank value of the blade pitch angle is higher than for other parameters. In Table 2.11, although the correlation coefficient between wind speed and drive train acceleration is higher than that between the blade pitch angle and drive train acceleration, the difference between the two correlation coefficients is not significant. Besides the blade pitch angle, other variables such as torque value, torque rate, and wind deviation, can also impact the drive train acceleration; however, the impact is not as significant as the blade pitch angle.

The analysis of data shows that the blade pitch angle is the most significant factor associated with the tower acceleration. The rank value of the blade pitch angle in Table 2.9 and Table 2.10 is the highest. The correlation coefficient between the blade pitch angle and the tower acceleration is almost identical to the correlation coefficient between the wind speed and the tower acceleration (see Table 2.11).

Table 2.9 Ranking produced by the predictor importance analysis for two turbines in data partition 3

Predictor Importance Analysis	Drive Train Acceleration		Tower Acceleration	
	Turbine 1 Predictor Rank	Turbine 2 Predictor Rank	Turbine 1 Predictor Rank	Turbine 2 Predictor Rank
Torque Value	42	38	44	49
Blade Pitch Angle Rate	37	29	52	44
Wind Deviation	12	13	31	25
Blade Pitch Angle	100	100	100	100
Wind Speed	90	91	84	89

Table 2.10 Ranking produced by the global sensitivity analysis for two turbines in data partition 3

Global Sensitivity Analysis	Drive Train Acceleration		Tower Acceleration	
	Turbine 1 Predictor Rank	Turbine 2 Predictor Rank	Turbine 1 Predictor Rank	Turbine 2 Predictor Rank
Torque Value	1.03	1.02	1.01	1.01
Blade Pitch Angle Rate	1.07	1.04	1.04	1.02
Wind Deviation	1.00	1.01	1.01	1.01
Blade Pitch Angle	1.72	2.93	1.76	1.81
Wind Speed	1.17	1.15	1.17	1.02

Table 2.11 Ranking produced by the correlation coefficient analysis for two turbines in data partition 3

Correlation Coefficient Analysis	Drive Train Acceleration		Tower Acceleration	
	Turbine 1 Correlation Coefficient	Turbine 2 Correlation Coefficient	Turbine 1 Correlation Coefficient	Turbine 2 Correlation Coefficient
Torque Value	-0.09	-0.10	-0.03	-0.09
Blade Pitch Angle Rate	0.08	0.01	0.09	0.02
Wind Deviation	0.00	0.02	-0.04	-0.02
Blade Pitch Angle	0.78	0.85	0.64	0.67
Wind Speed	0.84	0.86	0.66	0.69

2.5 Data analysis of wind turbine vibration in frequency domain

Besides the wind and control, malfunctions of turbine components may contribute to the vibrations of a wind turbine [16]. Usually, the aberrations may be caused by mechanical problems and are difficult to observe in the time domain. Projecting the time domain data into the frequency domain (power spectrum) shown in Figure 2.9 offers an alternative view. The x-axis in Figure 2.9 represents the frequency, and the y-axis is the power corresponding to the drive train acceleration.

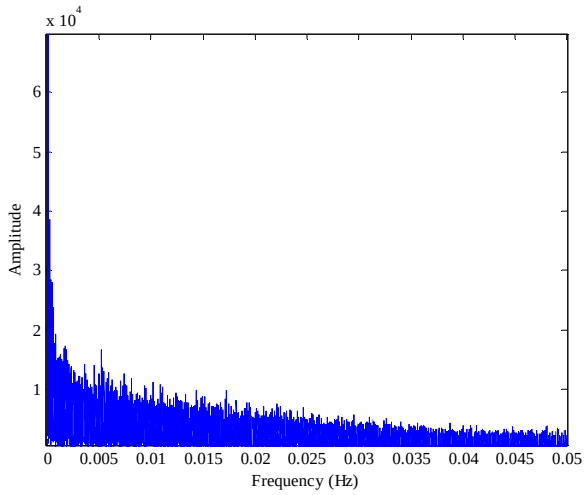

Figure 2.9 Spectrum from 0 to 0.05 Hz of the drive train acceleration of turbine 1

Usually, wind turbine vibrations caused by malfunctions of the power train are expressed as peaks in the spectrum at different frequencies. However, since the sampling time of the data set available for this study is only 10 seconds, only a small portion of the data frequency (up to 0.05 Hz) is reflected in the spectrum. Based on this limited analysis and information of turbine status from wind farm, an assumption that the turbine is operated in normal condition is made in this research and vibration caused by malfunction is excluded in consideration.

2.6 Summary

This chapter presented a preliminary study of wind turbine vibration data from two perspectives, time domain and frequency domain. To alleviate the impact of wind speed to wind turbine vibration, the data set is arbitrarily partitioned to three subsets according to three ranges of wind speed, [3.5m/s, 7m/s], [7m/s, 12m/s] and [12m/s, ∞].

These three ranges of wind speed are selected based on the shape of power curve which is similar to the sigmoid function.

Three approaches, the predictor importance analysis, global sensitivity analysis, and correlation coefficient analysis, were used to conduct quantitative analysis of the importance of parameters to wind turbine vibrations. Two parameters, the drive train acceleration and the tower acceleration, were used to study the wind turbine vibration. Rank values of the parameters selected for the data set were then derived by three different approaches. For the low wind speeds, e.g., between 3.5 m/s and 7m/s, the torque value and the torque rate of change were found to be meaningful parameters impacting the wind turbine vibration. For higher wind speeds, e.g., between 7 m/s and 12 m/s, the torque value and the blade pitch angle could potentially reduce the wind turbine vibrations. When wind speed was larger than 12 m/s, the blade pitch angle was suggested as the most dominant parameter that could potentially reduce the wind turbine vibrations.

The results of frequency domain analysis provided another angle of investigating wind turbine vibration. Power spectrum is utilized to illustrate vibrations in this domain. Malfunctions of wind turbine vibration could be observed as a peak of power at high frequency in the power spectrum. Unfortunately, due to the limitation of data, information of frequency higher than 0.05 was lost and patterns in high frequency was invisible. However, based on the available information in the power spectrum and turbine status from wind farm, an assumption that wind turbine was operated in normal condition was made. Thus, vibration potentially caused by malfunction of components installed in wind turbine was excluded in the consideration of this study.

CHAPTER 3.
MODELING WIND TURBINE VIBRATIONS BASED ON DATA DRIVEN APPROACH

3.1 Introduction

Wind energy was considered one of the most viable sources of sustainable energy. Its rapid growth in recent years has gained research attention aimed at investigating emerging problems. In the past, majority of these attentions were concentrated on domains such as wind energy conversion [10, 11], prediction of wind power [13], wind speed prediction [24, 45], wind farm layout design [3, 4, 5], and turbine monitoring [14, 15]. Mitigating the vibrations of a wind turbine is another avenue in wind energy research since vibrations are considered as a critical factor that could potentially trigger material fatigue, increase number of component failures, and shorten life-cycle of some components. Thus, mitigating wind turbine vibration in order to increase turbine availability and reduce cost of maintenance is interested by wind energy industry and is deserved to be investigated.

The past wind turbine vibration research has primarily focused on the building models based on first principles and simulation. Leithead et al. [17] studied dynamics of variable speed wind turbines and design of models to control wind turbines. Fadaeinedjad et al. [18] investigated the impact of voltage sag on vibration of the wind turbine tower. They used three simulation programs, TrubSim, FAST and Simulink, to model wind turbines. Murtagh et al. [19] investigated control wind turbine vibration by incorportaing a passive control device. However, the limitations of the previous research should also be considered. Firstly, conducting a laboratory experiment for a Megawatt-class turbine is challenging due to its large size. In addition, it was widely recognized that analysis of parametric models has limitations, as such models usually involve many assumptions, and therefore they might not adequately represent reality. With massive deployment of

wind farms in recent years, both the performance and maintenance of wind turbines have grown in importance. Thus, models accurately portraying wind turbine vibrations were needed.

Modeling turbine vibrations was complex, as many parameters were involved. A new approach designed to handle vibrations was needed. This chapter introduced data driven approaches to capture the dynamic equations of wind turbine vibration and establish accurate prediction models for wind turbine vibration. Five data-mining algorithms were used to model the relationships between the identified parameters and wind turbine vibrations, and the best one was selected for modeling and in-depth computational study.

3.2 Wind-speed based scenarios

In this study, the data set is further split into smaller subsets based on the following speed intervals [3.5 m/s, 5 m/s), [5 m/s, 6 m/s), [6 m/s, 7 m/s), [7 m/s, 8 m/s), [8 m/s, 9 m/s), [9 m/s, 10 m/s), [10 m/s, 11 m/s), [11 m/s, 12 m/s), and [12 m/s, 14 m/s]. Since each speed interval is narrow, the impact of the wind speed change can be neglected, and more accurate wind turbine vibration models can be built.

3.3 Wavelet analysis

Noisy data usually diminish accuracy of the models derived from such data. Wavelets are used to smooth the data and noise reduction before establishing vibration models. Wavelet analysis calls for the order and level of wavelet. The difference between the mean of the original value and the denoised value is used to select the best order and level. Comparative analysis is discussed to select the most appropriate combination of order and level Daubechies wavelets [46], namely DB7 Level 10, DB 7 Level 7, and DB 5 Level 5. Data set from 10/1/2008 12:00:10 AM to 10/8/2008 12:00:00 AM has been used in the comparative analysis. Table 3.1 presents the difference between the mean of

the original drive train acceleration and the mean of the denoised drive train acceleration for the three wavelets.

Table 3.1 Difference between the mean of the original and the denoised drive train acceleration

Wavelet Type	DB7 Level 10	DB 7 Level 7	DB 5 Level 5
Difference Between two Means	0.0092	0.0088	0.0004

In this study, no significant shift in the mean of acceleration is expected after denoising. According to Table 3.1, it is obvious that DB 5 Level 5 is better than other two transformations and thus it is selected.

To demonstrate the value of wavelet analysis, two experiments have been conducted. Neural Network (NN) models were built for original data sets and denoised data by DB 5 level 5. The DB 5 with level 5 denoised only the drive train acceleration and tower acceleration data. Table 3.2 presents the training results for a NN model based on the [7 m/s, 8 m/s) data subset of Turbine 1. Table 3.3 presents the test results for the same data subset. Four metrics, the mean absolute error (MAE, Eq. 3.1), the standard deviation of mean absolute error (SD of MAE, Eq. 3.2), the mean absolute percentage error (MAPE, Eq. 3.3), and the standard deviation of MAPE (SD of MAPE, Eq. 3.4), are used to evaluate the results, where $\hat{y}_i$ is the predicted drive train (or tower acceleration) and y_i is the observed value in the data set.

Table 3.2 Training results of the neural network model

Training	MAE	SD of MAE	MAPE	SD of MAPE
Original Data Set	5.68	4.80	3.90	353.19
Denoised Data Set	1.29	2.30	0.00	2.70

Table 3.3 Test results of the neural network model

Test	MAE	Std of MAE	MAPE	Std of MAPE
Original Data Set	5.57	4.74	0.19	2.35
Denoised Data Set	1.25	2.11	0.04	0.63

$$\text{Mean absolute error (MAE)} = \frac{1}{n}\sum_{i=1}^{n}|\hat{y}_i - y_i| \tag{3.1}$$

$$\text{Standard deviation of MAE} = \sqrt{\frac{1}{n}\sum_{i=1}^{n}(|\hat{y}_i - y_i| - \frac{1}{n}\sum_{i=1}^{n}|\hat{y}_i - y_i|)^2} \tag{3.2}$$

$$\text{Mean absolute percentage error (MAPE)} = \frac{1}{n}\sum_{i=1}^{n}(|\frac{\hat{y}_i - y_i}{y_i}|)\times 100\% \tag{3.3}$$

$$\text{Standard deviation of MAPE} = \sqrt{\frac{1}{n}\sum_{i=1}^{n}(|\frac{\hat{y}_i - y_i}{y_i}| - \frac{1}{n}\sum_{i=1}^{n}|\frac{\hat{y}_i - y_i}{y_i}|)^2}\times 100\% \tag{3.4}$$

Based on results in Table 3.2 and Table 3.3, it is obvious that denoising and smoothing data is beneficial for modeling. The large MAPE and SD of MAPE for the original dataset in Table 3.2 are caused by the small values in the training set and the nature of these two metrics. For example, some instances with values as small as 0.00002 are contained. A small error (the difference between the observed and predicted value) , such as 2, results in a large MAPE of (3.3) and a large SD of MAPE in (3.4).

3.4 Data-driven models

Data-driven models are used to represent the relationship between inputs, such as torque value, torque rate, wind speed and wind deviation, and outputs (the drive train

acceleration and tower acceleration). Such models differ from the physics-based functions, for example, the function describing the acceleration of a swing (see (Eq. 3.5)).

$$\text{Acceleration} = \frac{d^2x}{dt^2} = \ddot{x} = -x_0\omega^2 \cos \omega t \tag{3.5}$$

Unlike the parametric models, the data-driven models do not require knowing in advance the function mapping inputs into an output (see (Eq. 3.6)).

$$y = f(\vec{x}),\ \vec{x} = [x_1, x_2, ...x_n, v_1, v_2, ..v_n] \tag{3.6}$$

where y is the drive train acceleration or the tower acceleration measured by accelerometers, x_i are the non-controllable inputs (the wind deviation, wind speed), and v_j are the controllable inputs (the torque value, torque rate, blade pitch angle, and so on). The function $f(\bullet)$ is learned by data-mining algorithms.

Before a data-driven model is built, the most suitable data-mining algorithm needs to be selected. In this section, the performance of five classifiers, Neural Network (NN) [41, 42, 43], Support Vector Machine (SVM) [47, 48], Boosted Tree [39, 40], Standard C&RT, and Random Forest [49], is evaluated using two metrics, MAE (Eq. 3) and MAPE (Eq. 3.3). The data set, which is randomly selected across all wind speeds (Table 2), is used for training and testing.

The Neural Network (NN) is a biology-based computational model that is adaptive and robust. The Support Vector Machine, SVM, is used for classification and regression based on the concept of maximizing the margin between the data points of different classes. The last three data-mining algorithms are tree-based approaches. Boosted Tree applies the boosting method to regression trees. Standard C&RT, classification and regression tree, is a data-mining approach that builds an optimal tree structure to predict categorical or continuous variables. Random Forest is a data-mining algorithm composed of many decision trees, and it outputs the best values of an individual tree.

Table 3.4 and Table 3.5 illustrate the performance of the five classifiers for predicting the drive train acceleration and tower acceleration, respectively. The Neural Network (NN) model provides the lowest MAE and MAPE for both cases. Thus, NN model is selected as the most accurate model to predict wind turbine vibrations.

Table 3.4 Performance of five classifiers for predicting drive train acceleration

Drive Train Acceleration		
Classifier	MAE	MAPE
NN	1.17	0.07
SVM	8.64	0.27
Standard C&RT	4.23	0.16
Boosted Tree	3.20	0.20
Random Forest	2.06	0.09

Table 3.5 Performance of five classifiers for predicting tower acceleration

Tower Acceleration		
Classifier	MAE	MAPE
NN	4.54	0.11
SVM	13.72	0.27
Standard C&RT	10.86	0.22
Boosted Tree	6.91	0.15
Random Forest	5.26	0.11

All parameters used by the neural network model to extract models in Eqs. (3.7) - (3.8) are listed in Table 3.6.

$$y_1 = f(y_1(t-1), y_1(t-2), y_1(t-3), x_1, x_2, x_3, x_4, v_1, v_2) \quad (3.7)$$

$$y_2 = f(y_2(t-1), y_2(t-2), y_2(t-3), x_1, x_2, x_3, x_4, v_1, v_2) \quad (3.8)$$

where y_1 and y_2 represent the drive train acceleration and the tower acceleration, respectively. The function $f(\bullet)$ is learned by data-mining algorithms.

Table 3.6 Feature descriptions

Parameter	Description
y_1	Drive train acceleration
y_2	Tower acceleration
y_1(t-1)	Drive train acceleration at time t-1
y_1(t-2)	Drive train acceleration at time t-2
y_1(t-3)	Drive train acceleration at time t-3
y_2(t-1)	Tower acceleration at time t-1
y_2(t-2)	Tower acceleration at time t-2
y_2(t-3)	Tower acceleration at time t-3
x_1	Torque change rate
x_2	Wind speed
x_3	Wind deviation
x_4	Blade pitch angle change rate
v_1	Torque value
v_2	Blade pitch angle

3.5 Case study

As the neural network outperforms the other four data mining algorithms based on the sample data set, it is introduced to extract non-parametric predictive models of wind turbine vibration from the industrial data, i.e., the data set of Turbine 1 after pre-processing. In this study, data sets collected at two different turbines are used. The two data sets of are decomposed into subsets as described in Section 3.2. Each Turbine 1 data subset is then split into training and test data sets by random sampling. The training data set includes 2/3 of all data points and the test data set constitutes the remaining 1/3 data. The data subsets of Turbine 2 (external data sets) are applied to test the accuracy and

robustness of the models derived from Tribune 1 data. The parameters in Table 3.6 are selected to build models according to the functions (see Eq. (3.7) and (3.8)) learned by the neural network. Thus, two non-parametric models extracted from the data, one for the drive average train acceleration and another for the tower acceleration.

Table 3.7 presents test results from predicting the average drive train and the tower acceleration for 18 different scenarios. The model performance for each speed range (Scenarios 1 through 9) is measured with four metrics, MAE (Eq. 3.1), Standard Deviation of MAE (Eq. 3.2), MAPE (Eq. 3.3) and Standard Deviation of MAPE (Eq. 3.4).

The results included in Table 3.7 indicate that the predictions for the drive train acceleration are accurate as most of the MAPE values are lower than 0.03, which means that the prediction accuracy higher than 97%. In addition, the low value of the standard deviation of MAPE indicates small variability of error relative to the mean error.

The value of MAPE for tower acceleration oscillates about 0.07 which corresponds to 93% prediction accuracy. Considering the complexity of the underlying relationships this prediction accuracy is acceptable. One possible reason for the reduced prediction accuracy is that the impact of the rotor on the vibration of tower is less direct than that on the drive train.

Table 3.7 Test results for wind turbine vibration produced by the neural network model

Acceleration	Scenario	Wind Speed	MAE	SD of MAE	MAPE	SD of MAPE
Drive Train Acceleration	Scenario. 1	[3.5m/s - 5m/s)	0.5782	0.9249	0.0184	0.0202
	Scenario. 2	[5m/s - 6m/s)	0.4752	1.4199	0.0191	0.1598
	Scenario. 3	[6m/s - 7m/s)	0.5154	1.3468	0.0133	0.0437
	Scenario. 4	[7m/s - 8m/s)	1.2393	2.0922	0.0246	0.0430
	Scenario. 5	[8m/s - 9m/s)	1.2382	2.2780	0.0195	0.0370
	Scenario. 6	[9m/s - 10m/s	1.5762	3.0296	0.0042	0.3567
	Scenario. 7	[10m/s - 11m/s)	1.8956	3.3790	0.0162	0.4512
	Scenario. 8	[11m/s - 12m/s)	1.7312	2.9588	0.0173	0.0313
	Scenario. 9	[12m/s - 14m/s]	1.2692	2.1304	0.0120	0.5831
Tower Acceleration	Scenario. 1	[3.5m/s - 5m/s)	3.2221	4.8278	0.0955	0.1011
	Scenario. 2	[5m/s - 6m/s)	2.7683	5.6060	0.0709	0.1563
	Scenario. 3	[6m/s - 7m/s)	1.7724	4.2603	0.0410	0.1406
	Scenario. 4	[7m/s - 8m/s)	3.9584	6.4616	0.0882	0.2911
	Scenario. 5	[8m/s - 9m/s)	3.4913	6.2439	0.0545	0.0894
	Scenario. 6	[9m/s - 10m/s	5.2208	11.0250	0.0634	0.0970
	Scenario. 7	[10m/s - 11m/s)	9.5497	25.4213	0.0916	0.1691
	Scenario. 8	[11m/s - 12m/s)	8.4061	16.9336	0.0738	0.1099
	Scenario. 9	[12m/s - 14m/s]	5.9573	9.3430	0.0473	0.0752

The prediction performance of selected scenario, scenario 1 of Turbine 1, for both drive train and tower acceleration has been illustrated in scatter plots in Figure 3.1 to Figure 3.2 where the vertical axis represents the observed values and the horizontal axis represents the predicted ones. Figure 3.1 shows the prediction results of the first 200 points based on the test data for scenarioc1 (Table 3.7) in testing the drive train acceleration. Figure 3.2 illustrates the performance of the first 200 points for scenario 1 (Table 3.7) in testing the tower acceleration. Besides scatter plots, the run-charts, as shown in Figure 3.3 and Figure 3.4, were also included to display not only the prediction accuracy but also the time sequence of first 200 data points for testing both drive train acceleration and tower acceleration. Scatter plots and run-charts that illustrated prediction performance of other scenarios can be obtained in Appendix A.

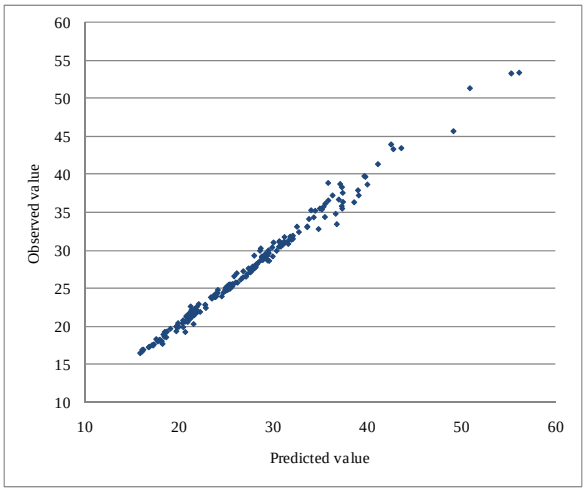

Figure 3.1 Scatter plot of the observed and predicted values of drive train acceleration for the first 200 points of turbine 1 in scenario 1

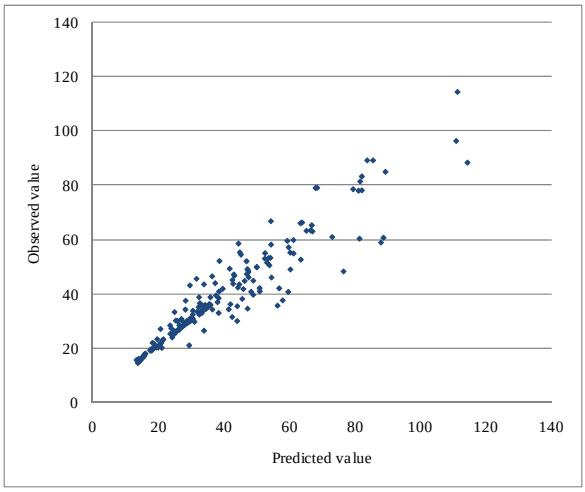

Figure 3.2 Scatter plot of the observed and predicted values of tower acceleration for the first 200 points of turbine 1 in scenario 1

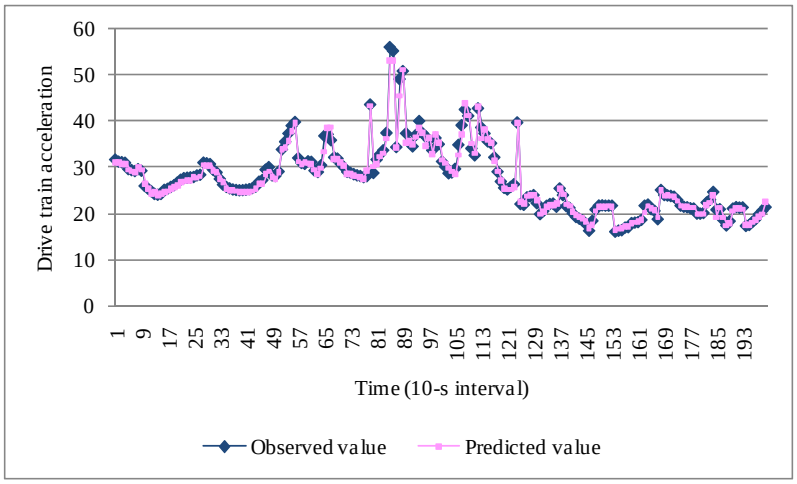

Figure 3.3 Run-chart of the observed and predicted values of drive train acceleration for the first 200 points of turbine 1 in scenario 1

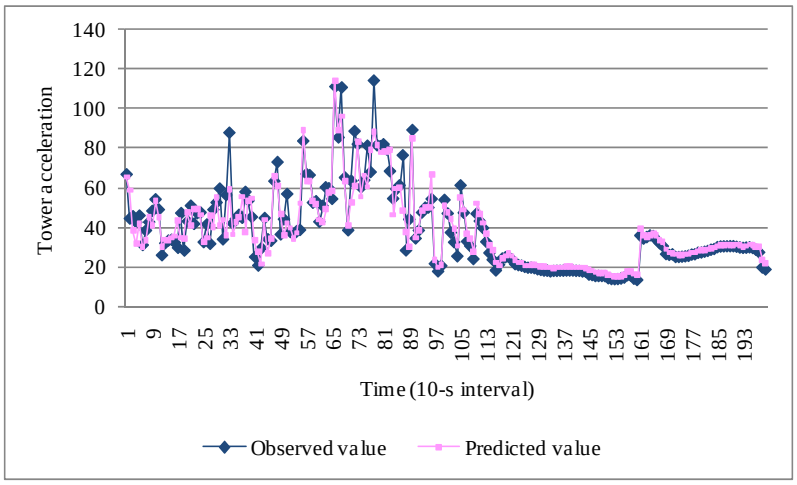

Figure 3.4 Run-chart of the observed and predicted values of tower acceleration for the first 200 points of turbine 1 in scenario 1

Table 3.8 presents test results for predicting the two types of accelerations, the drive train acceleration and tower acceleration, of the models extracted from data set of

Turbine 1 by applying the data set of Turbine 2. In the prediction of the drive train acceleration of Turbine 2, the models maintain their performance. The mean of the MAPE for predicting the drive train acceleration is about 0.0221, which indicates that the mean accuracy of the model is about 97.79%. This result is quite similar to the test results of data set of Turbine 1. In predicting the tower acceleration of Turbine 2, the mean MAPE is about 0.0998, which means that the mean accuracy across all models is about 91%. In this case, although its prediction accuracy drops slightly compared to the previous case (93%), the models are accurate for the type of the complex problem considered in this research. Thus, the results demonstrate that the models are accurate enough to model the relationships between the parameters and the targets (the drive train acceleration and the tower acceleration).

Table 3.8 Test results for wind turbine vibration of data set of turbine 2

Acceleration	Scenarios	Wind Speed	MAE	SD of MAE	MAPE	SD of MAPE
Drive Train Acceleration	Scenario. 1	[3.5m/s - 5m/s)	1.0903	2.9562	0.0240	0.0447
	Scenario. 2	[5m/s - 6m/s)	0.6721	1.5771	0.0171	0.0311
	Scenario. 3	[6m/s - 7m/s)	0.7282	1.5546	0.0158	0.0271
	Scenario. 4	[7m/s - 8m/s)	1.2036	2.1324	0.0208	0.0341
	Scenario. 5	[8m/s - 9m/s)	1.2575	2.5230	0.0175	0.0326
	Scenario. 6	[9m/s - 10m/s	1.7197	2.9600	0.0217	0.0339
	Scenario. 7	[10m/s - 11m/s)	2.3290	3.6028	0.0264	0.0377
	Scenario. 8	[11m/s - 12m/s)	2.6222	3.9620	0.0276	0.0398
	Scenario. 9	[12m/s - 14m/s]	3.0535	4.4006	0.0275	0.0377
Tower Acceleration	Scenario. 1	[3.5m/s - 5m/s)	6.1216	10.4774	0.0985	0.1302
	Scenario. 2	[5m/s - 6m/s)	5.3249	9.3070	0.0896	0.1835
	Scenario. 3	[6m/s - 7m/s)	4.8622	8.6557	0.0784	0.7400
	Scenario. 4	[7m/s - 8m/s)	4.4078	7.1761	0.0971	0.1391
	Scenario. 5	[8m/s - 9m/s)	3.5889	8.4652	0.0687	0.1370
	Scenario. 6	[9m/s - 10m/s	5.7685	8.0605	0.0998	0.0919
	Scenario. 7	[10m/s - 11m/s)	9.2428	12.4625	0.1130	0.1039
	Scenario. 8	[11m/s - 12m/s)	12.7809	12.9038	0.1400	0.1154
	Scenario. 9	[12m/s - 14m/s]	11.9156	11.6100	0.1128	0.1000

The data in scatter plots, Figure 3.5 and Figure 3.6, and run-charts, Figure 3.7 and Figure 3.8, illustrate prediction performance of scenario 1 of Turbine 2. For better visualization of the results, only the first 200 points are depicted in the figures. Each vertical axis represents the observed values and the horizontal the predicted values of the drive train acceleration (Figure 3.1) and the tower acceleration (Figure 3.2). Scatter plots and run-charts of other scenarios were are listed in Appendix B.

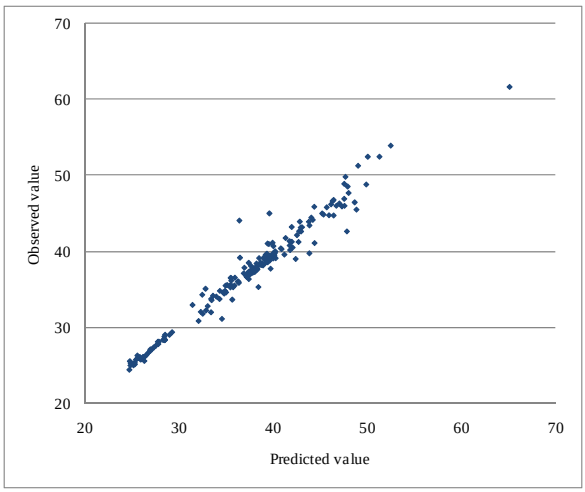

Figure 3.5 Scatter plot of the observed and predicted values of the drive train acceleration for the first 200 points of turbine 2 in scenario 1

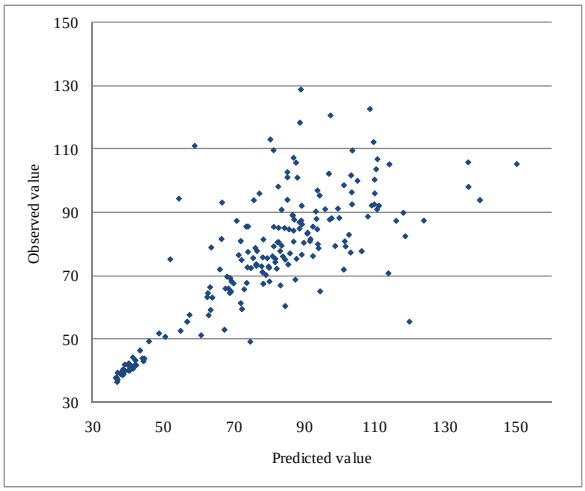

Figure 3.6 Scatter plot of the observed and predicted values of the tower acceleration for the first 200 points of turbine 2 in scenario 1

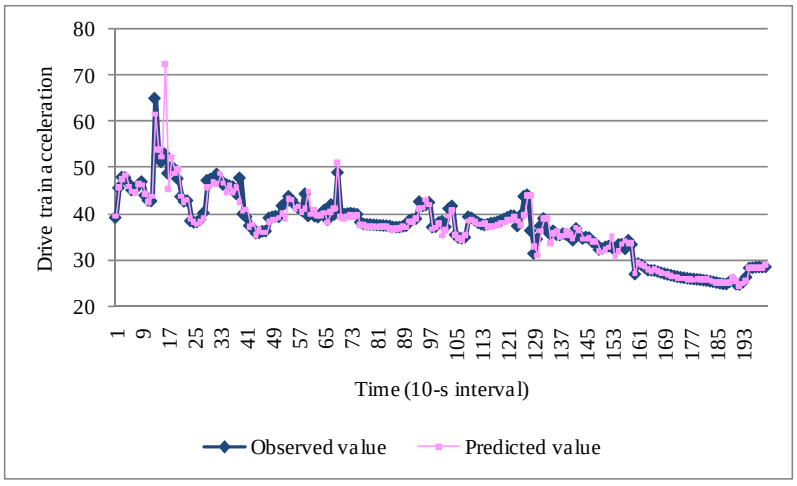

Figure 3.7 Run-chart of the observed and predicted values of the drive train acceleration for the first 200 points of turbine 2 in scenario 1

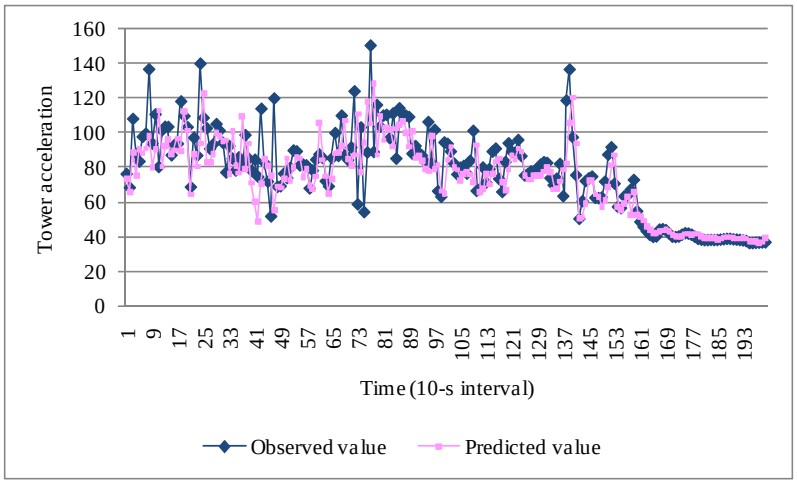

Figure 3.8 Run-chart of the observed and predicted values of the tower acceleration for the first 200 points of turbine 2 in scenario 1

In this study, based on results provided by two tables, Table 3.7 and Table 3.8, the MAPE of the models for predicting both two accelerations indicate that modeling the wind turbine vibration with data-driven models is feasible and the accuracy of prediction is acceptable.

3.6 Summary

This chapter introduced a methodology to model wind turbine vibration based on a data driven perspective. In algorithm selection, five data mining algorithms were compared in model extraction from data sets collected at two randomly selected wind turbines. The models have been extensively tested and the best model, derived by the neural network algorithm, was applied to 18 data sets (scenarios). Performance of all models was evaluated using different metrics (MAE, SD of MAE, MAPE and SD of MAPE). The ultimate goal of this research was to drive an accurate model to predict vibrations of the drive train acceleration and tower acceleration. Such models will play

important role in devising control strategies, like minimizing wind turbine vibrations. Since these models are non-parametric, in general, conventional optimization algorithms cannot be applied to solve them, rather evolutionary algorithms are needed. Such computational intelligence approaches will be introduced in the next chapter.

CHAPTER 4.
OPTIMIZATION OF WIND TURBINE PERFORMANCE WITH DATA DRIVEN MODELS

4.1 Introduction

The interest in renewable energy has increased in recent years due to environmental concerns and growing awareness of the limited supply of fossil fuels. The anticipated increase in the cost of electricity generated from fossil fuels due to carbon taxation has become a catalyst in the quest for clean energy. Wind energy has been the most successfully commercialized among all forms of renewable energy [50]. Research in wind energy has significantly intensified in power generation, energy conversion, wind farm design and so on in the recent years. Optimization has been considered as one critical issue tightly involved in wind energy research areas. Boukhezzar et al. [51] designed a non-linear controller for optimizing the power of the DFIG generator. Abdelli et al. [52] applied a multi-objective genetic algorithm to optimize the efficiency of a small scale turbine.

The goal of this paper is to develop models optimizing wind turbine performance in three objectives, maximization of the power produced by a wind turbine, and reduction of vibrations of the turbine's drive train and tower.

Numerous studies of wind power models have been reported in the literature [51-53]. A passive control method using a tuned mass damper to mitigate vibrations of the blades and tower of a wind turbine was presented in [19]. The research reported in [20] discussed the estimation of aeroelastic damping of operational wind turbine modes based on experiments. The majority of the published research falls into parametric and physics-based models. This paper illustrates non-linear and non-parametric models for optimization of wind power and vibration using a data-driven approach. Such an

approach has been successfully applied to optimize power plants and industrial processes [54].

The focus of this chapter is on vibrations attributed to the control of wind turbines, e.g., control of the generator torque and blade pitch. Two parameters, drive train acceleration and tower acceleration, are selected to represent vibrations of the drive train and tower. Two generalized data-driven models of wind turbine vibrations are developed, one to predict the drive train accelerations and the other to predict the tower accelerations. The power output is also modeled by a similar methodology. Neural network [41, 42, 43] is applied to extract these data-driven models from industrial (wind turbine) data. The three models are then integrated into a multi-objective optimization model [55]. As the models are nonparametric and nonlinear, obtaining analytical form solutions is difficult, and therefore an evolutionary strategy algorithm [56, 57, 58] is used to solve them. Different control preferences lead to numerous control strategies.

The data used in this research was obtained from a large (150MW) wind farm, and its sampling frequency is 0.1 Hz. Since the frequency of wind turbine vibrations is higher than 0.1 Hz, the information loss due to the low (0.1 Hz) frequency of available data has been reflected in the research results. To address the information loss, a 1-min (lower frequency) data set is derived from the 0.1 Hz (10-s) data set. Computational experiments with the two data sets, i.e., 10-s and 1-min, demonstrate a potential for further reduction of turbine vibrations. Due to the limited data frequency, this chapter investigates the potential for vibration reduction by adjusting certain controllable parameters, such as blade pitch angle and generator torque. Industrial implementation of the approach proposed in this paper calls for higher frequency data.

4.2 Modeling wind turbine vibrations and power output

4.2.1 Data description

Two types of data sets, 10-s data and 1-min data of a wind turbine, are used in this research. The 10-s data was collected from a SCADA system, and the 1-min data set was derived by averaging the values of all parameters across each 60-s period from the 10-s data set. The total length of each data set is two months. The SCADA system contains values of more than 120 parameters; however, only certain parameters that could be potentially related to wind turbine vibrations and their power output were selected based on the domain expertise and past studies in wind energy. Tables 4.1 and 4.2 demonstrate the general format of the data sets used in this research.

Table 4.1 Sample data set of 10-s data collected from SCADA system

Time	Torque	…….	Drive Train Acc	Drive Train Acc (t-1)
19/10/08 3:01:10 PM	42.1586	…….	63.2651	61.5034
19/10/08 3:01:20 PM	45.5093	…….	59.9151	63.2651
…….	…….	…….	…….	…….

Table 4.2 Sample 1-min data computed based on the 10-s data

Time	Torque	…….	Drive Train Acc	Drive Train Acc (t-1)
10/19/08 3:01 PM	40.7994	…….	59.7646	59.5475
10/19/08 3:02 PM	36.9941	…….	54.8406	56.1781
…….	…….	…….	…….	…….

The columns in Tables 1 and 2 represent the parameters related to wind turbine vibrations and the power output. All data is time stamped.

4.2.2 Data pre-processing

Data pre-processing is critical to the data mining for correctness and accuracy of the results. Some of the data errors may have been caused by sensor failures, transmission errors, and failures of various subsystems. The errors usually appear as data exceeding physical constraints or missing values. All incorrect data was deleted from the data sets used in this paper.

4.2.3 Wind turbine vibration model

In this chapter, understanding and modeling vibrations of a wind turbine from the operational data collected from the turbine is presented. Two significant vibration sources are considered: vibrations due to the air passing through the wind turbine and vibrations due to the forces originating with the control system that affects the torque and the blade pitch angle. The values of the drive train acceleration recorded by the SCADA system are used to represent the vibration of the drive train of a wind turbine, while the tower vibration is represented by the acceleration measurements from the tower. The parameters used in this section are selected based on data analysis and domain knowledge.

In this research, drive train part acceleration is measured by a sensor installed at the bottom back of a nacelle. Since two identical drive train acceleration values are reported by the SCADA system, an average value of the two is used in this paper. The vibration of the drive train system is expressed in (4.1).

$$y_1(t) = f_1(y_1(t-1), v_1(t), v_1(t-1), x_1(t), x_1(t-1), x_2(t), x_2(t-1)) \quad (4.1)$$

where all parameters are time t dependent, and y_1 represents the drive train vibrations; v_1 is the wind speed, x_1 is the torque, x_2 is the blade pitch angle, and $t-1$ is the previous sampling time period. Parameter selection is mainly based on domain knowledge. Details are presented in Table 8. In addition, the symbol $f_1(\bullet)$ represents model (4.1) derived from the data with a neural network algorithm.

The sensor to measure tower acceleration is located near the connection of a nacelle and a tower. The model of a tower vibration is presented in (4.2).

$$y_2(t) = f_2(y_2(t-1), v_1(t), v_1(t-1), x_1(t), x_1(t-1), x_2(t), x_2(t-1)) \quad (4.2)$$

The parameters of model (4.2) are identical to those in model (4.1) with y_2 representing the tower vibrations. The symbol $f_2(\bullet)$ is used to represent model (4.2) extracted with a neural network.

In models (4.1) and (4.2), the torque value x_1 at time t and blade pitch angle x_2 at time t are considered as controllable parameters used to realize the potential for controlling vibrations of a wind turbine. Wind speed at time t and the past states of all parameters are considered as non-controllable parameters.

4.2.4 Power output model

It is known that the power extracted from the wind is expressed as the nonlinear expression in (4.3).

$$P = \frac{1}{2}\rho\pi R^2 C_p(\lambda, \beta)v^3 \quad (4.3)$$

where the air flow density is represented by ρ, R is the rotor radius, v is the wind speed, and $C_p(\lambda, \beta)$ is the power coefficient function of the blade pitch angle β and the tip-speed ratio λ. Model (4.3) does not exactly match the actual power curve illustrated in Figure 4.1. In this power curve, a given wind speed value is mapped onto a range of power values for a variety of reasons, including sensor errors and faults of various types; for example, a small error in wind speed *v* could result in a large error of the power output due to the cube relationship. To model actual power curves, neural networks, k-NN (k nearest neighbor), and other data-mining algorithms can be used. In this paper, a neural network model $f_3(\bullet)$ is used to estimate power output, and it is expressed in (4.4).

$$y_3(t) = f_3(v_1(t), v_1(t-1), x_1(t), x_1(t-1), x_2(t), x_2(t-1)) \quad (4.4)$$

The notation used here is identical to the notation of model (4.1).

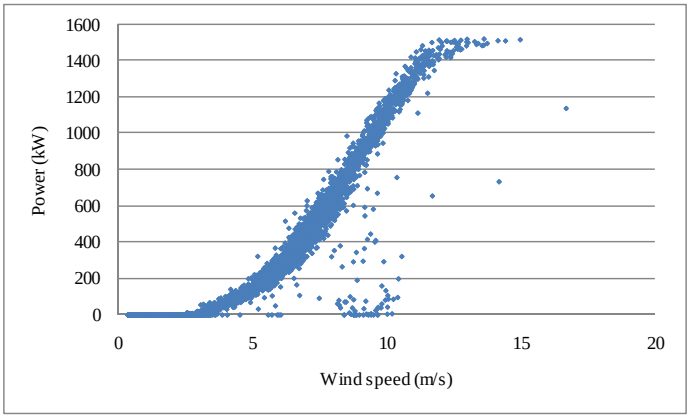

Figure 4.1 Power curve of a 1.5 MW turbine

4.2.5 Validation of the models

The same data denoising procedure introduced in Chapter 3 is applied to filter the noisy data of the drive train acceleration and tower acceleration here. To build data-driven models, the 10-s and 1-min data sets are divided into a training data set (2/3 of all data) and a test data set (1/3) of all data. In the 10-s data set, there are a total of 204894 instances, and in the 1-min data there are a total of 34149 instances. Each training data set is used to train a neural network, while the test data set is used to test the accuracy of data-derived models. Four metrics (4.5) – (4.8) are used to evaluate the quality of models.

$$\text{Mean absolute error (MAE)} = \frac{1}{n}\sum_{i=1}^{n}|\hat{y}_i - y_i| \tag{4.5}$$

$$\text{Standard deviation of MAE} = \sqrt{\frac{1}{n}\sum_{i=1}^{n}(|\hat{y}_i - y_i| - \frac{1}{n}\sum_{i=1}^{n}|\hat{y}_i - y_i|)^2} \tag{4.6}$$

$$\text{Mean absolute percentage error (MAPE)} = \frac{1}{n}\sum_{i=1}^{n}\left(\left|\frac{\hat{y}_i - y_i}{y_i}\right|\right)\times 100\% \quad (4.7)$$

$$\text{Standard deviation of MAPE} = \sqrt{\frac{1}{n}\sum_{i=1}^{n}\left(\left|\frac{\hat{y}_i - y_i}{y_i}\right| - \frac{1}{n}\sum_{i=1}^{n}\left|\frac{\hat{y}_i - y_i}{y_i}\right|\right)^2}\times 100\% \quad (4.8)$$

Table 4.3 presents the test results of three neural network (NN) models extracted from the 10-s data set. The mean value of the drive train acceleration in this data set is 67.24 and the standard deviation (SD) of the drive train acceleration is 36.81. As shown in Table 4.3, the MAE of the drive train acceleration predicted by the NN model is 1.27, the corresponding MAPE is 0.02, which means that the model is 98% accurate. For the tower acceleration, the mean value of the tower acceleration is 72.83 and the SD is 45.40. The MAE in predicting tower acceleration is 4.73 and the SD is 8.92. The MAPE is 0.06, i.e., the model is 94% accurate. Although the MAPE is quite impressive, the SD of MAPE, which equals 0.10, is somewhat large. This indicates that the accuracy of the model predicting tower acceleration is not steady. However, considering the complexity of the tower acceleration itself, this result is acceptable for tower vibration analysis. The mean value of the power generated is 633.83 and the SD is 460.36. The MAE of the model predicting power is 9.86. The corresponding MAPE for the power prediction is 0.03, i.e., the model is 97% accurate.

Table 4.3 Test results of the NN models for 10-s data

Predicted Parameter	MAE	SD of MAE	MAPE	SD of MAPE
Drive train acceleration	1.27	2.52	0.02	0.03
Tower acceleration	4.73	8.92	0.06	0.10
Generated power	9.86	13.78	0.03	0.08

Figures 4.2 to 4.4 illustrate the first 50 predicted and observed values of the 10-s test data set for the three models: drive train acceleration (Figure 4.2), tower acceleration (Figure 4.3), and power (Figure 4.4).

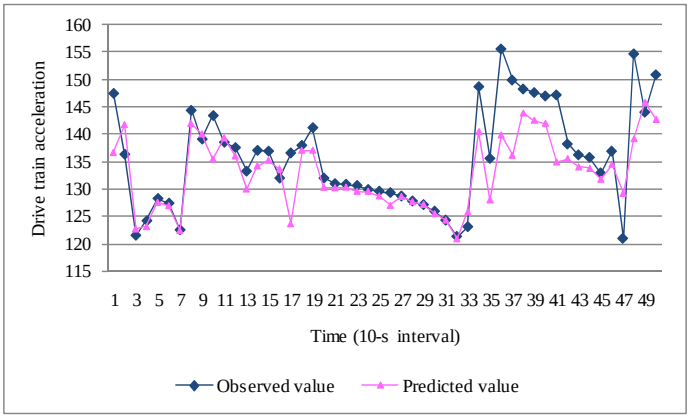

Figure 4.2 The first 50 test points of the drive train acceleration for 10-s data

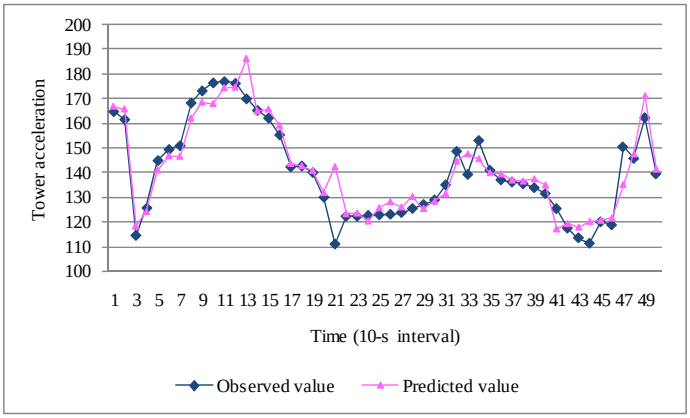

Figure 4.3 The first 50 test points of the tower acceleration for 10-s data

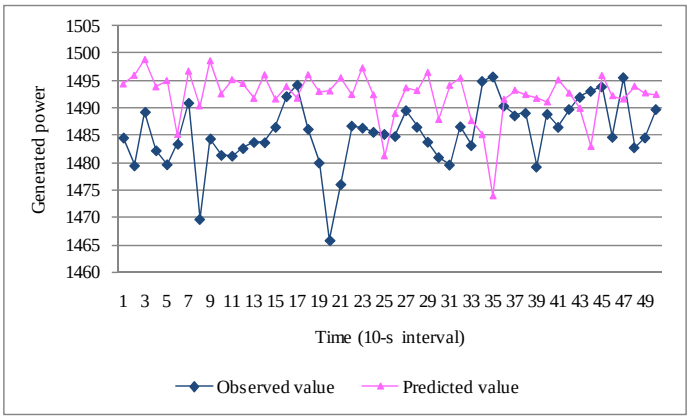

Figure 4.4 The first 50 test points of the power output for 10-s data

The test results for three models extracted from the 1-min data set are included in Table 4.4. The MAE of the drive train acceleration is 0.77, and the MAPE of 0.01 implies a 99% accuracy of the model. For the model to predict the tower acceleration, the MAPE is 0.03, i.e., the model is 97% accurate. The MAPE of the model predicting the generated power is 0.03 (97% model accuracy). Although the model accuracy is impressive, the standard deviation is relatively high. The results indicate that even though the models can quite accurately predict acceleration and power output, some predicted instances could involve a significant error.

Table 4.4 Testing results of the NN models for 1-min data

Predicted Parameter	MAE	SD of MAE	MAPE	SD of MAPE
Drive train acceleration	0.77	1.58	0.01	0.01
Tower acceleration	2.76	7.97	0.03	0.04
Generated power	8.99	13.83	0.03	0.15

Figure 4.5 presents the first 50 points of the observed and predicted values of the drive train accelerations. Figure 4.6 illustrates the first 50 points for the tower acceleration, and Figure 4.7 shows the power prediction results.

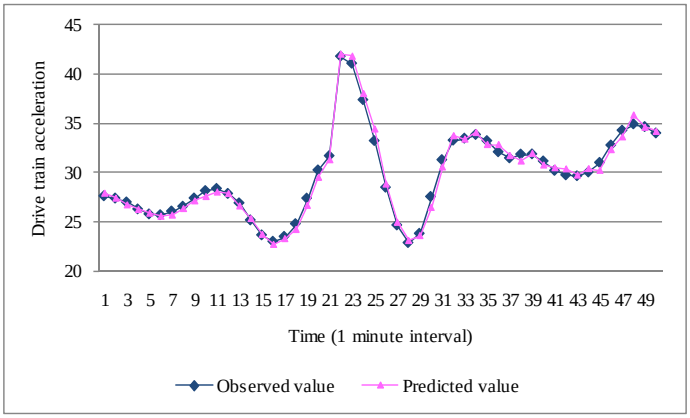

Figure 4.5 The first 50 test points of the drive train accelerations for 1-min data

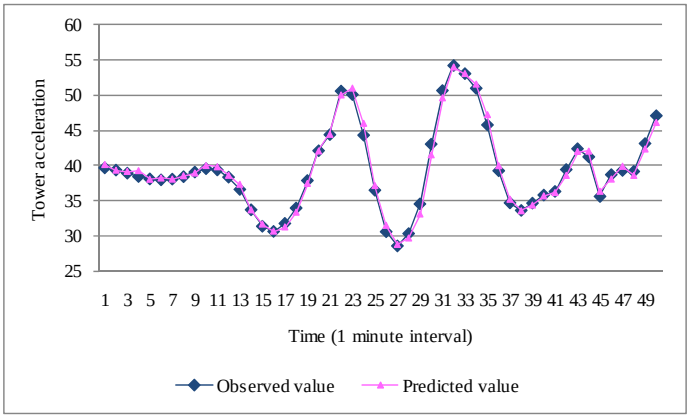

Figure 4.6 The first 50 test points of the tower acceleration for 1-min data

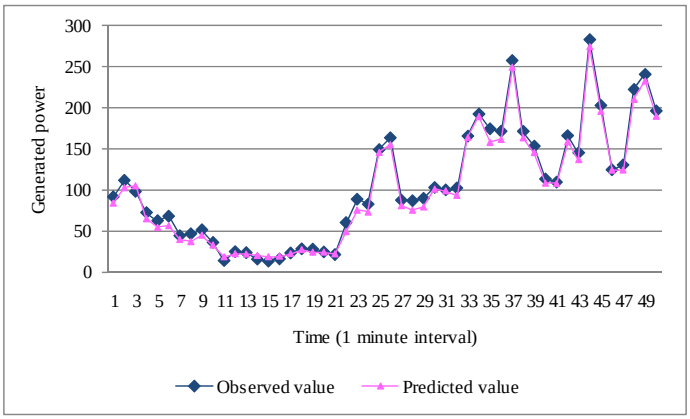

Figure 4.7 The first 50 test points of the power output 1-min data

4.3 Multi-objective optimization model

In modeling vibrations and power output, torque and blade pitch angle are considered as controllable parameters. Parameters such as wind speed and past states of non-controllable parameters serve as inputs to the data-driven models. Both the generator torque and the blade pitch angle impact vibrations of the drive train and the tower.

In the model considered in this paper, the drive train acceleration, the tower acceleration, and the inverse of power output are the three objectives to be minimized. Solutions of this model become control strategies for the wind turbine. This multi-objective minimization model is formulated in (4.9).

$$
\begin{gathered}
\min(Obj_1, Obj_2, Obj_3) \\
subject\ to \\
y_1(t) = f_1(y_1(t-1), v_1(t), v_1(t-1), x_1(t), x_1(t-1), x_2(t), x_2(t-1)) \\
y_2(t) = f_2(y_2(t-1), v_1(t), v_1(t-1), x_1(t), x_1(t-1), x_2(t), x_2(t-1)) \\
y_3(t) = f_3(v_1(t), v_1(t-1), x_1(t), x_1(t-1), x_2(t), x_2(t-1)) \\
\max\{0, \text{currentSettings} - 50\} \le x_1(t) \le \min\{100, \text{currentSettings} + 50\} \\
\max\{-5, \text{currentSettings} - 5\} \le x_2(t) \le \min\{15, \text{currentSettings} + 5\}
\end{gathered}
\tag{4.9}
$$

where $Obj_1 = y_1(t)$, $Obj_2 = y_2(t)$ and $Obj_3 = 1/y_3(t)$ are the three objectives to be minimized.

Table 8 lists all parameters used in model (4.9). The first three parameters in Table 8 represent the three objectives to be minimized. Two controllable parameters, $x_1(t)$ and $x_2(t)$, are the torque and the blade pitch angle at time *t*. The remaining variables on the list in Table 4.5 are the non-controllable parameters at time *t* and *t -1*.

Table 4.5 Description of parameters

Parameter	Description
$y_1(t)$	Average drive train acceleration at time *t*
$y_2(t)$	Tower acceleration at time *t*
$y_3(t)$	Generated power at time *t*
$y_1(t\text{-}1)$	Average drive train acceleration at time *t-1*
$y_2(t\text{-}1)$	Tower acceleration at time *t-1*
$x_1(t)$	Generator torque at time *t*
$x_1(t\text{-}1)$	Generator torque at time *t-1*
$x_2(t)$	Blade pitch angle at time *t*
$x_2(t\text{-}1)$	Blade pitch angle at time *t-1*
$v_1(t)$	Wind speed at time *t*
$v_1(t\text{-}1)$	Wind speed at time *t-1*

The two inequality constraints in model (4.9) impose the upper and lower bounds on the two controllable parameters, i.e., they define the feasible ranges for these parameters. The range for the torque value $x_1(t)$ at time t is between $\max\{0, \text{CurrentSetting} - 50\}$ and $\min\{100, \text{CurrentSetting} + 50\}$. The torque value was normalized in the interval [0, 100%]. The change of the torque value in two consecutive time intervals (10-s or 1-min) is limited to 50% of the maximal torque. This value is determined by considering the turbine specifications and realistic control. Based on manufacturing specifications, the generator torque is limited to 10090 Nm, and the

maximum change rate of the torque is 4500 Nm/s, which corresponds to 45% of the maximum torque per second. The average blade pitch angle $x_2(t)$ at time t is in the range $\max\{-5, \text{CurrentSetting} - 5\}$ and $\min\{15, \text{CurrentSetting} + 5\}$. The values of the blade pitch angle change in the interval [-5°, 15°]. The values were determined based on the maximum and minimum value of the blade pitch angle in the data set considered in this research. The maximum one time (10-s or 1-min) change of the blade pitch angle is fixed at 5°.

Table 4.6 provides correlation coefficients [24] between controllable parameters and the three parameters considered as the model objectives, i.e., drive train acceleration, tower acceleration, and power. Although the relationship between these parameters is nonlinear, the linear relationship expressed with the correlation coefficient provides certain insights into dependencies among them. As illustrated in Table 4.6, torque and blade pitch angle are correlated to a different degree to the three parameters in the model's objective. These correlation coefficients indicate that changing the values of the torque and the blade pitch angle impacts power output, drive train acceleration and tower acceleration simultaneously. Thus, optimization of the trade-off between vibrations and power becomes a challenge.

Table 4.6 Correlation coefficients between turbine parameters

Parameter	Blade pitch angle	Torque	Power produced	Tower acceleration	Drive train acceleration
Blade pitch angle	1.00	0.43	0.44	0.46	0.39
Torque	0.43	1.00	0.99	0.77	0.90
Power produced	0.44	0.99	1.00	0.77	0.90
Tower acceleration	0.46	0.77	0.77	1.00	0.83
Drive train acceleration	0.39	0.90	0.90	0.83	1.00

To recognize the importance of the three model objectives in model (4.9), a weighted sum of these objectives is presented in (4.10). The weights indicate different control preferences.

$$\begin{gathered}
\min\ (w_1 y_1(t) + w_2 y_2(t) + w_3(1/\, y_3(t))) \\
subject\ to \\
y_1(t) = f_1(y_1(t-1), v_1(t), v_1(t-1), x_1(t), x_1(t-1), x_2(t), x_2(t-1)) \\
y_2(t) = f_2(y_2(t-1), v_1(t), v_1(t-1), x_1(t), x_1(t-1), x_2(t), x_2(t-1)) \\
y_3(t) = f_3(v_1(t), v_1(t-1), x_1(t), x_1(t-1), x_2(t), x_2(t-1)) \\
\max\{0, \text{currentSettings} - 50\} \le x_1(t) \le \min\{100, \text{currentSettings} + 50\} \\
\max\{-5, \text{currentSettings} - 5\} \le x_2(t) \le \min\{15, \text{currentSettings} + 5\}
\end{gathered} \tag{4.10}$$

The notation is the same as in model (4.9). The weight assignment to the objectives serves as a mechanism for solution selection among many non-dominant solutions contained in the Pareto set.

4.4 Solving the multi-objective optimization model

4.4.1 Strength Pareto Evolutionary Algorithm

Model (4.9) is learned by a neural network rather than provided in an analytical form. To solve this multi-objective minimization model, evolutionary algorithms are the most natural choice. Here a particular evolutionary strategy (ES) algorithm, the Strength Pareto Evolutionary Algorithm (SPEA) [56], is used to solve model (4.9). The steps of the SPEA are presented next [56].

1. Initialize three sets, parent set (S_p), offspring set (S_o) and elite set (S_e). Generate μ_c individuals (solutions) randomly to conduct the first generation of population.

2. Repeat until the stopping criteria (number of generations, N) is satisfied

2.1. Search the best non-dominated solutions in S_o. Add all non-dominated solutions to S_e.

2.2. Search and delete all dominated solutions in S_e.

2.3. Apply a clustering technique to reduce the size of S_e, if S_e is too large.

2.4. Assign fitness to solutions in S_e and S_o.

2.5. Apply a binary tournament selection to select μ_p parents from the $S_o \bigcup S_e$ to form a population of parents, and store this population in S_p.

2.6. Recombine two parents from S_p to generate a new population.

2.7. Mutate μ_c individuals in S_o by the mutation operator and assign fitness values to them.

3. Check number of generations; if it equals N, then Stop.

The solutions to the multi-objective minimization model (4.9), the torque value and the blade pitch angle, are encoded as vectors. These solutions are treated as individuals defined as (x^i, σ^i) at the i^{th} generation, where $x^i = [x_1^i(t), x_2^i(t)]^T$ and $\sigma^i = [\sigma_1^i, \sigma_2^i]^T$. The elements $x_1^i(t)$ and $x_2^i(t)$ of the solution vector x^i represent the torque and the blade pitch angle at the i^{th} generation. The parameter σ^i represents the vector of standard deviations of the normal distribution with mean equal to zero. In this vector, σ_1^i and σ_2^i are the standard deviations associated with torque and blade pitch angle. Two uniform distributions, $U[0.4, 4]$ and $U[0.2, 2]$, are applied to initialize the values of elements in the vector of standard deviations σ^i.

Recombination of parents in SPEA is expressed in (4.11):

$$\left(\frac{\sum_{j \in S_p} x_j^i}{2}, \frac{\sum_{j \in S_p} \sigma_j^i}{2}\right) \tag{4.11}$$

where S_p denotes the parent set.

Eq. (4.11) implies that every two selected individuals in the parent population are recombined to produce a child. Another key part of SPEA is the mutation operator. Individuals in this research are mutated using the two equations (4.12) and (4.13).

$$\sigma^i = \sigma^i \bullet [e^{N(0,\tau')+N_1(0,\tau)}, e^{N(0,\tau')+N_2(0,\tau)}] \tag{4.12}$$

$$x^i = x^i + N(0, \sigma^i) \tag{4.13}$$

where $N(0, \tau')$ is a normal distribution with the mean equal to 0 and a standard deviation of τ'. $N_k(0, \tau)$ is another normal distribution with the mean 0 and standard deviation equal τ for $k = 1, 2$. In Eq. (13), $N(0, \sigma^i)$ is also a normal distribution but with a mean of 0 and the standard deviation computed from Eq. (12).

4.4.2 Tuning parameters of the evolutionary strategy algorithm

Numerous SPEA parameters need to be determined ahead of computation. In this research, parameters such as τ, τ', tournament size, and the number of parents used in recombination, are arbitrarily selected, as they do not significantly impact computational results. The value of τ is 0.5, τ' = 0.3536, the tournament size is four, and the number of recombined parents is two. Besides these parameters, the value of two other parameters needs to be determined: the selection pressure and the population size. The selection pressure is the ratio of the parent set size divided by the size of the offspring set (see (4.14))

$$\text{SP} = N_p / N_{off} \tag{4.14}$$

where SP = the selection pressure, N_p = the size of parent set (S_p), and N_{off} = the size of offspring set (S_o).

Two experiments are conducted to tune selection pressure and population size of the evolutionary strategy (ES) algorithm applied to 10-s and 1-min data sets. The first experiment was established based on an instance randomly selected from the 10-s data set. The second experiment was implemented based on an instance that has the same time range as the instance of experiment one from the 1-min data set. Table 4.7 presents details of the two instances used in two experiments.

Table 4.7 Two experiments for tuning selection pressure and population size

One instance selected from the 10-s data set of Experiment 1		One instance selected from the 1-min data set of Experiment 2	
Time	10/18/08 10:55:10 PM	Time	10/18/08 10:55 PM
$x_1(t)$	100.93	$x_1(t)$	100.43
$x_1(t\text{-}1)$	100.06	$x_1(t\text{-}1)$	100.58
$v_1(t)$	12.32	$v_1(t)$	14.42
$v_1(t\text{-}1)$	14.11	$v_1(t\text{-}1)$	14.96
$y_3(t)$	1484.47	$y_3(t)$	1481.49
$y_2(t)$	164.64	$y_2(t)$	169.72
$y_2(t\text{-}1)$	167.20	$y_2(t\text{-}1)$	170.22
$x_2(t)$	6.77	$x_2(t)$	10.68
$x_2(t\text{-}1)$	8.21	$x_2(t\text{-}1)$	11.41
$y_1(t)$	147.43	$y_1(t)$	142.68
$y_1(t\text{-}1)$	139.09	$y_1(t\text{-}1)$	144.27

Ten different selection pressures are considered: SP-1 (2parents/2offspring), SP-2 (2parents/4offspring), SP-3 (2parents/6offspring), SP-4 (2parents/8offspring), SP-5 (2parents/10offspring), SP-6 (2parents/12offspring), SP-7 (2parents/14offspring), SP-8 (2parents/16offspring), SP-9 (2parents/18offspring) and SP-10 (2parents/20offspring). Three extreme cases of the selection pressure accelerating the convergence of the ES algorithm are considered, minimizing the drive train acceleration only (Case 1), minimizing the tower acceleration only (Case 2), and minimizing the inverse of power only (Case 3). These three extreme cases can be expressed with three weight assignments used in model (10). In Case 1, $w_1 = 1$, $w_2 = 0$ and $w_3 = 0$; in Case 2, $w_1 = 0$, $w_2 = 1$ and $w_3 = 0$; and in Case 3, $w_1 = 0$, $w_2 = 0$ and $w_3 = 1$.

Table 4.8 illustrates the convergence of the ES algorithm as a function of the selection pressure (SP) for experiment 1. To determine the best SP, the evolutionary strategy algorithm has run for 1500 generations for each selection pressure. As shown in

Table 4.8, the fastest average convergence of the ES algorithm corresponds to SP-9. The ES algorithm converges in Case 1 at the 106th generation. It is observed that the ES algorithm converges at the 180th and 41st generation in Case 2 and Case 3, respectively. The selection pressure SP-9 in Table 4.8 involves the smallest average number of generations at 109.

Table 4.8 Convergence for 10 values of the selection pressure in experiment 1

Selection Pressure	Case 1 Convergence Speed	Case 2 Convergence Speed	Case 3 Convergence Speed	Average Convergence Speed
SP-1 (2parents/2offspring)	968	1420	163	850.33
SP-2 (2parents/4offspring)	637	1170	478	761.67
SP-3 (2parents/6offspring)	97	974	96	389.00
SP-4 (2parents/8offspring)	97	974	96	389.00
SP-5 (2parents/10offspring)	134	419	59	204.00
SP-6 (2parents/12offspring)	108	736	60	301.33
SP-7 (2parents/14offspring)	110	277	35	140.67
SP-8 (2parents/16offspring)	87	214	47	116.00
SP-9 (2parents/18offspring)	106	180	41	109.00
SP-10 (2parents/20offspring)	171	306	15	164.00

Table 4.9 illustrates the convergence for different values of the selection pressure in experiment 2 with the best convergence attained for SP-10. The ES algorithm in Case 1 and Case 2 converges at the 36th generation and in Case 3 at the 55th generation.

Table 4.9 Convergence for 10 values of the selection pressure in experiment 2

Selection Pressure	Case 1 Convergence Speed	Case 2 Convergence Speed	Case 3 Convergence Speed	Average Convergence Speed
SP-1 (2parents/2offspring)	190	190	253	211.00
SP-2 (2parents/4offspring)	466	466	31	321.00
SP-3 (2parents/6offspring)	258	258	178	231.33
SP-4 (2parents/8offspring)	35	35	80	50.00
SP-5 (2parents/10offspring)	99	99	52	83.33
SP-6 (2parents/12offspring)	292	292	48	210.67
SP-7 (2parents/14offspring)	149	149	28	108.67
SP-8 (2parents/16offspring)	83	83	41	69.00
SP-9 (2parents/18offspring)	15	15	118	49.33
SP-10 (2parents/20offspring)	36	36	55	42.33

In addition to the analysis of the selection pressure, two population sizes for each experiment are evaluated, where one of them is five times larger than the base population. For example, the two populations in experiment 1 are denoted as PS1 (2 parents/18 offspring) and PS2 (10 parents/90 offspring). Larger population sizes are not considered here due to the excessive computational cost of the ES algorithm.

Table 4.10 illustrates the convergence of the ES algorithm for two population sizes of experiment 1. As shown in Table 4.10, the fastest convergence is attained for population size PS2 with 10 parents and 90 offspring. The minimum inverse of power (Case 3) is attained at the 1st generation. The latter is due to the fact that the maximum torque value was included in the initial solution. In Case 1 and Case 2, the ES algorithm converges at the 18^{th} and 51^{st} generation. In this experiment, the average number of generations was much lower than for the case with a population size of 2 parents and 18 offspring (see Table 4.7).

Table 4.10 Convergence of the ES algorithm for two populations of experiment 1

Population Size	Case 1 Convergence Speed	Case 2 Convergence Speed	Case 3 Convergence Speed	Average Convergence Speed
PS1(2parents/18 offspring)	106	180	41	109.00
PS2(10parents/90 offspring)	18	51	1	23.33

Table 4.11 shows that the population with 2 parents and 20 offspring leads to the best performance in experiment 2. For this population size, the ES algorithm converges at the 36^{th} generation in Case 1. It also converges at the 36^{th} generation in Case 2, and in Case 3 at the 55^{th} generation.

Table 4.11 Convergence of the ES algorithm for two populations of experiment 2

Population Size	Case 1 Convergence Speed	Case 2 Convergence Speed	Case 3 Convergence Speed	Average Convergence Speed
PS1(2parents/20 offspring)	36	36	55	42.33
PS2(10parents/100 offspring)	49	49	137	78.33

4.5 Computational results

Three types of computational results will be discussed in this section. First, the results of a single-point optimization based on the 10-s data set are introduced. Then, the optimization results over a period of 11-min (multi-point) are presented for three extreme cases, which are defined later in this section. Finally, a comparison between the optimization for the 10-s data set and 1-min data set is discussed to demonstrate the impact on mitigating wind turbine vibrations over a 10-min period.

4.5.1 Single-point optimization

Optimizing a trade-off between wind turbine vibrations and the power output produces a set of non-dominant solutions. An instance of the 10-s data set shown in Table 10 is selected to compute the solution set. Table 4.12 presents a partial solution set for this instance. As presented in Table 4.7, the original average drive train acceleration is 147.43, the original tower acceleration is 164.64 and the original generated power is 1484.47. Each solution in Table 4.12 represents different settings of torque value (TV) and blade pitch angle (BPA). For example, Solution 4 in Table 4.12 shows that for the torque value (TV) of 67.6 and blade pitch angle (BPA) at 15, the average drive train acceleration is reduced from 147.43 to 136.71, and the tower acceleration could be reduced from 164.64 to 120.34. However, the turbine generated power is reduced from

1484.47 to 1031.21. Under this control strategy, the respective gains of the drive train acceleration and the tower acceleration are 7.27% and 26.90%, respectively. However, the reduced vibrations also reduced the power output by -30.53%. Solution 7 illustrates a modest gain in tower accelerations. As presented in Table 4.12, the tower accelerations are reduced from 164.64 to 119.41, i.e., the gain is 27.48%. Simultaneously, the drive train acceleration is reduced from 147.43 to 136.98, and the turbine generated power is reduced from 1484.47 to 1005.11. The respective gains are 7.09% and -32.29%.

Table 4.12 Partial solution set generated by the evolutionary strategy algorithm

Solution No.	Solution ($x_1(t)$, $x_2(t)$)	$y_1(t)$	Gain of $y_1(t)$	$y_2(t)$	Gain of $y_2(t)$	$y_3(t)$	Gain of $y_3(t)$
1	(90.0, 8.81)	136.86	7.17%	160.61	2.45%	1460.96	-1.58%
2	(90.0, 7.34)	136.85	7.18%	164.47	0.10%	1460.80	-1.59%
3	(63.9, 15.00)	136.96	7.10%	119.42	27.47%	1007.14	-32.16%
4	(67.6, 15.00)	136.71	7.27%	120.34	26.90%	1031.21	-30.53%
5	(50.9, -3.23)	122.57	16.86%	356.37	-116.45 %	785.72	-47.07%
6	(90.0, 8.09)	136.88	7.15%	162.46	1.33%	1462.77	-1.46%
7	(63.4, 15.00)	136.98	7.09%	119.41	27.48%	1005.11	-32.29%

Figure 4.8 shows the non-dominated solutions of the elite set in a three-dimensional space. The vertical axis represents tower acceleration. One horizontal axis represents the drive train acceleration and the other power output.

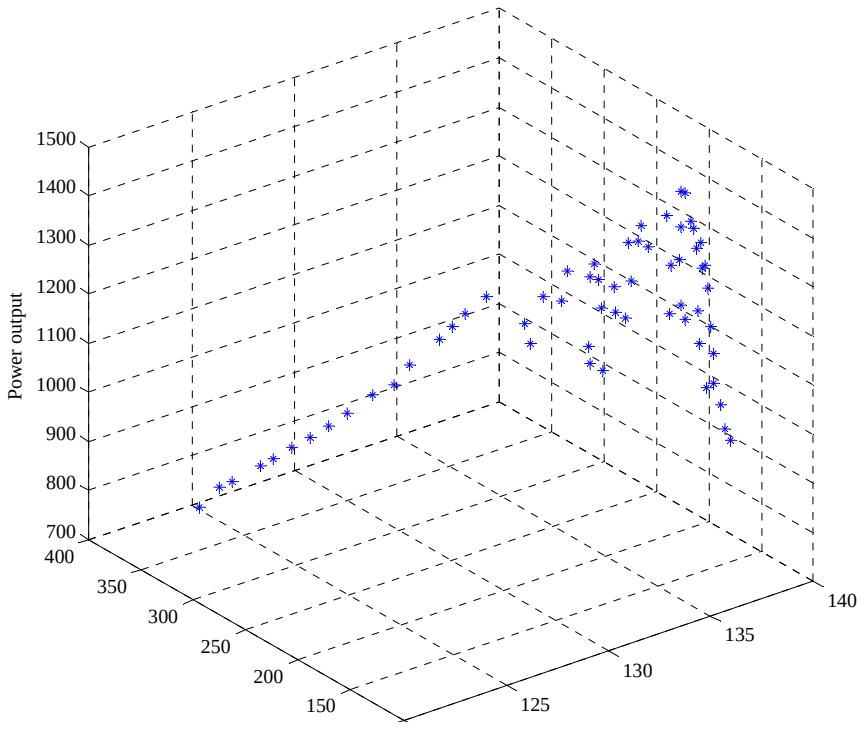

Figure 4.8 Solution of the elite set in a 3-dimensional space

4.5.2 Multi-point optimization

The results presented in Table 4.12 involved one instance only. In this section, multi-point optimization will be introduced, and the same three cases discussed in Section 4.2 are considered. The data from 10/19/08 2:43:00 AM to 10/19/08 2:54:00 AM (a total of 11 minutes of 10-s data) is used in this study. Optimization results for three cases are presented.

Figure 4.9 illustrates the optimization results of Case 1. The corresponding control strategies are illustrated in Figures 4.10 and 4.11. Figure 4.10 shows the original and computed torque. Figure 4.11 illustrates the original and the computed blade pitch angle. The mean reduction of the drive train acceleration over the 11-min time period is

shown in Table 4.13. The mean of the drive train acceleration has been reduced from 131.67 to 119.67 (a 9.16% gain).

Table 4.13 Gains in vibration reductions of the drive train for Case 1

Case 1 (Minimize $y_1(t)$)	Minimum value (mean)	Original value (mean)	Gain (mean)
Average drive train acceleration	119.61	131.67	9.16%

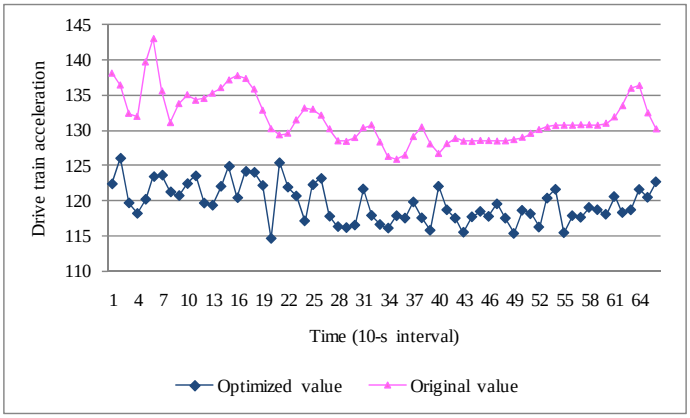

Figure 4.9 The optimized and original drive train acceleration of Case 1 for 10-s data

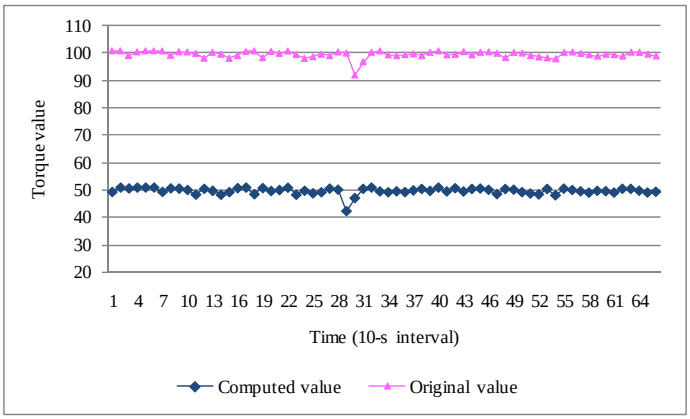

Figure 4.10 The computed and original torque value of Case 1 for 10-s data

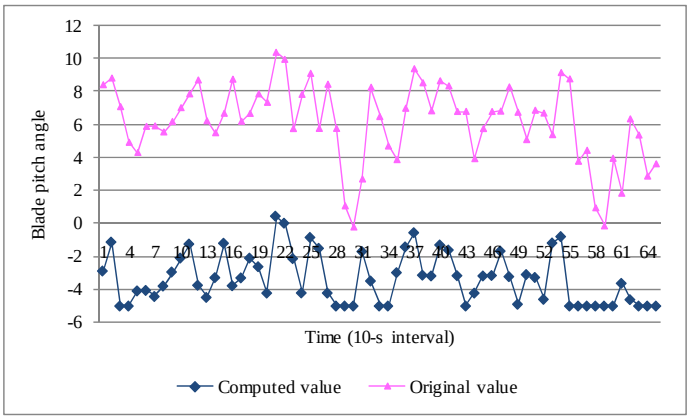

Figure 4.11 The computed and original average blade pitch angle of Case 1 for 10-s data

Figure 4.12 presents the results of Case 2. Figure 4.13 illustrates the computed torque and the original torque. Figure 4.14 shows the computed blade pitch angle (controls) and the original blade pitch angle. In controlling the tower vibrations, the value of torque and blade pitch angle should both be decreased at the same time. Table 4.14 presents the mean gain of reduced tower accelerations over the 11-min period. The mean

value of minimum tower acceleration is 86.38. The mean of the original tower acceleration is 127.47. The tower acceleration has been reduced by 32.23%.

Table 4.14 Gain in reduction tower vibrations for Case 2

Case 2 (Minimize $y_2(t)$)	Minimum value (mean)	Original value (mean)	Gain (mean)
Tower acceleration	86.38	127.47	32.23%

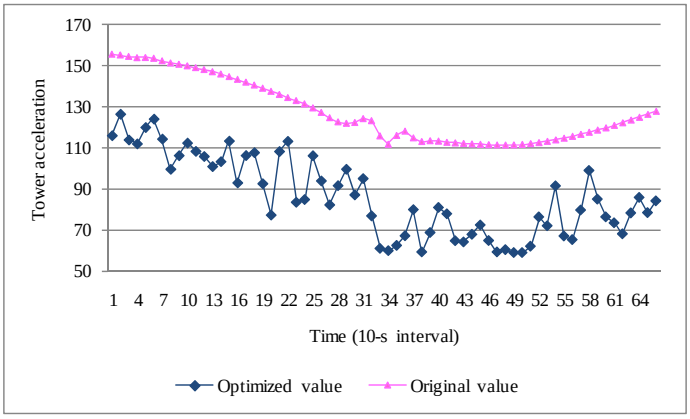

Figure 4.12 The optimized and original tower acceleration of Case 2 for 10-s data

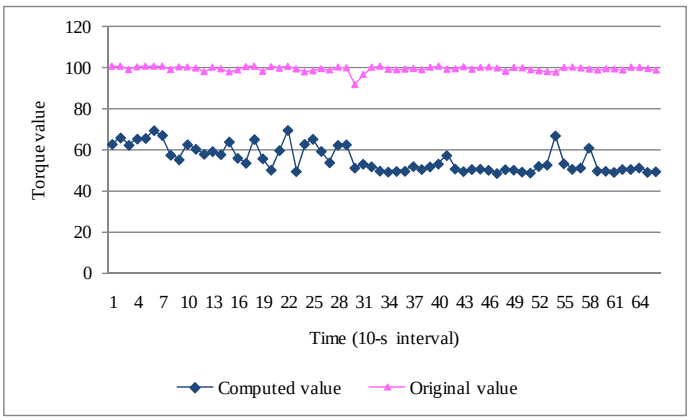

Figure 4.13 The computed and original torque value of Case 2 for 10-s data

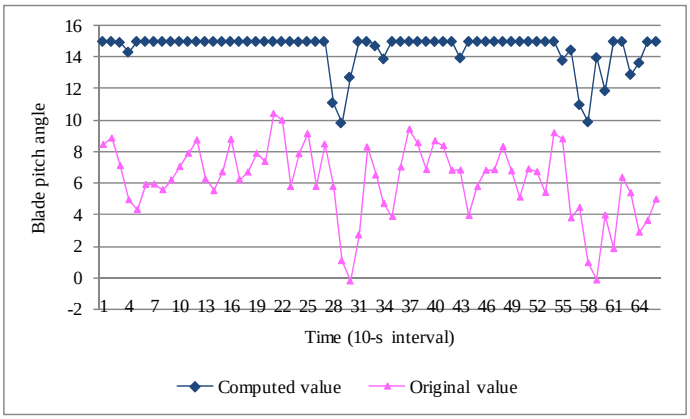

Figure 4.14 The computed and original blade pitch angle of Case 2 for 10-s data

Figure 4.15 shows the optimization results for Case 3 over the 11-min period. The original and computed values of the torque and the blade pitch angle are shown in Figure 4.15 and Figure 4.16, respectively. In this case, the simulation results indicate that to obtain the maximum power output does not necessarily require a maximum torque value but an increase of the mean blade pitch angle. Table 4.15 shows a mean gain of 1.05% in maximizing power output. The average of the maximized power output shown in Table 4.15 is 1498.02, and the mean original power output is 1482.42.

Table 4.15 Gains in power output for control strategy of Case 3

Case 3 (Maximize $y_3(t)$)	Optimized value (mean)	Original value (mean)	Gain (mean)
Power output	1498.02	1482.42	1.05%

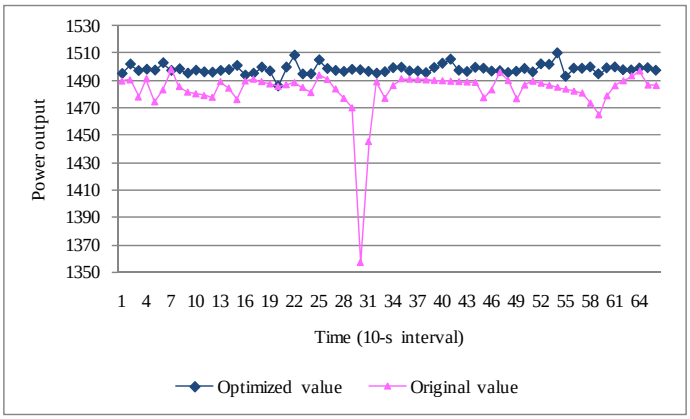

Figure 4.15 The optimized and original power output of Case 3 for 10-s data

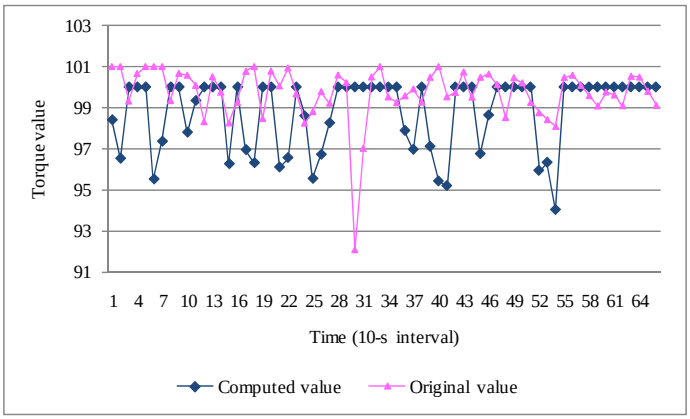

Figure 4.16 The computed and original torque value of Case 3 for 10-s data

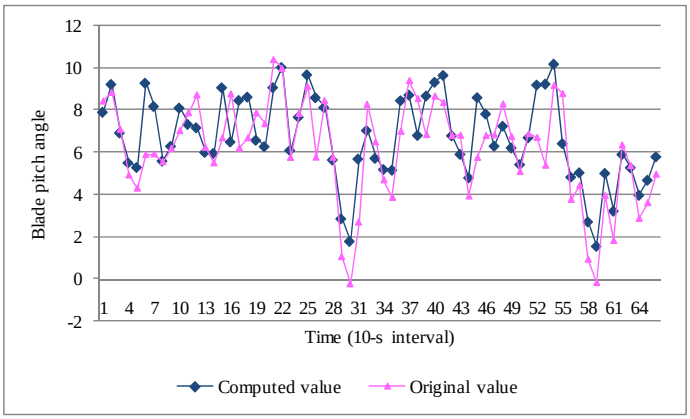

Figure 4.17 The computed and original mean blade pitch angle of Case 3 for 10-s data

In this section, only three sets of weight assignments for the multi-objective optimization model were considered. Methods for optimal generation of weights need to be considered in the future.

4.5.3 Analysis of computational results

In this section, computational experience with 10-s and 1-min data sets is presented. The information loss due to the reduced data sampling frequency is addressed. The results (all mean values) included in Table 4.16 summarize the gains in vibration reduction due to increased data sampling frequency by considering three cases for two types of data sets. Ten minutes worth of 10-s data (from 10/19/2008 2:43:00 AM to 10/19/2008 2:52:50 AM) was selected, and the mean gains are compared to the results obtained of the same 1-min data. Table 4.16 illustrates that the gain in reduction of the drive train vibration based on the model extracted from 10-s data is 9.10%. This gain is larger than the one for the model extracted from the 1-min data set (5.87%). For Case 2, shown in Table 4.16, the mean reduction of the tower acceleration for the 10-s data set is 31.76%, and the mean gain for the 1-min data set is 18.46%. Even though in Case 3 the

gain of the power output for the 10-s data set is larger than the gain of the power for the 1-min data set, it is not as significant as the gain in reducing vibrations. This is due to the different characteristics of the power output and vibration in high frequency, as well as the bounded wind turbine power, here at 1.5 MW. These results indicate that using the current data frequency (0.1Hz) could limit even larger gains in vibrations. Using higher frequency data would likely unleash additional gains in vibrations reduction. The accelerometer and the SCADA system available for this research are typical of the present industrial standard and did not offer higher frequency vibration data.

Table 4.16 Comparison of computational results
for 10-s data set and 1-min data set over 10 min horizon

Mean Value			
Minimize Drive Train Acceleration	Optimized Drive Train Acceleration	Original Drive Train Acceleration	Gain
10-s data set	119.53	131.49	9.10%
1-min data set	124.06	131.79	5.87%
Minimize Tower Acceleration	Optimized Tower Acceleration	Original Tower Acceleration	Gain
10-s data set	87.22	127.82	31.76%
1-min data set	106.26	130.32	18.46%
Maximize Power Output	Optimized Power Output	Original Power Output	Gain
10-s data set	1497.99	1481.72	1.10%
1-min data set	1497.79	1482.57	1.03%

4.6 Summary

In this chapter a multi-objective optimization model involving wind turbine power output, vibration of drive train, and vibration of tower was studied. A data-driven approach for model development was introduced. The drive train vibration and tower

acceleration were represented with accelerations of the drive train and the tower. Models developed for prediction of vibrations and the power produced by the turbine were trained by Neural Network and their accuracies were tested. Although the power output was considered as an objective, its negative relationship with other two objectives indicate that it also served as a bound constraining the mitigation aimed at curtailing drive train vibration and tower vibration.

Industrial data sets used in the study were collected by a SCADA system. The original data set was sampled at 10-s intervals (0.1 Hz frequency). Although the research showed that the data collected by the industry-accepted frequency could not be sufficient to fully mitigate turbine vibrations, the methodology presented in this paper could be used once suitable data becomes available. Bounded by the data availability, a 1-min data set was derived by averaging instances in the original 10-s data set to present effect of information loss in modeling and optimization. Both data sets were used to model drive train vibration, tower vibration and the power output of a wind turbine. The prediction accuracy of the derived models was tested with independent data sets. Four metrics, MAE, SD of MAE, MAPE and SD of MAPE, all defined in the paper, were introduced to evaluate the performance of data-driven models. Comparative study of computational experiments demonstrated that the potential to reduce vibration of the drive train and tower by optimized control.

The multi-objective optimization model was solved with an evolutionary strategy algorithm. The impact of selection pressure and population size on the efficiency of the evolutionary strategy algorithm was studied. The optimization results generated based on three weight assignment cases presented the potential gains of vibration mitigation and power maximization by adjusting two controllable variables, the generator torque and the blade pitch angle. The computational results demonstrated that the gains in reduced wind turbine vibrations and increased power output were larger for the 10-s data sets than those

for the 1-min data sets. All 1-min data sets were obtained by averaging the corresponding 10-s data.

The objective of this chapter, building accurate data-driven models to study the impact of turbine control on their vibrations and power output and demonstrating the optimization results of wind turbine performance, was accomplished.

CHAPTER 5

CONCLUSION

A data-driven methodology to analyze wind turbine vibrations was introduced. It included analysis of wind turbine vibration data, building wind turbine vibration models, and investigating optimization of wind turbine performance by considering power generation and vibrations. The research reported in the Thesis shed light on a new perspective of reducing wind turbine vibrations. Chapter 2 introduced the data analysis of wind turbine vibration from two different angles, time domain and frequency domain. In the time domain analysis, data set was decomposed to three partitions according to the wind speed values. This data decomposition strategy provided a way to isolate the turbine vibrations attributed to both the drive train and the tower from the impact of other factors such as the wind itself, malfunctions of mechanical systems (e.g., shaft misalignments), and so on. Importance analysis of boosting tree algorithm, Global sensitivity analysis of Neural Network algorithm and Correlation Coefficient analysis were applied to investigate turbine parameters that could potentially impact wind turbine vibrations. The frequency domain analysis provided a different angle of investigating turbine vibrations. Fourier analysis transforms data from time domain to frequency domain.

In Chapter 3, models to predict vibration of drive train and tower of wind turbine were studied. Wavelet analysis was introduced to smooth the value of drive train and tower acceleration as accelerometers were very sensitive to noise. Benefits of data denoising were discussed by comparing models based on original data and denoised data. Five data mining algorithms, Neural Network, Support Vector Machine, Standard Classification and Regression Tree, Boosting tree for regression and Random Forests for regression, were used to build models for drive train and tower vibrations. Data set were decomposed according to narrower range of wind speeds to further isolate vibration contributed by wind turbine control.

In Chapter 4 optimization of wind turbine performance was studied. A multi-objective optimization model for maximizing power generation and reducing turbine vibrations was presented. Models for predicting generated power, drive train acceleration and tower acceleration were constructed by a Neural Network algorithm. An evolutionary strategy algorithm was employed to solve the overall model. Gains of power maximization and vibration mitigation under different weight assignments for objectives are presented.

One of the challenges for future research is to develop schemes for selection of Pareto optimal solutions. Adaptive control of wind turbine by considering the tradeoff between supply and demand of electricity is another avenue of research. In management of wind farm, both power production and maintenance cost are essential to managers. Operation of wind turbine in full capacity is not always a necessary and wise choice since abusing of system can lead to high maintenance cost due to, in part, frequent replacement of wind turbine components. Predictive control for wind turbine vibrations can be also another interesting topic for further research. The motivation of developing predictive model for wind turbine vibrations is providing suggested control settings to improve the manipulation of wind turbine.

APPENDIX A

FIGURES ILLUSTRATING PREDICTION PERFORMANCE OF TURBINE 1

Scenario 2

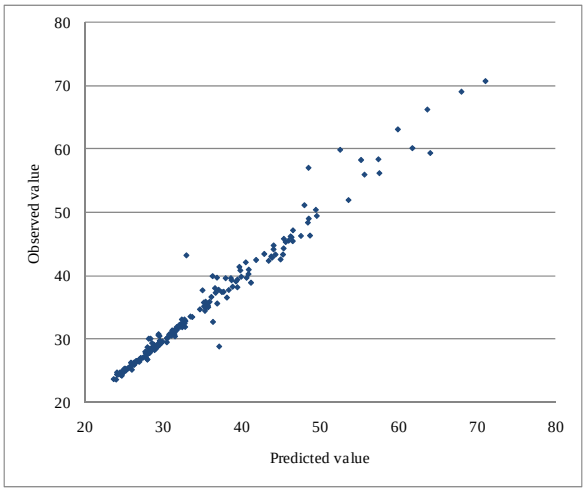

Figure A.1 Scatter plot of the observed and predicted values of drive train acceleration for the first 200 points of Turbine 1 in Scenario 2

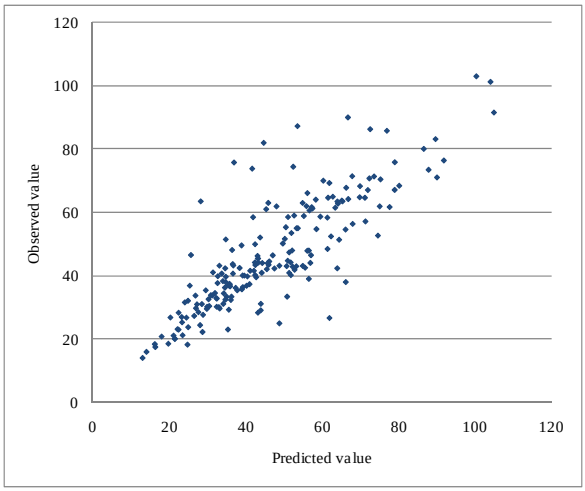

Figure A.2 Scatter plot of the observed and predicted values of tower acceleration for the first 200 points of Turbine 1 in Scenario 2

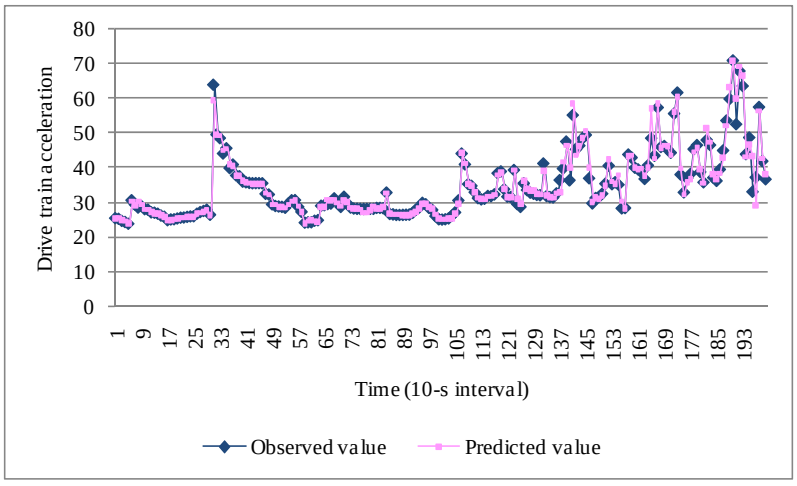

Figure A.3 Run-chart of the observed and predicted values of drive train acceleration for the first 200 points of Turbine 1 in Scenario 2

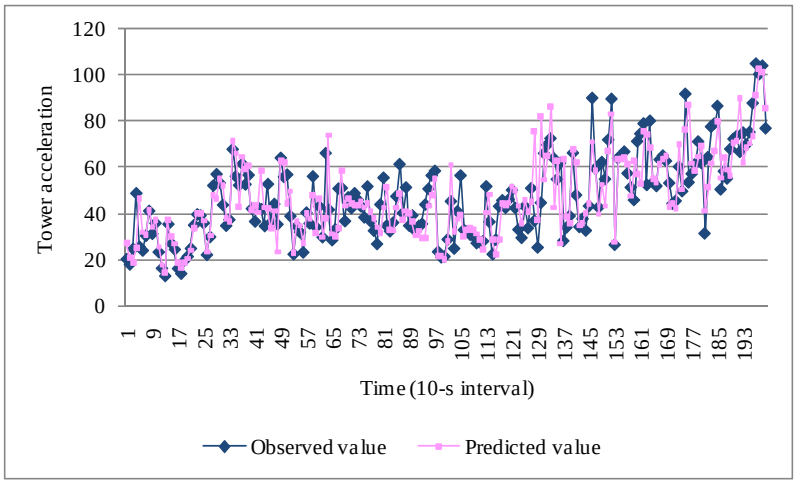

Figure A.4 Run-chart of the observed and predicted values of tower acceleration for the first 200 points of Turbine 1 in Scenario 2

Scenario 3

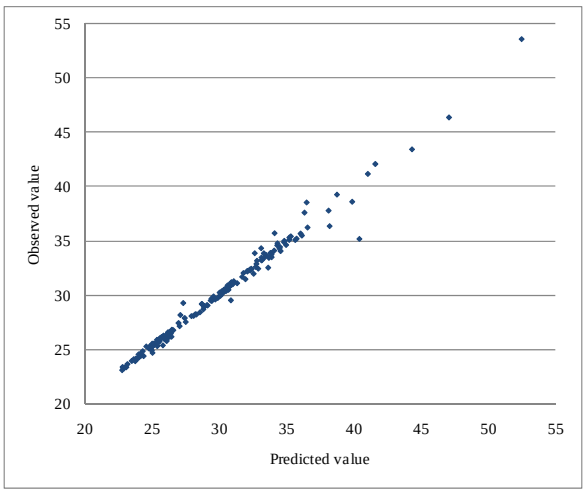

Figure A.5 Scatter plot of the observed and predicted values of drive train acceleration for the first 200 points of Turbine 1 in Scenario 3

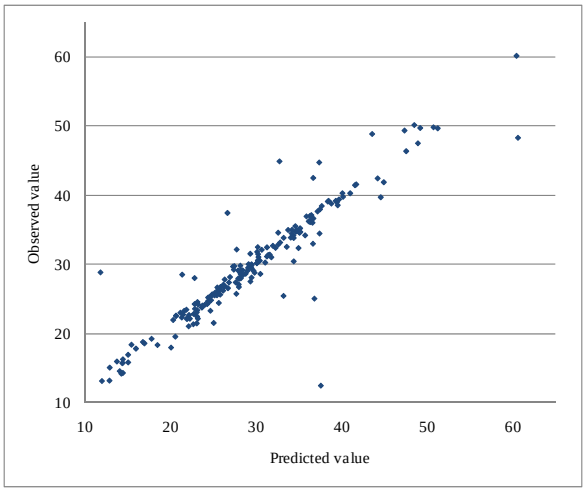

Figure A.6 Scatter plot of the observed and predicted values of tower acceleration for the first 200 points of Turbine 1 in Scenario 3

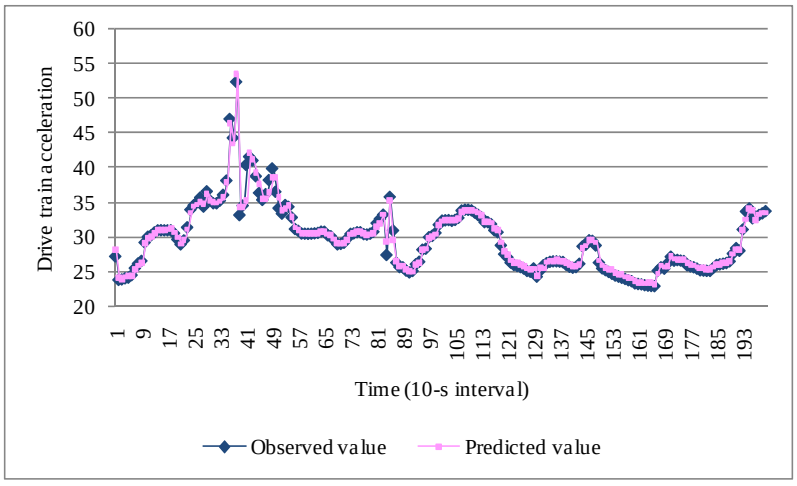

Figure A.7 Run-chart of the observed and predicted values of drive train acceleration for the first 200 points of Turbine 1 in Scenario 3

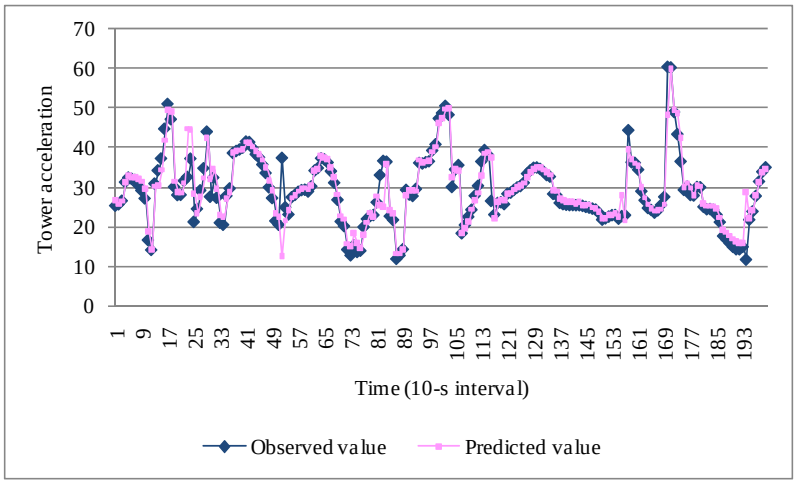

Figure A.8 Run-chart of the observed and predicted values of tower acceleration for the first 200 points of Turbine 1 in Scenario 3

Scenario 4

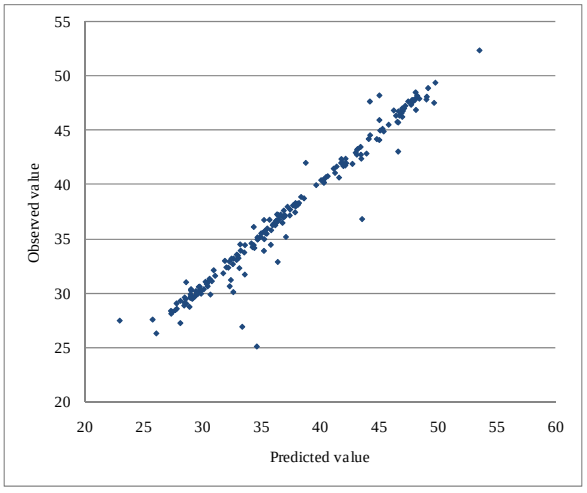

Figure A.9 Scatter plot of the observed and predicted values of drive train acceleration for the first 200 points of Turbine 1 in Scenario 4

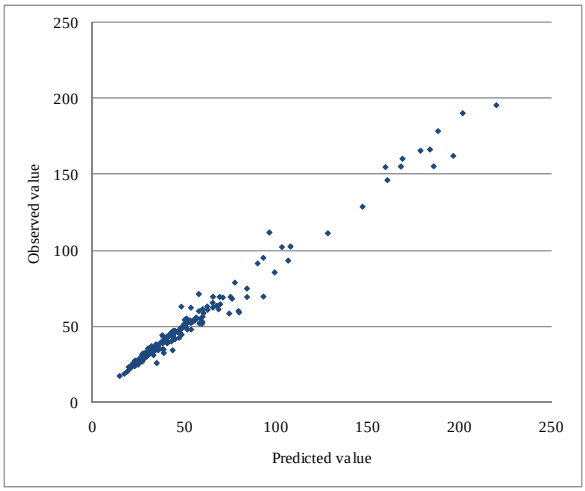

Figure A.10 Scatter plot of the observed and predicted values of tower acceleration for the first 200 points of Turbine 1 in Scenario 4

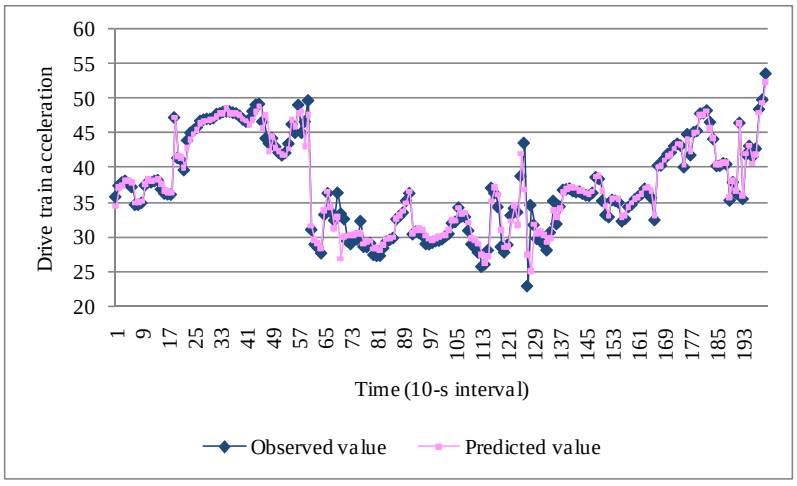

Figure A.11 Run-chart of the observed and predicted values of drive train acceleration for the first 200 points of Turbine 1 in Scenario 4

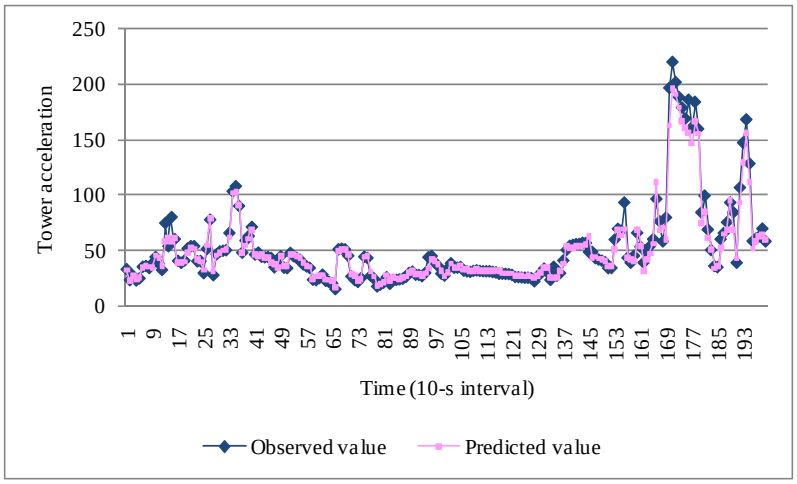

Figure A.12 Run-chart of the observed and predicted values of tower acceleration for the first 200 points of Turbine 1 in Scenario 4

Scenario 5

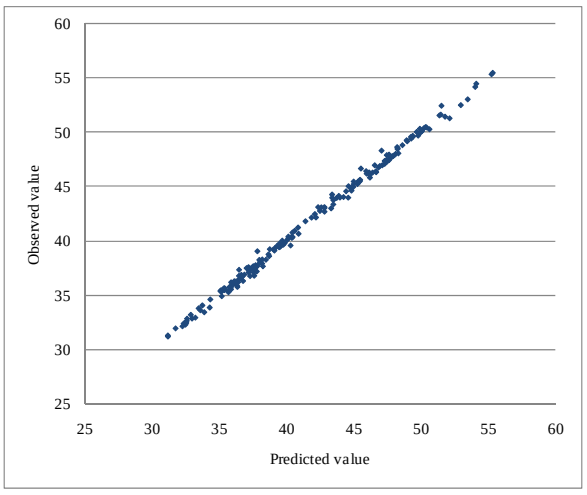

Figure A.13 Scatter plot of the observed and predicted values of drive train acceleration for the first 200 points of Turbine 1 in Scenario 5

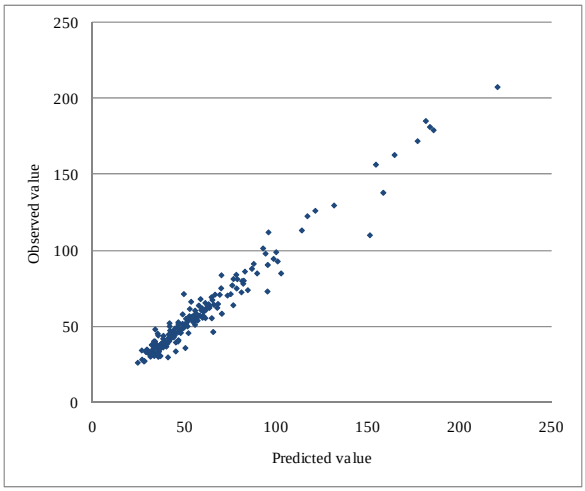

Figure A.14 Scatter plot of the observed and predicted values of tower acceleration for the first 200 points of Turbine 1 in Scenario 5

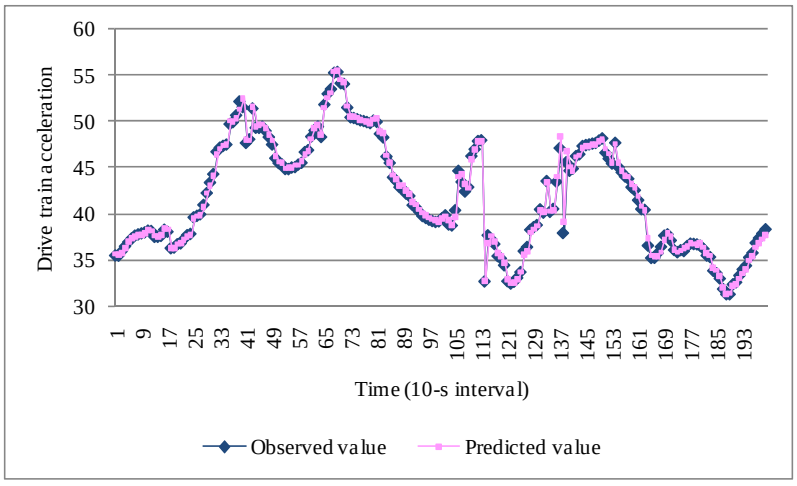

Figure A.15 Run-chart of the observed and predicted values of drive train acceleration for the first 200 points of Turbine 1 in Scenario 5

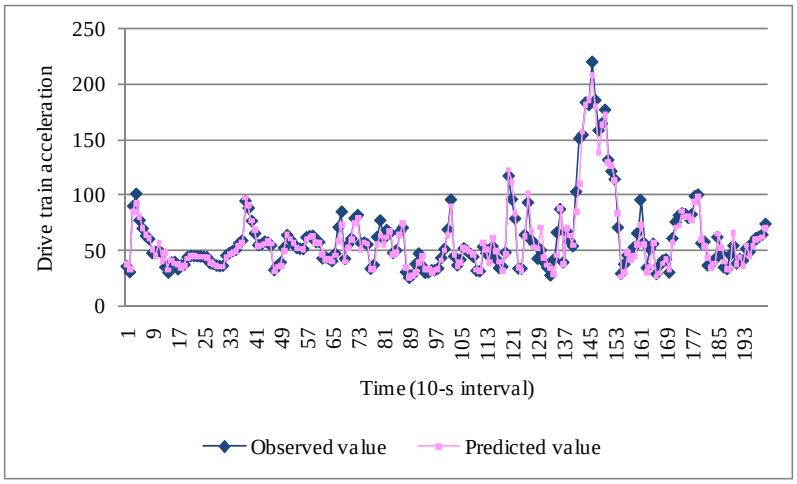

Figure A.16 Run-chart of the observed and predicted values of tower acceleration for the first 200 points of Turbine 1 in Scenario 5

Scenario 6

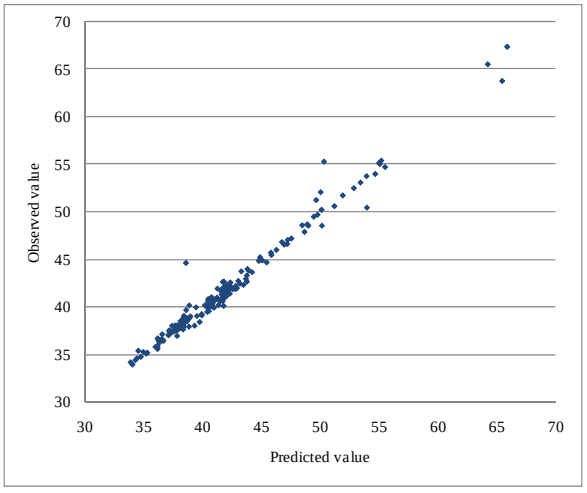

Figure A.17 Scatter plot of the observed and predicted values of drive train acceleration for the first 200 points of Turbine 1 in Scenario 6

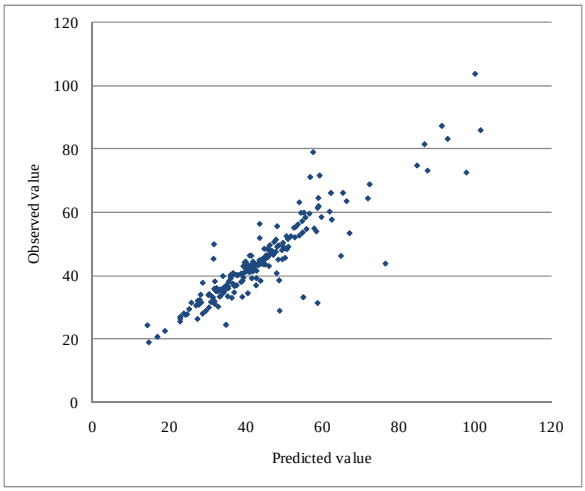

Figure A.18 Scatter plot of the observed and predicted values of tower acceleration for the first 200 points of Turbine 1 in Scenario 6

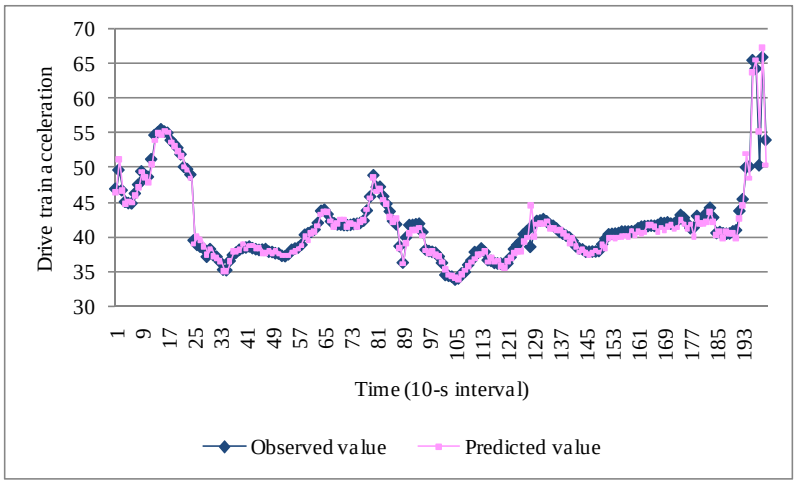

Figure A.19 Run-chart of the observed and predicted values of drive train acceleration for the first 200 points of Turbine 1 in Scenario 6

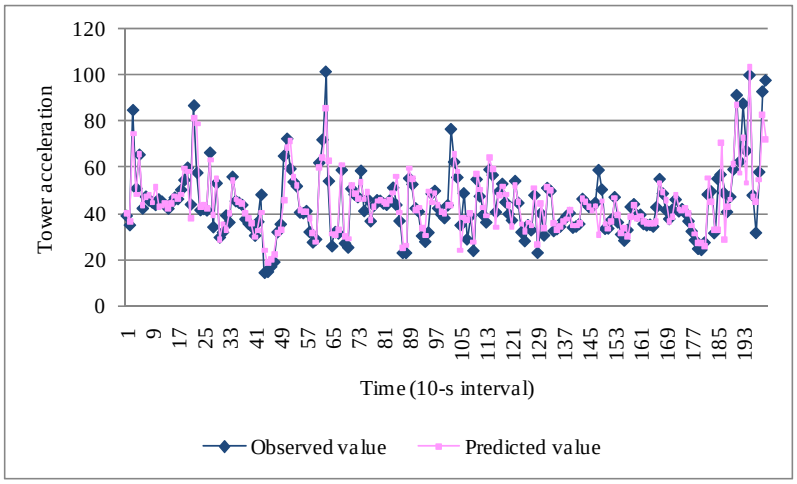

Figure A.20 Run-chart of the observed and predicted values of tower acceleration for the first 200 points of Turbine 1 in Scenario 6

Scenario 7

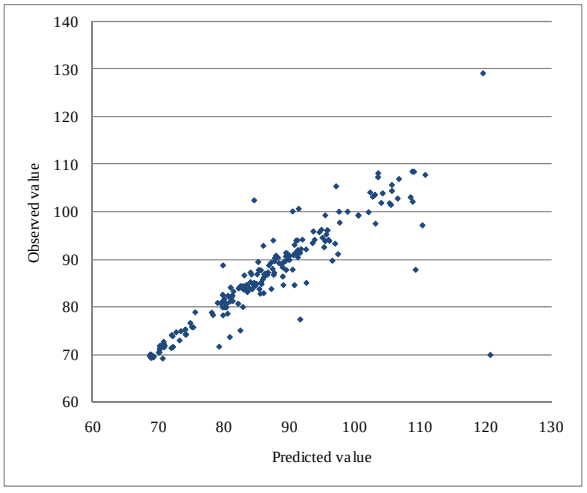

Figure A.21 Scatter plot of the observed and predicted values of drive train acceleration for the first 200 points of Turbine 1 in Scenario 7

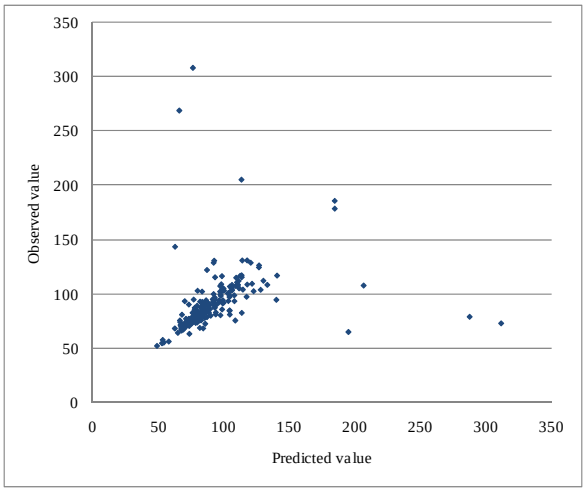

Figure A.22 Scatter plot of the observed and predicted values of tower acceleration for the first 200 points of Turbine 1 in Scenario 7

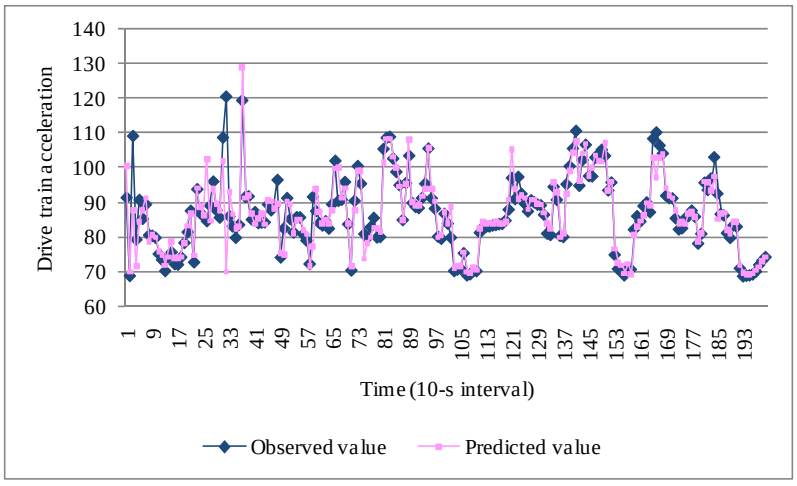

Figure A.23 Run-chart of the observed and predicted values of drive train acceleration for the first 200 points of Turbine 1 in Scenario 7

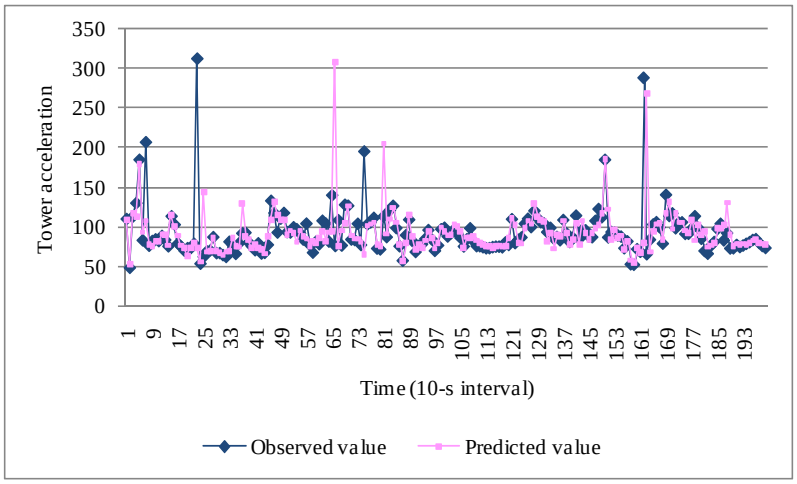

Figure A.24 Run-chart of the observed and predicted values of tower acceleration for the first 200 points of Turbine 1 in Scenario 7

Scenario 8

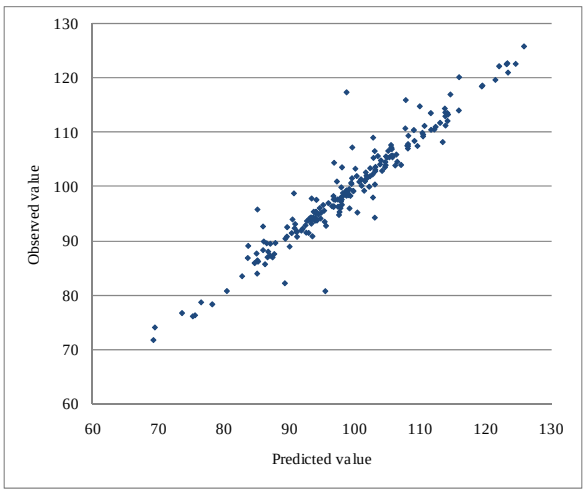

Figure A.25 Scatter plot of the observed and predicted values of drive train acceleration for the first 200 points of Turbine 1 in Scenario 8

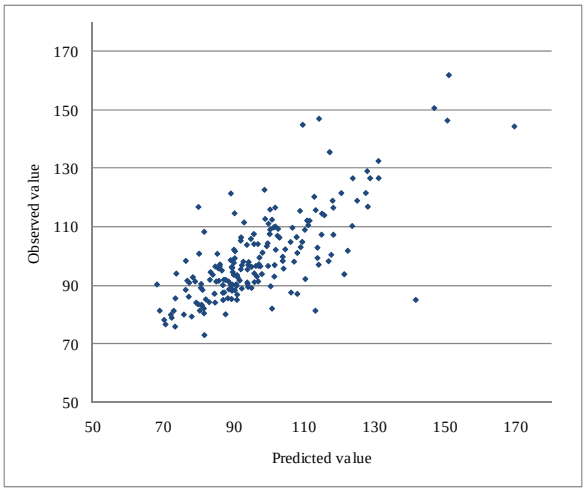

Figure A.26 Scatter plot of the observed and predicted values of tower acceleration for the first 200 points of Turbine 1 in Scenario 8

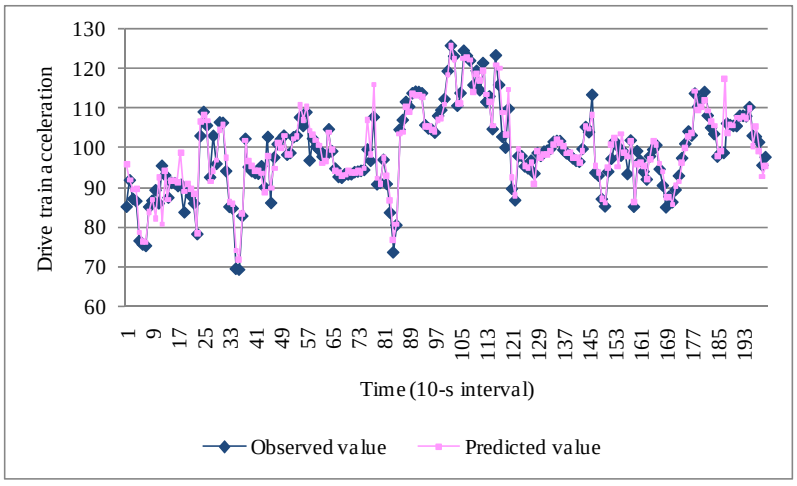

Figure A.27 Run-chart of the observed and predicted values of drive train acceleration for the first 200 points of Turbine 1 in Scenario 8

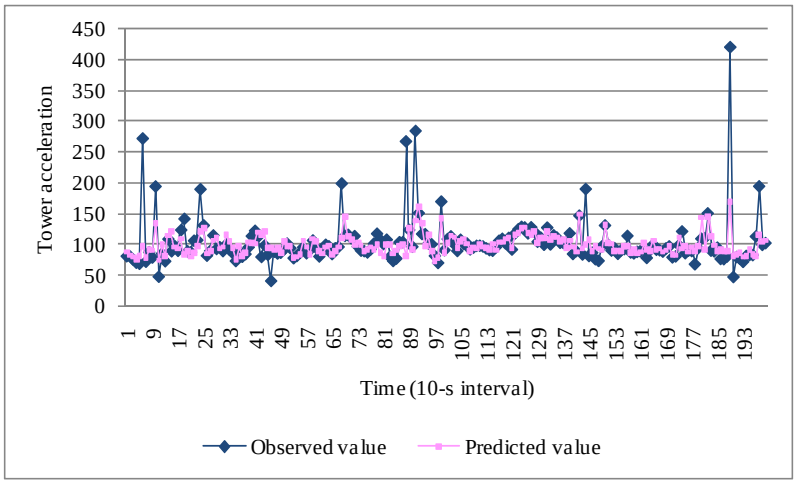

Figure A.28 Run-chart of the observed and predicted values of tower acceleration for the first 200 points of Turbine 1 in Scenario 8

Scenario 9

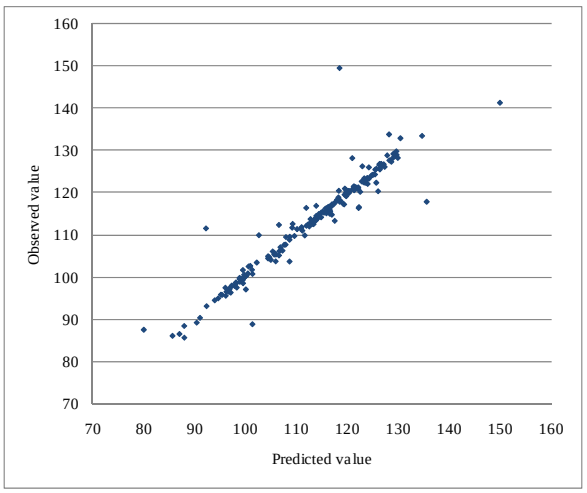

Figure A.29 Scatter plot of the observed and predicted values of drive train acceleration for the first 200 points of Turbine 1 in Scenario 9

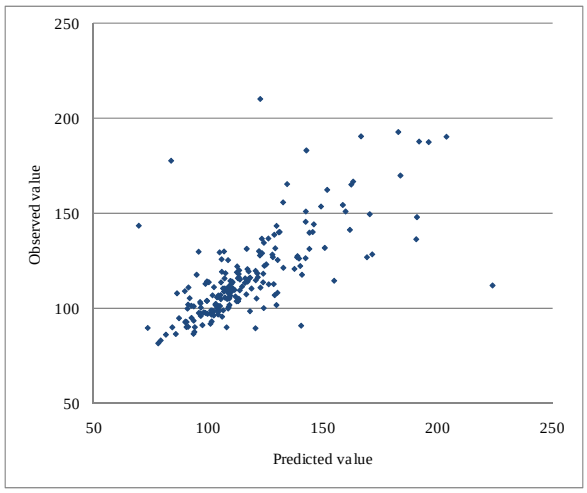

Figure A.30 Scatter plot of the observed and predicted values of tower acceleration for the first 200 points of Turbine 1 in Scenario 9

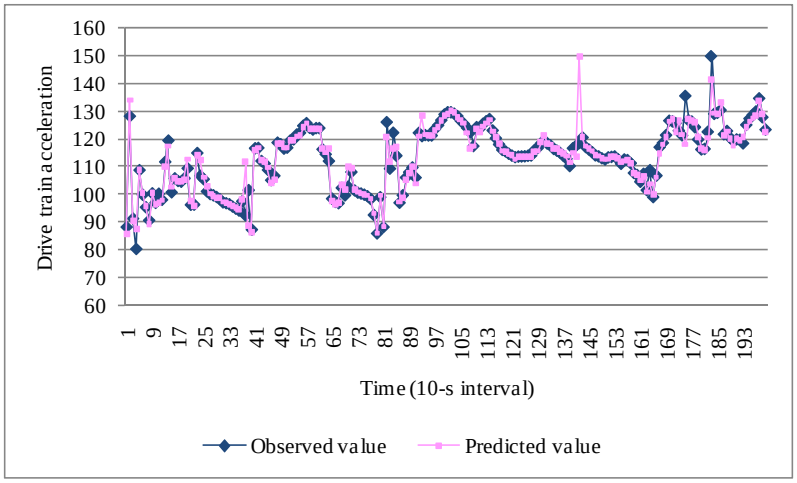

Figure A.31 Run-chart of the observed and predicted values of drive train acceleration for the first 200 points of Turbine 1 in Scenario 9

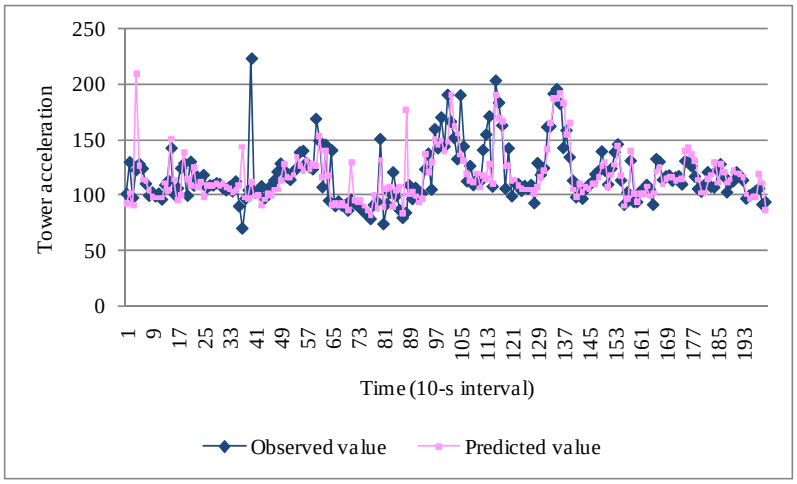

Figure A.32 Run-chart of the observed and predicted values of tower acceleration for the first 200 points of Turbine 1 in Scenario 9

APPENDIX B

FIGURES ILLUSTRATING PREDICTION PERFORMANCE OF TURBINE 2

Scenario 2

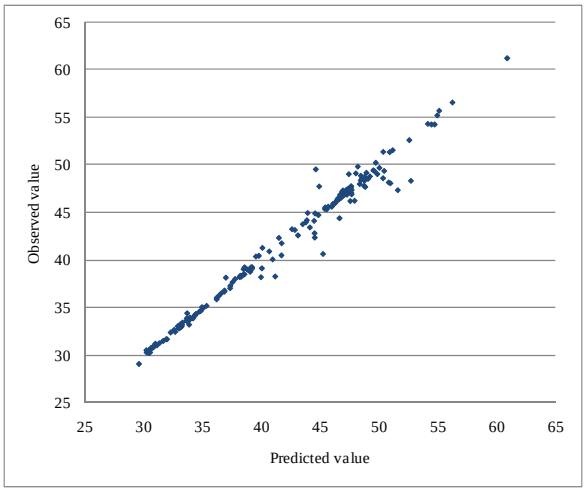

Figure B.1 Scatter plot of the observed and predicted values of the drive train acceleration for the first 200 points of Turbine 2 in Scenario 2

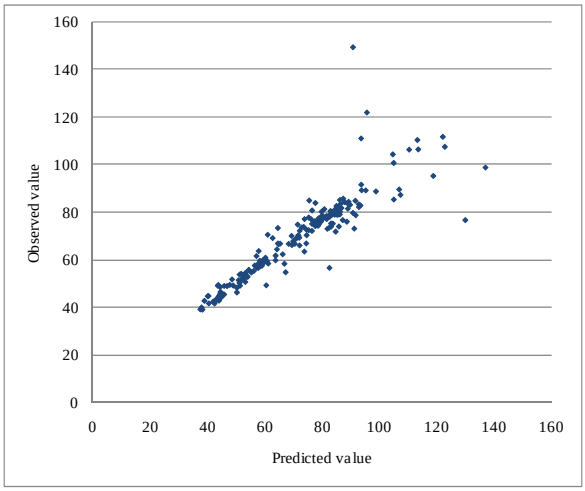

Figure B.2 Scatter plot of the observed and predicted values of the tower acceleration for the first 200 points of Turbine 2 in Scenario 2

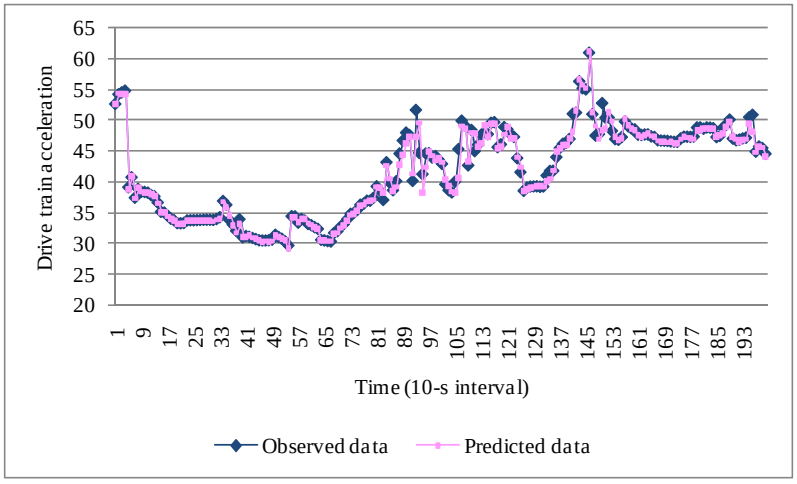

Figure B.3 Run-chart of the observed and predicted values of the drive train acceleration for the first 200 points of Turbine 2 in Scenario 2

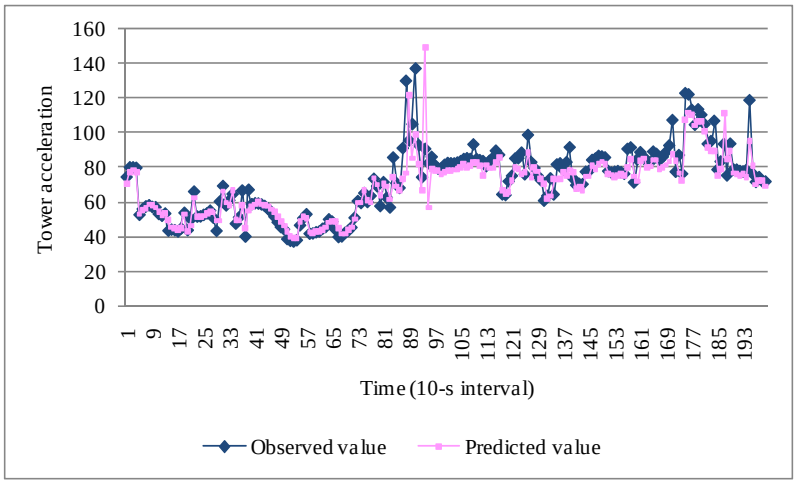

Figure B.4 Run-chart of the observed and predicted values of the tower acceleration for the first 200 points of Turbine 2 in Scenario 2

Scenario 3

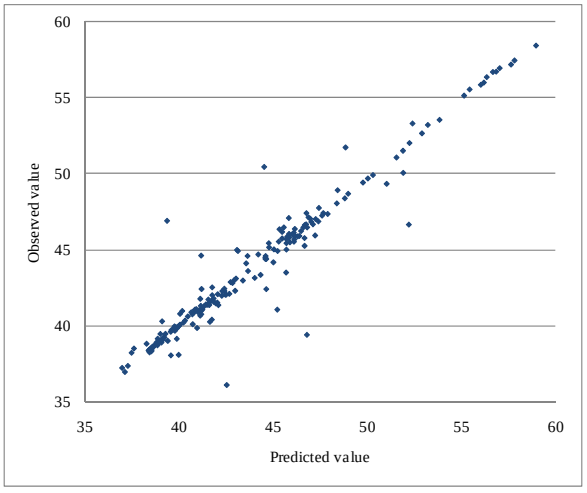

Figure B.5 Scatter plot of the observed and predicted values of the drive train acceleration for the first 200 points of Turbine 2 in Scenario 3

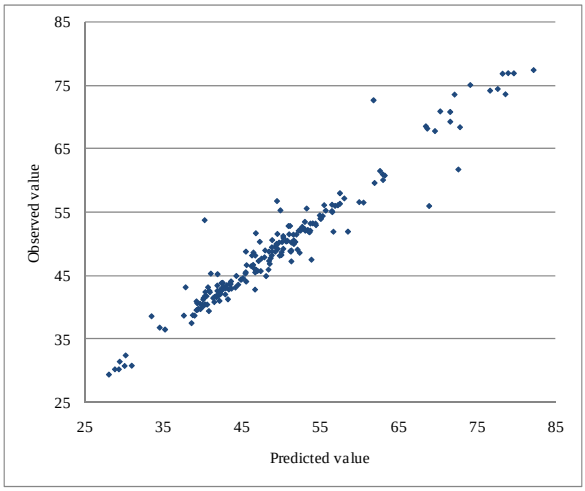

Figure B.6 Scatter plot of the observed and predicted values of the tower acceleration for the first 200 points of Turbine 2 in Scenario 3

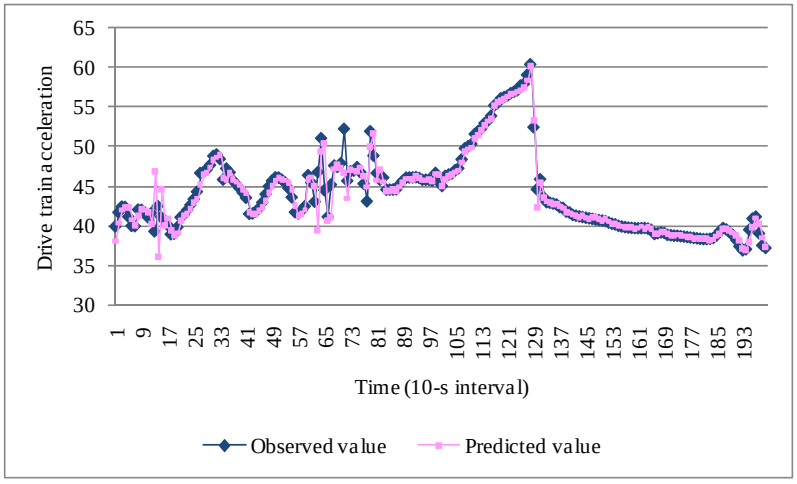

Figure B.7 Run-chart of the observed and predicted values of the drive train acceleration for the first 200 points of Turbine 2 in Scenario 3

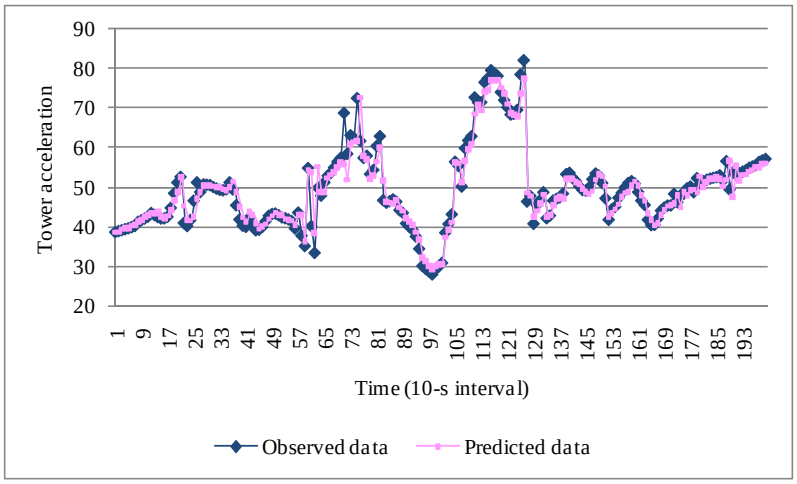

Figure B.8 Run-chart of the observed and predicted values of the tower acceleration for the first 200 points of Turbine 2 in Scenario 3

Scenario 4

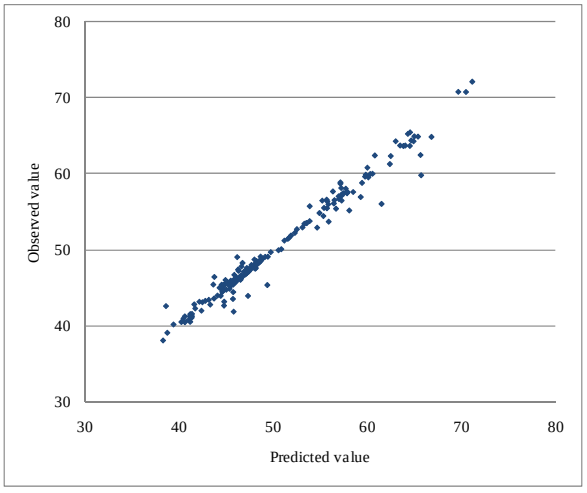

Figure B.9 Scatter plot of the observed and predicted values of the drive train acceleration for the first 200 points of Turbine 2 in Scenario 4

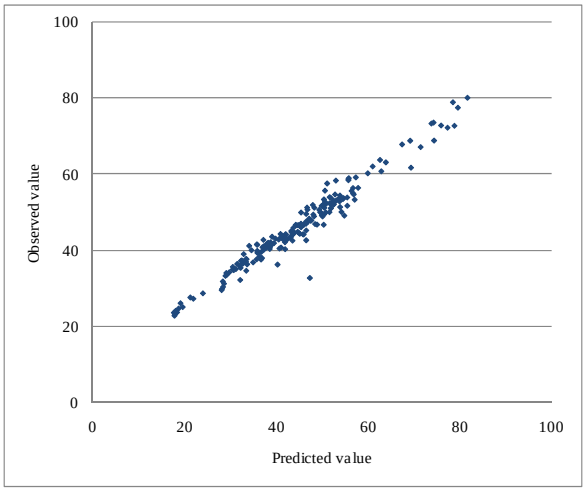

Figure B.10 Scatter plot of the observed and predicted values of the tower acceleration for the first 200 points of Turbine 2 in Scenario 4

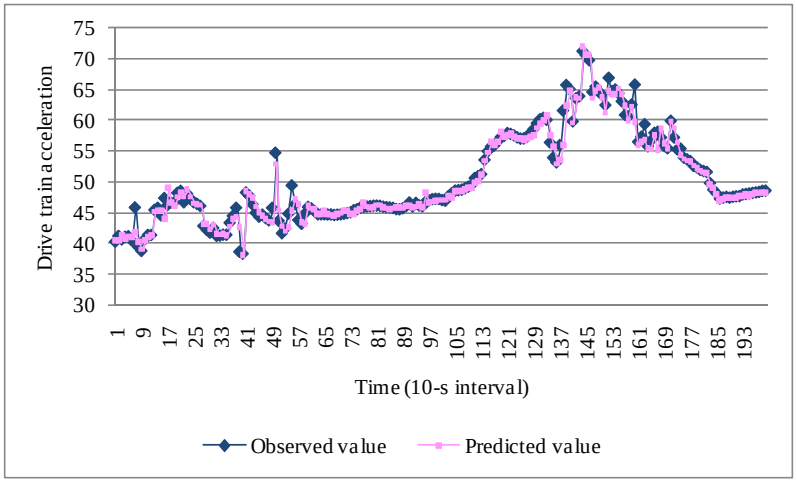

Figure B.11 Run-chart of the observed and predicted values of the drive train acceleration for the first 200 points of Turbine 2 in Scenario 4

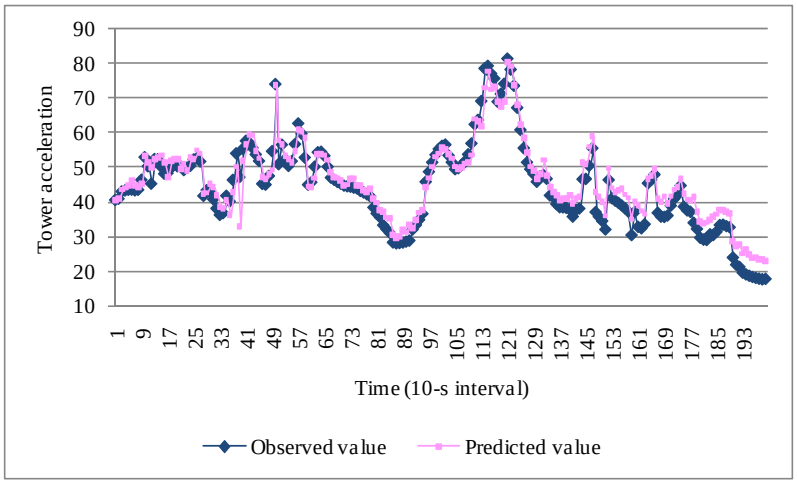

Figure B.12 Run-chart of the observed and predicted values of the tower acceleration for the first 200 points of Turbine 2 in Scenario 4

Scenario 5

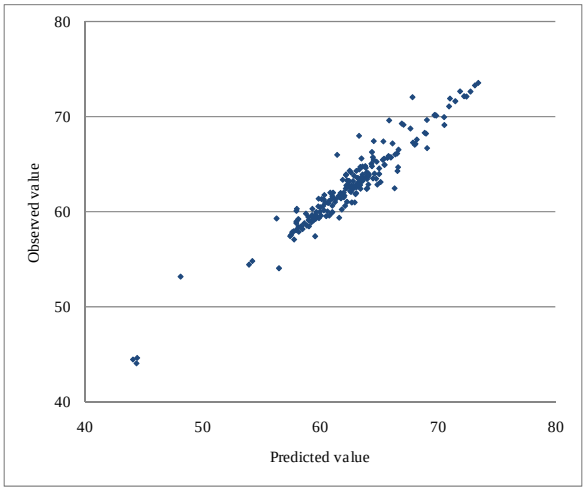

Figure B.13 Scatter plot of the observed and predicted values of the drive train acceleration for the first 200 points of Turbine 2 in Scenario 5

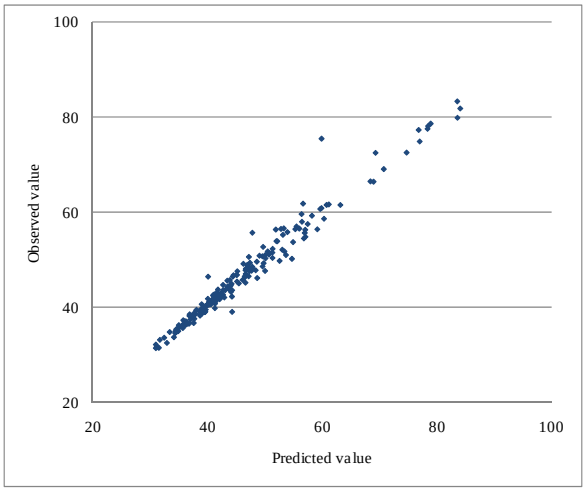

Figure B.14 Scatter plot of the observed and predicted values of the tower acceleration for the first 200 points of Turbine 2 in Scenario 5

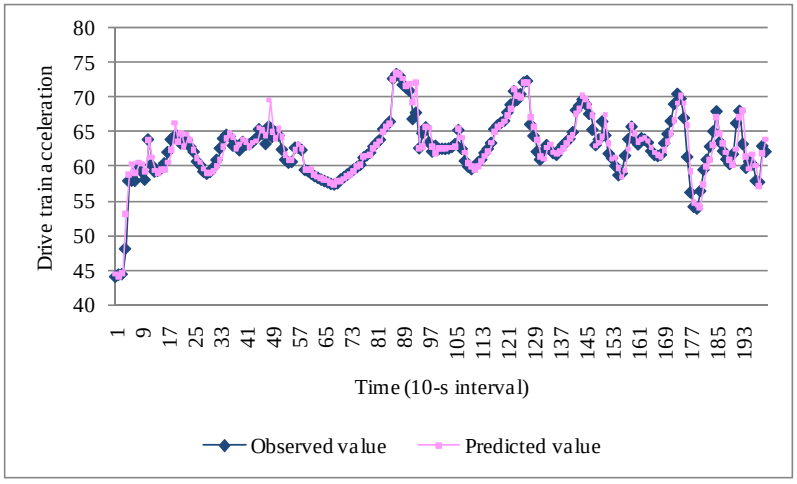

Figure B.15 Run-chart of the observed and predicted values of the drive train acceleration for the first 200 points of Turbine 2 in Scenario 5

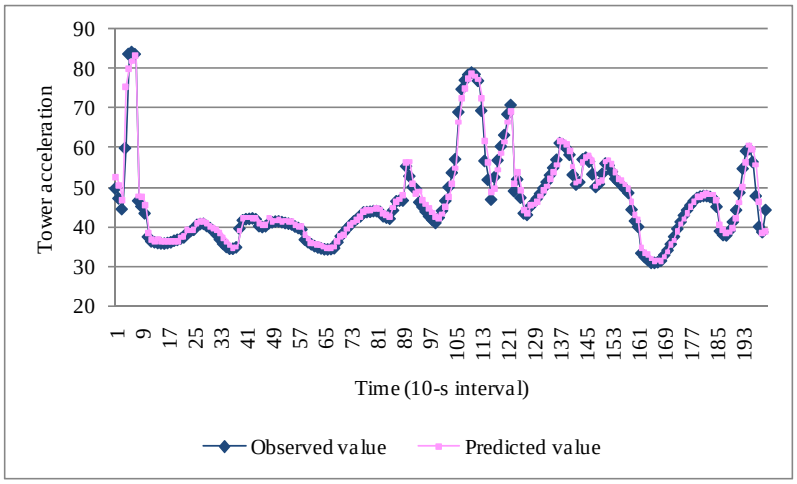

Figure B.16 Run-chart of the observed and predicted values of the tower acceleration for the first 200 points of Turbine 2 in Scenario 5

Scenario 6

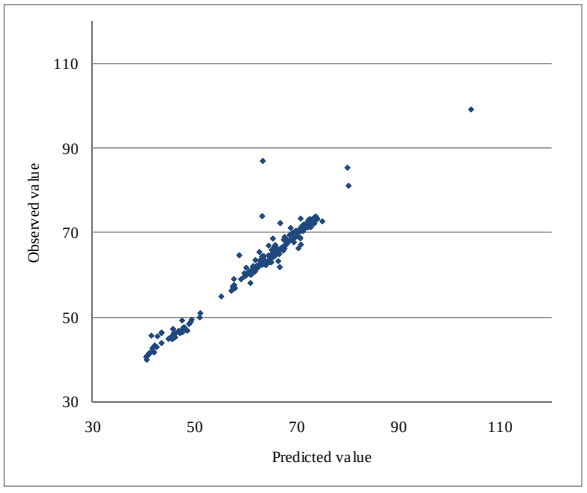

Figure B.17 Scatter plot of the observed and predicted values of the drive train acceleration for the first 200 points of Turbine 2 in Scenario 6

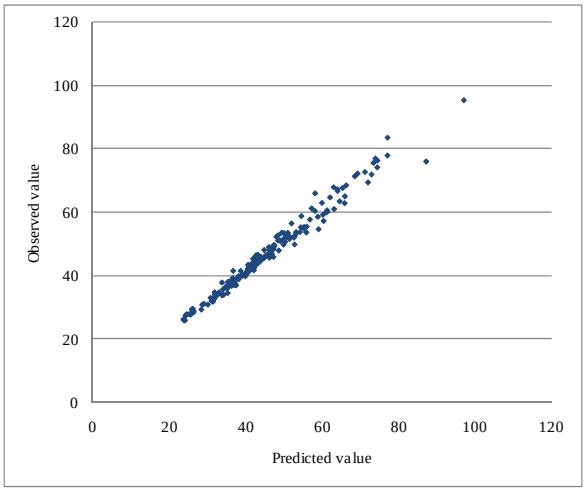

Figure B.18 Scatter plot of the observed and predicted values of the tower acceleration for the first 200 points of Turbine 2 in Scenario 6

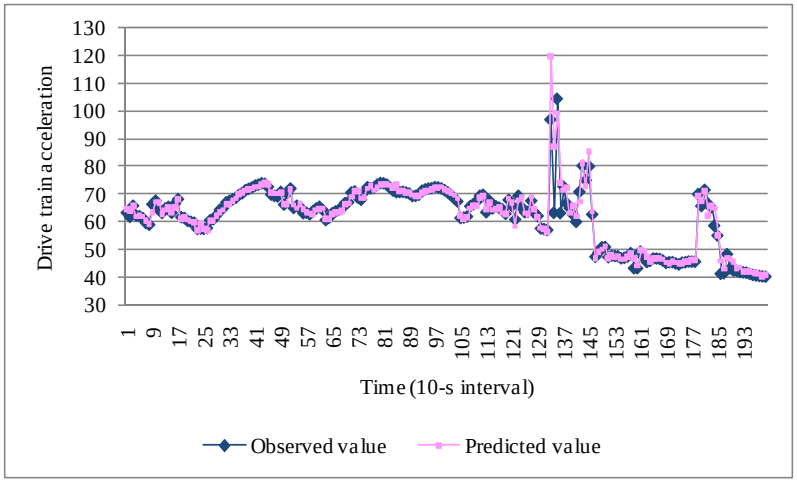

Figure B.19 Run-chart of the observed and predicted values of the drive train acceleration for the first 200 points of Turbine 2 in Scenario 6

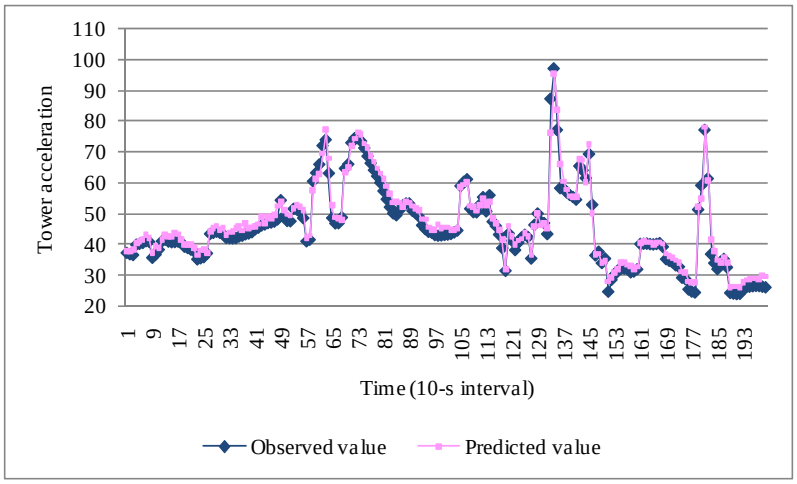

Figure B.20 Run-chart of the observed and predicted values of the tower acceleration for the first 200 points of Turbine 2 in Scenario 6

Scenario 7

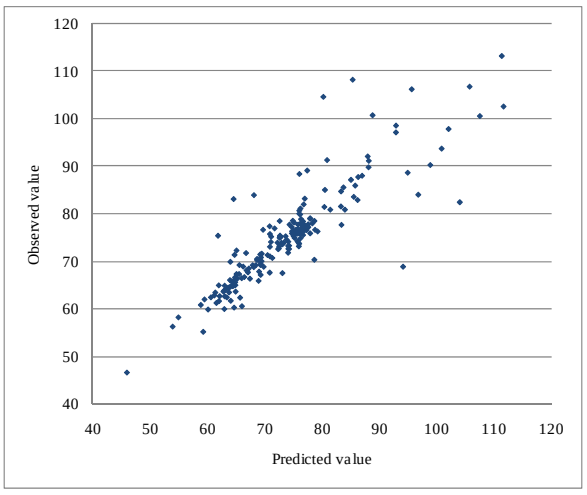

Figure B.21 Scatter plot of the observed and predicted values of the drive train acceleration for the first 200 points of Turbine 2 in Scenario 7

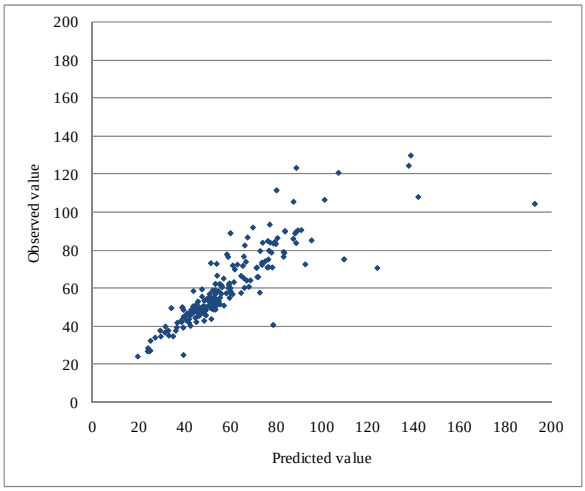

Figure B.22 Scatter plot of the observed and predicted values of the tower acceleration for the first 200 points of Turbine 2 in Scenario 7

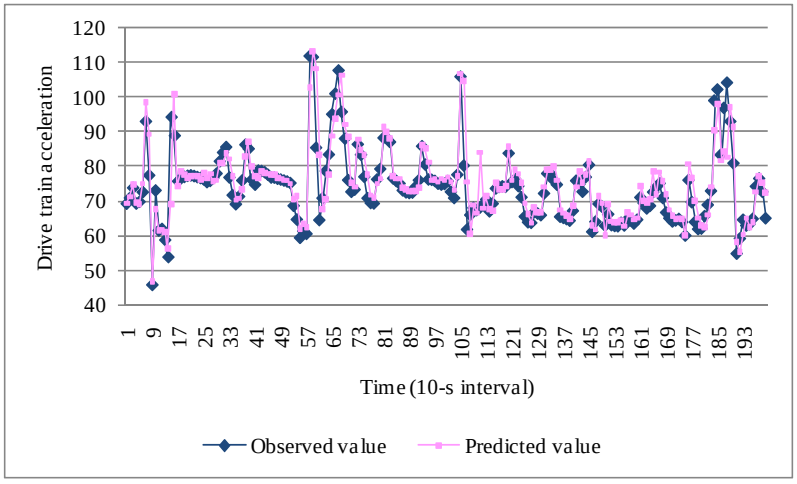

Figure B.23 Run-chart of the observed and predicted values of the drive train acceleration for the first 200 points of Turbine 2 in Scenario 7

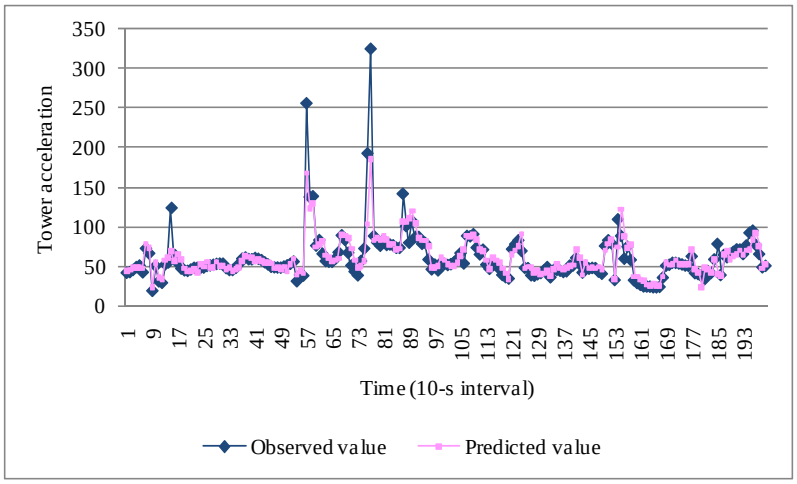

Figure B.24 Run-chart of the observed and predicted values of the tower acceleration for the first 200 points of Turbine 2 in Scenario 7

Scenario 8

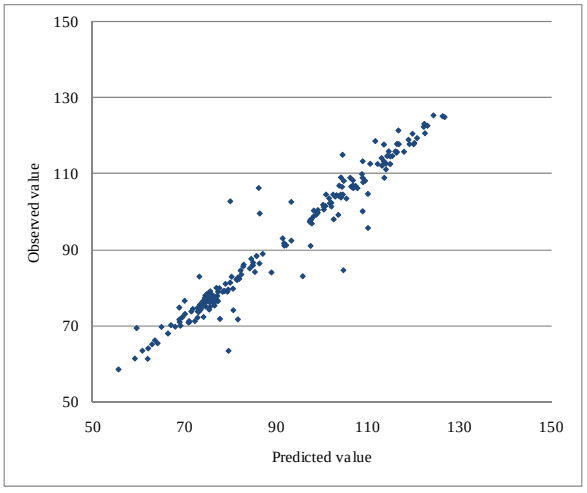

Figure B.25 Scatter plot of the observed and predicted values of the drive train acceleration for the first 200 points of Turbine 2 in Scenario 8

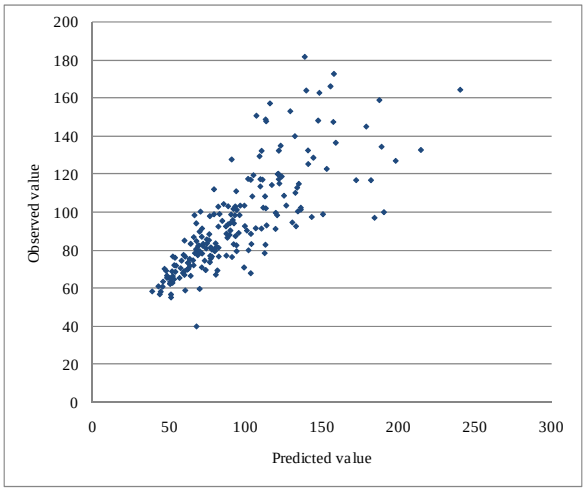

Figure B.26 Scatter plot of the observed and predicted values of the tower acceleration for the first 200 points of Turbine 2 in Scenario 8

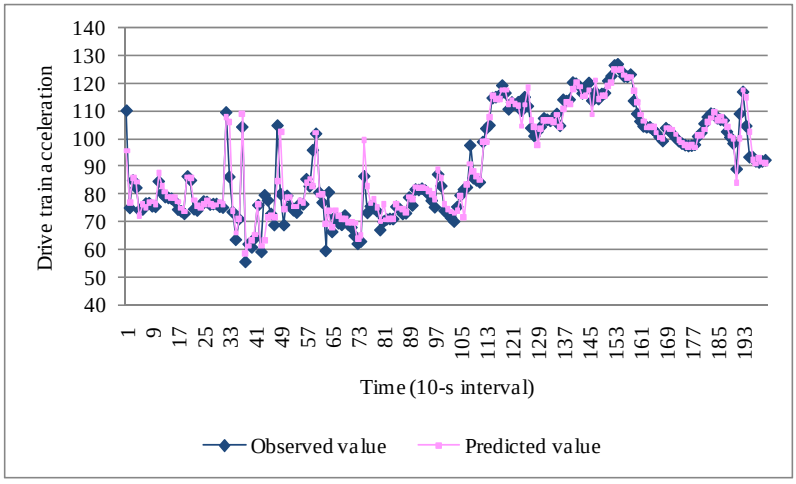

Figure B.27 Run-chart of the observed and predicted values of the drive train acceleration for the first 200 points of Turbine 2 in Scenario 8

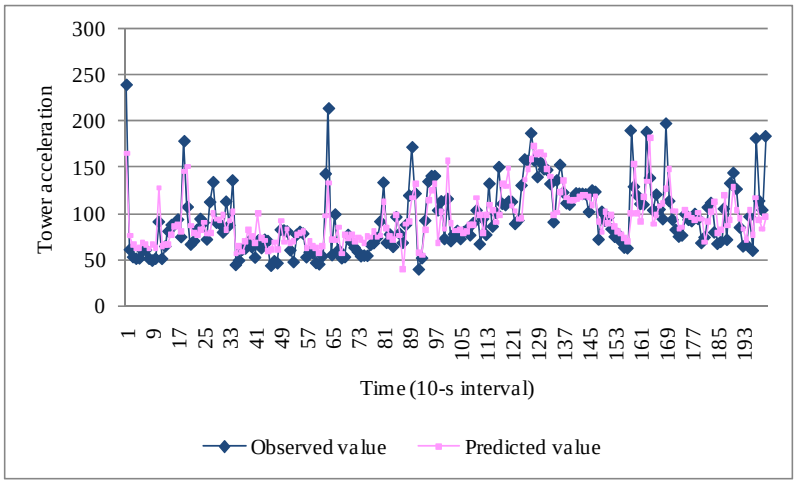

Figure B.28 Run-chart of the observed and predicted values of the tower acceleration for the first 200 points of Turbine 2 in Scenario 8

Scenario 9

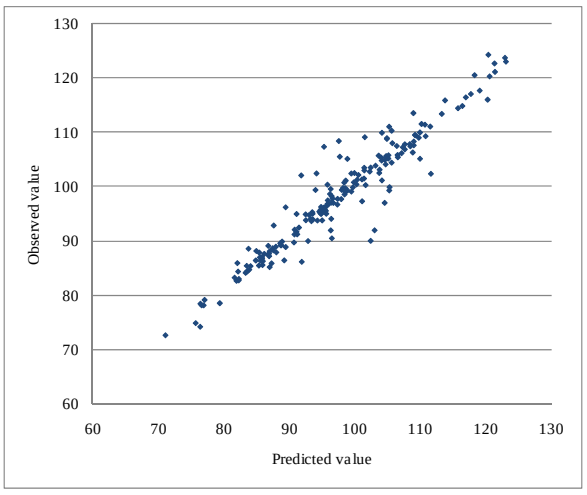

Figure B.29 Scatter plot of the observed and predicted values of the drive train acceleration for the first 200 points of Turbine 2 in Scenario 9

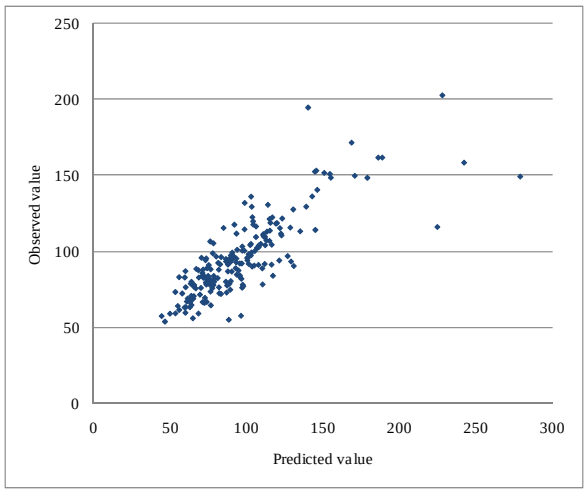

Figure B.30 Scatter plot of the observed and predicted values of the tower acceleration for the first 200 points of Turbine 2 in Scenario 9

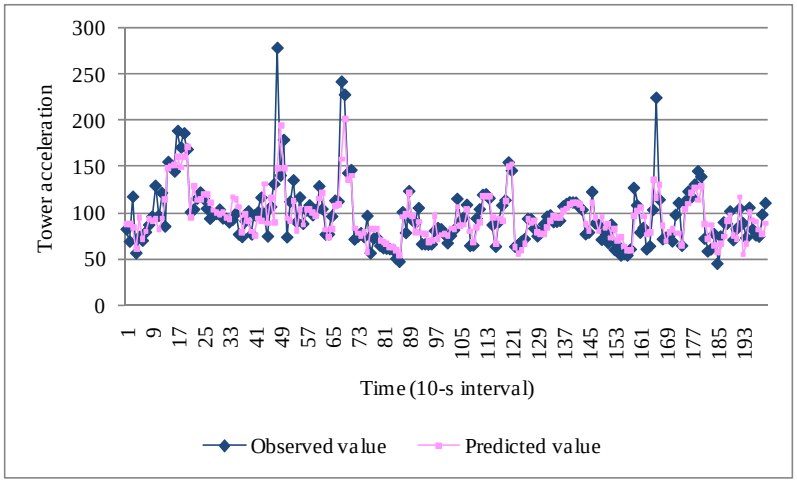

Figure B.31 Run-chart of the observed and predicted values of the drive train acceleration for the first 200 points of Turbine 2 in Scenario 9

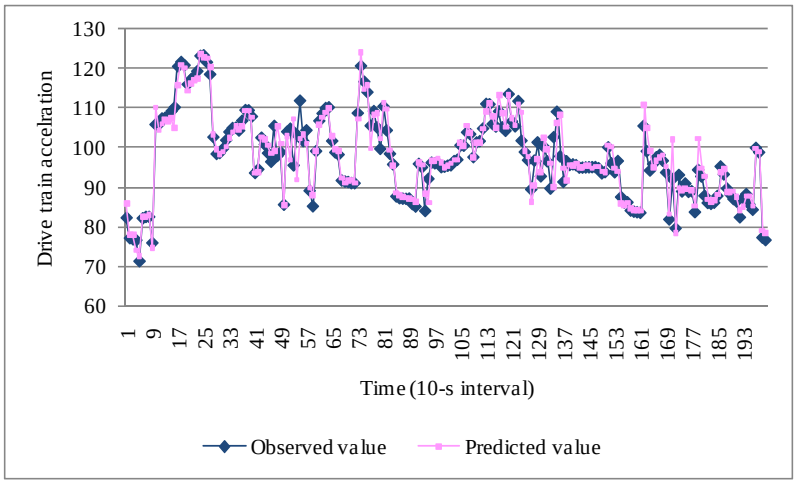

Figure B.32 Run-chart of the observed and predicted values of the tower acceleration for the first 200 points of Turbine 2 in Scenario 9

REFERENCES

[1] D. Laino, C. Butterfield, R. Thresher, and D. Dodge, "Evaluation of select IEC standard wind turbine design cases on the combined experiment wind turbine model," *Wind Energy*, American Society of Mechanical Engineers, Solar Energy Division (Publication) SED, Vol. 14, pp. 47-48, 1993.

[2] K. Saranyasoontorn, and L. Manuel, "A comparison of wind turbine design loads in different environments using inverse reliability techniques," *Wind Energy*, Vol. 126, No. 4, pp. 1060-1068, 2004.

[3] R. Barthelmie, S. Frandsen, M. Nielsen, S. Pryor, P. Rethore, and H. Jørgensen, "Modelling and measurements of power losses and turbulence intensity in wind turbine wakes at Middelgrunden offshore wind farm", *Wind Energy*, Vol. 10, No. 6, pp. 517-528, 2007.

[4] J. Mora, J. Barón, J. Santos, and M. Payán, "An evolutive algorithm for wind farm optimal design," *Neurocomputing*, Vol. 70, No. 16, pp. 2651-2658, 2007.

[5] A. Leite, C. Borges, and D. Falcão, "Probabilistic Wind Farms Generation Model for Reliability Studies Applied to Brazilian Sites," *IEEE Transactions on Power Systems*, Vol. 21, No. 4, pp. 1493-1501, 2006.

[6] T. Senjyu, R. Sakamoto, N. Urasaki, T. Funabashi, H. Fujita, and H. Sekine, "Output power leveling of wind turbine generator for all operating regions by pitch angle control," *IEEE Transactions on Energy Conversion*, Vol. 21, No. 2, pp. 467-475, 2006.

[7] H. Ko, K. Lee, M. Kang and H. Kim, "Power quality control of an autonomous wind-diesel power system based on hybrid intelligent controller," *Neural Networks*, Vol. 21, No. 10, pp. 1439-1446, 2008.

[8] K. Johnson, L. Pao, M. Balas and L. Fingersh, "Control of variable-speed wind turbines: standard and adaptive techniques for maximizing energy capture," *IEEE Control Systems Magazine*, Vol. 26, pp. 70-81, 2006.

[9] I. Munteanu, N. Cutululis, A. Bratcu and E. Ceanga, "Optimization of variable speed wind power systems based on a LQG approach," *Control Engineering Practice*, Vol. 13, No. 7, pp. 903-912, 2005.

[10] Md. Arifujjaman, M. Iqbal and J. Quaicoe, "Performance comparison of grid connected small wind energy conversion systems," *Wind Engineering*, Vol. 33, No. 1, pp. 1-18, 2009.

[11] Ö. Mutlu, E. Akpınar and A. Balıkcı, "Power quality analysis of wind farm connected to Alaçatı substation in Turkey," *Renewable Energy*, Vol. 34, No. 5, pp. 1312-1318, 2009.

[12] A. Kusiak, H. Zheng, and Z. Song, "Wind Farm Power Prediction: A Data-Mining Approach," *Wind Energy*, Vol. 12, No. 3, pp. 275-293, 2009.

[13] A. Kusiak, H. Zheng and Z. Song, "Short-Term Prediction of Wind Farm Power: A Data-Mining Approach," *IEEE Transactions on Energy Conversion*, Vol. 24, No. 1, pp. 125-136, 2009.

[14] A. Kusiak, H. Zheng and Z. Song, "On-line Monitoring of Power Curves," *Renewable Energy*, Vol. 34, No. 6, pp. 1487-1493, 2009.

[15] A. Kusiak, H. Zheng and Z. Song, "Models for Monitoring Wind Farm Power," *Renewable* Energy, Vol. 34, No. 3, pp. 583-590, 2009.

[16] V. Wowk, *Machinery Vibration: Measurement and Analysis*, McGraw-Hill, 1991.

[17] W. Leithead and B. Connor, "Control of variable speed wind turbines: dynamic models," *International Journal of Control*, Vol. 73, No. 13, pp. 1173-1189, 2000.

[18] R. Fadaeinedjad, G. Moschopoulos, M. Moallem, "Investigation of voltage sag impact on wind turbine tower vibrations," *Wind Energy*, Vol. 11, No. 4, pp. 351-375, 2008

[19] P.J. Murtagh, A. Ghosh, B. Basu, B.M. Broderick, "Passive control of wind turbine vibrations including blade/tower interaction and rotationally sampled turbulence," *Wind Energy*, Vol. 11, No. 4, pp. 305-317, 2008

[20] M. H. Hansen, K. Thomsen, P. Fuglsang and T. Knudsen, "Two methods for estimating aeroelastic damping of operational wind turbine modes from experiments," *Wind Energy*, Vol. 9, No.1-2, pp. 179 – 191, 2006.

[21] P. Louka, G. Galanis, N. Siebert, G. Kariniotakis, P. Katsafados, I. Pytharoulis, and G. Kallos, "Improvements in wind speed forecasts for wind power prediction purposes using Kalman filtering," *Journal of Wind Engineering and Industrial Aerodynamics*, Vol. 96, No. 12, pp. 2348-2362, 2008.

[22] P. Flores, A. Tapia and G. Tapia, "Application of a control algorithm for wind speed prediction and active power generation," *Renewable Energy*, Vol. 30, No. 4, pp. 523-536, 2005.

[23] T. H. M. El-Fouly, E. F. El-Saadany and M. M. A. Salama, "One Day Ahead Prediction of Wind Speed and Direction," *IEEE Transaction on Energy Conversion*, Vol. 23, No. 1, pp. 191 – 201, 2008.

[24] I. G. Damousis, M. C. Alexiadis, J. B. Theocharis and P. S. Dokopoulos, "A fuzzy model for wind speed prediction and power generation in wind parks using spatial correlation," *IEEE Transaction on Energy Conversion*, Vol. 19, No. 2, pp. 352-361, 2004.

[25] G. Contaxis and J. Kabouris, "Short Term Scheduling in A Wind/Diesel Autonomous Energy System," *IEEE Transactions on Power System*, Vol. 6, No. 3, pp. 1161-1167, 1991

[26] E. Anahua, St. Barth and J. Peinke, "Markovian Power Curves for Wind Turbines," *Wind Energy*, Vol. 11, pp. 219-232, 2008

[27] L. Landberg, "Short-term prediction of the power production from wind farms," *Journal of Wind Engineering and Industrial Aerodynamics*, vol. 80, pp. 207-220, 1999.

[28] J. Z. Chu, S. S. Shieh, S. S. Jang, C. I. Chien, H. P. Wan and H. H. Ko, "Constrained optimization of combustion in a simulated coal-fired boiler using artificial neural network model and information analysis," *Fuel*, vol. 82, pp. 693-703, 2003.

[29] H. Rusinowski, M. Szega, A. Szlk and R. Wilk, "Methods of choosing the optimal parameters for solid fuel combustion in stoker-fired boilers," *Energy Conversion and Management*, vol. 43, pp. 1363-1375, 2002.

[30] D. Büche, P. Stoll, R. Dornberger and P. Koumoutsakos, "Multiobjective evolutionary algorithm for the optimization of noisy combustion processes," *IEEE Transactions on Man, Control, and Cybernetics – Part C*, vol. 32, pp. 460-473, 2002.

[31] S. Y. Wang, G. L. Bai, Y. Cao and B. Li, "An algorithm of simulating human intelligent control for combustion system," in *IEEE International Conference on Intelligent Processing Systems*, 1997, pp. 786-771.

[32] R. Cass and B. Radl, "Adaptive process optimization using functional-link networks and evolutionary optimization," *Control Engineering Practice*, vol. 4, pp. 1579-1584, 1997.

[33] A. Kusiak, Z. Song, and H. Zheng, "Anticipatory Control of Wind Turbines with Data-Driven Predictive Models," *IEEE Transactions on Energy Conversion*, Vol. 24, No. 3, pp. 766-774, 2009.

[34] D. Li, C. He and Y. Fu, "Optimization of internal electric connection system of large offshore wind farm with hybrid genetic and immune algorithm" in *3rd International Conference on Deregulation and Restructuring and Power Technologies*, 2008, pp. 2476-2481.

[35] M. Prats, J. Carrasco, E. Galván, J. Sánchez, L. Franquelo and C. Batista, "Improving transition between power optimization and power limitation of variable speed, variable pitch wind turbines using fuzzy control techniques" in *IECON Proceedings (Industrial Electronics Conference)*, 2000, pp. 1497-1502.

[36] B. Sareni, A. Abdelli, X. Roboam and D. Tran, "Model simplification and optimization of a passive wind turbine generator," *Renewable Energy*, Vol. 34, No.12, pp. 2640-2650, 2009.

[37] E. HAU, *Wind-turbines: Fundamentals, Technologies, Application and Economics*. Springer, 2000.

[38] D. B. Fernando, D. B. Hernán and J. M. Ricardo, *Wind Turbine Control Systems: Principles, Modelling and Gain Scheduling Design*. Springer, 2007

[39] J. Friedman, "Stochastic gradient boosting," *Stanford University Statistics Department*, 1999.

[40] J. H. Friedman, "Greedy function approximation: A gradient boosting machine," *The Annals of Statistics*, Vol. 29, pp. 1189-1232, 2001.

[41] H.T. Siegelmann and E.D. Sontag, "Analog computation via neural networks," *Theoretical Computer Science*, Vol. 131, No. 2, pp. 331-360, 1994.

[42] G. V. Cybenko, "Approximation by Superpositions of a Sigmoidal function," *Mathematics of Control, Signals and Systems*, Vol. 2, pp. 303-314, 1989.

[43] M. Smith, *Neural Networks for Statistical Modeling*. Van Nostrand Reinhold, 1993.

[44] R. A. Fisher, "Frequency distribution of the values of the correlation coefficient in samples from an indefinitely large population," *Biometrika*, Vol. 10, pp. 507-521, 1915.

[45] M. Monfared, H. Rastegar, H. M. Kojabadi, "A new strategy for wind speed forecasting using artificial intelligent methods," *Renewable Energy*, Vol. 34, No. 3, pp. 845-848, 2009.

[46] I. Daubechies, *Ten Lectures on Wavelets*, Society for Industrial and Applied Mathematics, Philadelphia, PA, 1992.

[47] B. Schölkopf, C. J.C. Burges, and A. J. Smola, *Advances in Kernel Methods: Support Vector Learning*. Cambridge, MA: MIT Press, 1999.

[48] I. Steinwart and A. Christmann, *Support Vector Machines*. New York: Springer-Verlag. 2008.

[49] L. Breiman, "Random Forests," *Machine Learning*, vol. 45, pp. 5-32, 2001.

[50] *http://en.wikipedia.org/wiki/Wind power*

[51] B. Boukhezzar and H. Siguerdidjane, "Nonlinear control with wind estimation of a DFIG variable speed wind turbine for power capture optimization," *Energy Conversion and Management*, Vol. 50, No. 4, pp. 885-892, 2009.

[52] A. Abdelli, B. Sareni and X. Roboam, "Optimization of a small passive wind turbine generator with multiobjective genetic algorithms," *International Journal of Applied Electromagnetics and Mechanics*, Vol. 26, No. 3-4, pp. 175-182, 2007

[53] B. Boukhezzar, H. Siguerdidjane and M. Maureenhand, "Nonlinear control of variable-speed wind turbines for generator torque limiting and power optimization," *Journal of solar energy engineering*, Vol. 128, No. 4, pp. 516-530, 2006.

[54] Z. Song and A. Kusiak, "Constraint-Based Control of Boiler Efficiency: A Data-Mining Approach," *IEEE Transactions on Industrial Informatics*, Vol. 3, No. 1, pp. 73-83, 2007.

[55] R. Steuer, *Multiple Criteria Optimization: Theory, Computations, and Application*, Wiley New York: 1986.

[56] E. Zitzler and L. Thiele, "Multiobjective evolutionary algorithms: a comparative case study and the strength Pareto approach," *IEEE Transactions on Evolutionary Computation*, Vol. 3, No. 4, pp. 257-271, 1999.

[57] Z. Song and A. Kusiak, “Optimization of Temporal Processes: A Model-Predictive Control Approach,” *IEEE Transactions on Evolutionary Computation*, Vol. 13, No. 1, pp. 169-179, 2009.

[58] K. Deb, *Multi-Objective Optimization using Evolutionary Algorithms*, Wiley: New York, 2001.